High Throughput 3D Hydrogel Cell and Tissue Encapsulation Assay to Measure Matrix Metalloproteinase and Metabolic Activity

Dissertation

Presented in Partial Fulfillment of the Requirements for the Degree Doctor of Philosophy in the Graduate School of The Ohio State University

By

Abdulaziz Saud W. Fakhouri, M.S.

Graduate Program in Biomedical Engineering

The Ohio State University

2019

Dissertation Committee

Jennifer Leight Ph.D., Advisor

Jessica Winter Ph.D.

Keith Gooch Ph.D.

Abstract

Currently, most assays for cancer chemotherapeutic screening and development utilize two dimensional (2D) culturing systems. These 2D systems lack aspects of the *in vivo* microenvironment creating a poor *in vitro* representation that significantly affects cellular responses. To recapitulate the *in vivo* cellular microenvironment more closely, three dimensional (3D) cell culture systems have been developed and utilized. However, 3D cell culture systems are more complex, making analysis of cellular responses more difficult. Therefore, most high throughput (HT) 3D assays have been limited to measurements of cell viability. Yet other cellular functions play critical role in diseases and are promising pharmacological targets. There is a need for a HT 3D culturing system that enables the measurement of cellular functions, other than viability, for drug testing applications. To address this need, we developed, characterized, validated and demonstrated the utility of a HT 3D culturing system to measure matrix metalloproteinase (MMP) and metabolic activity, simultaneously. MMPs are critical regulators of tissue homeostasis and are upregulated in many diseases, such as arthritis and cancer. The developed assay produced edge effect, drift, Z'-factor, %CV, inter-plate, and inter-day fold shifts of the signals that were within the acceptable range for HT applications, designating it suitable for screening applications. Human MMP-1, -2 and -9 resulted in a significant increase in signal intensity. Encapsulation of several cell types,

utilizing two different MMP-degradable peptides, produced robust signals above background noise and within the linear range of the assay. Finally, the utility of the system to measure cellular MMP activity in response to chemotherapeutics was demonstrated. Fibrosarcoma cell line (HT1080) was treated with several drugs, known to alter MMP activity, over a range of concentrations. Interestingly, sorafenib (SOR), a small molecule multi-kinase inhibitor utilized in clinical trials, increased MMP activity in a dose-dependent. This assay combines 3D cellular encapsulation and MMP activity detection in a HT format, which makes it suitable for drug screening and development applications.

Historically, immortalized cancer cell lines have been used for the vast majority of *in vitro* cancer studies due to their unlimited proliferation and ease of use. However, cell lines lack the tumor heterogeneity and native microenvironment encountered *in vivo,* factors that also affect cellular responses. To more closely approximate the heterogeneity observed with *in vivo* tumor cells, human tissue samples have been used in patient derived xenografts (PDX) and tumor organotypic slice culture models. However, PDX and organotypic slice culture models are unsuitable for HT applications because they are expensive and have long turnaround time to produce results. A simple and efficient system that enables culturing human tissue is needed. To address this need, we developed a 3D *ex vivo* culture system which maintained viability of human tissue samples derived from patients undergoing surgeries. Moreover, MMP and metabolic activity were measured in tissue size dependent manner. After further characterization, we envision

that this system will enable drug screening utilizing human tissue samples for drug development and personalized medicine applications.

Dedication

((How can those who know be equal to those who don't know?! None will be mindful of this except people of reason.)) (Az-Zumar, verse 9, Holy Qur'an)

I would like to dedicate this dissertation, first of all, to God, who guided me to light throughout my entire life and made me who I am today. I would like to praise, thank and worship him. On a similar level, I would like to dedicate this dissertation to my parents, my mother Rola and father Saud. Since the day I took my first breath, they never stopped loving, caring and supporting me in all means. This whole Ph.D. is another way of thanking them for what they have done, and I hope it would payback a fraction. I eagerly would love to dedicate this dissertation and Ph.D. to my wife, Mirah Bashiti, the wife of my dreams and love of my life. She always lifts me up, when I am down. She is always there when I need her, she is one of a kind, and I would never reach this point without her. Indeed, ~~behind~~ beside every man a great/amazing/wonderful woman, and words are incompetent to express what she deserves. In addition to her, this dissertation is dedicated to my children, Saud and Qamar, who did not help! Yet they have my heart and love. I would like also to dedicate this dissertation to my siblings, Sarah, Faisal, and Sultan, who I always can count on. Thank you very much siblings! You are the absolute best! Finally, I would like to dedicate this dissertation to my great advisor Dr. Jennifer Leight, as her

first Ph.D. student. Her door was always open and never been closed to her students. Thank you Dr. Leight for your help, guidance and advice, this Ph.D. would never be done without your support. Through all the mountains and oceans we went through, she was always doing her best to educate, advice and support. We are lucky to have you! Thank you a million!

Acknowledgments

I would like to acknowledge all my friends and family who helped me through this journey. I would like to thank my lab mates Ameya, Jessica, Joshua, Caitlin, Anthony, Catherine, Mohammed, and all the Leight lab members for their help and support. I am so glad that I was among such nice people. I would like to acknowledge and thank my candidacy and dissertation committee members Dr. Leight, Dr. Gooch, Dr. Winter and Dr. Kniss for their service, advice and support. I would like to thank all BME department advisors and mentors, they were always happy to help, I am so proud to be the student of some. I would like to thank Dr. Yee (City of Hope, Duarte, CA) for providing us with patient tissue samples. Finally, I would like to acknowledge Ohio Cancer Research (OCR), OH, USA for funding part of this work as well as King Saud University (KSU) and Saudi Arabian Cultural Mission (SACM), Riyadh, KSA for sponsoring me through my Ph.D.

Thank you all!

Vita

Jun. 2006……...…. High School Diploma, Riyadh, KSA.

Sep. 2006 to Feb. 2012….. B.S., King Saud University, Riyadh, KSA.

Feb. 2011 to Sep. 2012..... Service Engineer, General Electric Healthcare, Riyadh, KSA.

Sep. 2012 to Sep. 2018….. Demonstrator, King Saud University, Riyadh, KSA.

Aug. 2013 to May 2015 …. M.S., The Ohio State University, Columbus, Ohio, USA.

Jun. 2015 to Present ……. Ph.D., The Ohio State University, Columbus, Ohio, USA.

Sep. 2018 to Present …….. Lecturer, King Saud University, Riyadh, KSA.

Publications

Fakhouri, A. S., Weist, J. L., Tomusko, A. R., & Leight, J. L. (2019). High-Throughput Three-Dimensional Hydrogel Cell Encapsulation Assay for Measuring Matrix Metalloproteinase Activity. *ASSAY and Drug Development Technologies*, *17*(3), 100–115. https://doi.org/10.1089/adt.2018.877

Fakhouri, A. S., & Leight, J. L. (2019). Measuring Global Cellular Matrix Metalloproteinase and Metabolic Activity in 3D Hydrogels. *JoVE (Journal of Visualized Experiments)*, (143), e59123. https://doi.org/10.3791/59123.

Fakhouri, F. S., **Fakhouri, A. S.,** & Torres-Rodriguez, J. J. (2018). *U.S. Patent No. US9987009B2*. Washington, DC: U.S. Patent and Trademark Office. Retrieved from https://patents.google.com/patent/US9987009B2/en

Fields of Study

Major Field: Biomedical Engineering

Specialization: Biosensors, Fluorescence, Biomaterials, Hydrogels, 3D Cell Encapsulation, High Throughput Assays, Assay Development, Matrix Metalloproteinases, Metabolic Activity.

Table of Contents

List of Tables

List of Figures

Chapter 1. Introduction

Development of new drugs to treat human disease is a long and expensive process, with some estimating it takes at ten years and a billion dollars to develop a new drug (Ledford, 2011). Yet, this one drug that makes it to market is less than 5% of drugs tested at or before clinical trials (Singh M, Close DA, Mukundan S, Johnston PA, & Sant S, 2015), while the rest fail, 60% due to high toxicity (unwanted side effects or off-target activities) or lack of clinical efficacy (Hopkins, 2008; Kola, 2008). This very low percentage of drugs translated into effective treatments in clinics indicates that there is a gap in the path of drug development between *in vitro* high throughput (HT) compound screening and *in vivo* animal testing and clinical trials. To bridge such a gap, there is a need for comprehensive pre-clinical assays that more closely reflect the *in vivo* disease accurately. This dissertation focuses on bridging the gap between current HT 2D assays, utilized for drug screening and development, and patient derived xenograft (PDX) models, that more accurately predict clinical responses and are used to study treatment outcomes prior to clinical trials. *In vitro*, it is well established that 3D cell culture systems often more closely represent the *in vivo* cellular responses than traditional 2D cell culture methods. Therefore, bridging this gap could be achieved by utilizing 3D cell culturing methodologies and developing them to suit the requirements of HT applications, then improving the mimicry *in vitro* to enhance prediction of clinical responses *in vivo*. HT 2D

culture assays enable the discovery of thousands of drugs to treat diseases. Yet, their effectiveness in predicting clinical outcomes has been limited to their ability to accurately represent *in vivo* cellular responses, preventing further treatment development for cancer. Therefore, 3D cultures are being developed and utilized for HT applications such as drug screening and development. However, HT 3D culture system utility is limited by the increased cost, labor, and time required for 3D culturing and the incompatibility of many non-viability assays to HT approaches. For example, other cellular functions beyond viability such as protease activity are important pharmacological targets. Furthermore, isolated cells used in 3D cultures are homogenous, without native microenvironment, or disease pathology, all of which have significant effect on cellular response to therapeutics. There is a need for a HT 3D culture system that combines HT approaches for measuring cellular functions and provides a closer representation of *in vivo* similar to PDX models. To address this need, we developed a HT 3D hydrogel system that enables the measurement of cellular functions, specifically matrix metalloproteinase (MMP) activity, efficiently and is suitable for drug screening. Moreover, to more closely recapitulate the *in vivo* tumor, we improved our HT 3D hydrogel culture assay to encapsulate patient-derived breast adipose fine needle aspirate biopsies (FNAB) and tissue dissections for *ex vivo* culture. Using this culture system, MMP and metabolic activity were detected in a size dependent manner. Preliminary results of *ex vivo* culture provide sufficient evidence to further characterize viability and histological fidelity of encapsulated tissue samples, and to validate MMP activity with standard assays. All of

which will provide a powerful *in vitro* drug testing tool that has HT outcomes and a closer representation to *in vivo*.

1.1. 3D Cell Culture

1.1.1. 2D and 3D Cultures: Features and Effects on Cellular Functions

Two dimensional (2D) culturing systems have contributed significantly to understanding basic cellular behavior and functions for drug development. Yet, a growing body of evidence supports the notion that 2D culturing systems influence cellular behavior and functions differently than three dimensional (3D) culturing systems. 3D culture provides environmental cues similar to those experienced by cells *in vivo,* which are absent in 2D cultures, such as soluble gradients, cell-cell, and cell-matrix adhesion (Baker & Chen, 2012; Duval et al., 2017; Hoarau-Véchot, Rafii, Touboul, & Pasquier, 2018). Unlike cells in 3D culture, cells in 2D culture experience forced apical-basal polarity and can only adhere and migrate in one plane (Baker & Chen, 2012; Duval et al., 2017). Such differences between 3D and 2D cultures have significant effects on cellular behavior and functions including, cellular differentiation, morphology, migration, and drug resistance. 3D culture can restore the differentiation state of chondrocytes after 2D culture plates (Benya & Shaffer, 1982) and improve the direct reprogramming of fibroblasts into cardiomyocytes utilizing microRNAs (Li et al., 2016). Additionally, breast cancer cells MCF7 cultured in 3D collagen scaffold had heterogeneous morphology, higher expression of pro-angiogenic growth factors and matrix metalloproteinases (MMP), upregulated epithelial to mesenchymal transition (EMT) markers, and higher

tumorigenicity when implanted *in vivo*, as compared to cells cultured on 2D plates (Chen et al., 2012). Previously mentioned examples demonstrated several differences in cellular functions between 2D and 3D cultures. However, they utilized 3D gels in comparison to traditional 2D tissue culture plates, thus observed differences in cellular functions may be caused by dimensionality or other confounding factors.

In order to determine if the observed changes in functions were caused by dimensionality or other factors, for example stiffness, a number of studies have been conducted in which cells were cultured on top of gels (2D) or within gels (3D) with the same stiffness. For example, human mesenchymal stem cells differentiate to osteoblasts when cultured on top of stiff gels (2D) but differentiate to chondrocytes when cultured within the same stiff gel (3D) (Hogrebe & Gooch, 2016). Fibroblasts in 3D gels are more spindle shaped and migrate faster as compared to 2D gels (Hakkinen, Harunaga, Doyle, & Yamada, 2011). Glioblastoma multiform (GBM) stem-like cells encapsulated within 3D collagen based gels exhibited higher resistance to receptor tyrosine kinase inhibitors than when cultured on top of 2D collagen gels (Fernandez-Fuente, Mollinedo, Grande, Vazquez-Barquero, & Fernandez-Luna, 2014). These examples are few of many that demonstrate the influence of culture dimensionality on cellular functions.

1.1.2. 3D High Throughput Culturing Technologies

Mounting evidence has demonstrated that 3D *in vitro* culture systems can recapitulate critical aspects of the *in vivo* cellular microenvironment. Therefore, several *in vitro* 3D

culture technologies have been adapted for HT screening applications, including microfluidics, micromolding, scaffolds (hydrogels), and spheroids, and covered in depth by several recent reviews (Duval et al., 2017; Hoarau-Véchot et al., 2018; Ryan et al., 2016). Microfluidics approaches use micro- and nano-photolithographic fabrication to create biocompatible devices, which mimic various environmental structures found *in vivo*. Microfluidic devices typically are constructed from the polymer poly(dimethyl siloxane) (PDMS) due to its biocompatibility with cell culture, resistance to biological deterioration, and ability to create a variety of structures on a microscale (Whitesides, 2006). Microfluidics have been utilized to mimic organs (i.e. organ-on-chip) *in vitro* for many applications, such as lung-on-chip to test pharmaceutical compounds efficacy before moving forward to animal or clinical studies (Esch, Bahinski, & Huh, 2015; Huh et al., 2013, 2010). While, microfluidic technology allows routine establishment of complex structure and multicellular formation, it requires highly trained users, complex lithographic equipment and expensive clean rooms to produce initial microfluidic prototypes, all of which are constantly utilized if ongoing adjustments are required. This long process to fabricate prototypes makes utilization of microfluidic devices challenging in widespread applications.

Similar to microfluidics, micromolding also depend on PDMS molds to create microstructures that are molded on culturing surfaces such as poly(ethelyne glycol) dimethacrylate (PEGDMA) and hyaluronic acid (HA) hydrogels (Fukuda et al., 2006; Singh M et al., 2015). Micromolds have been used to produce morphologically

reproducible 3D multicellular spheroids from cervical and breast cancer cell lines (Singh M et al., 2015). This reproducibility is due to low well-to-well and plate-to-plate variations, which enables micromolding to be compliant to HT applications (Ryan et al., 2016). Similar to microfluidic devices, micromolding also require PDMS molds made with photolithography techniques, requiring highly trained personnel and expensive equipment. Further, micromolded structures may get damaged easily if careful pipetting techniques are not practiced. Both microfluidics and micromolding contributed in understanding basic structural microenvironmental effects on cellular behavior and functions, however, they share the same limitations in complexity and cost.

Scaffold technology is one of the most widely used 3D culturing techniques. Scaffolds provide a physical cellular anchorage platform, like the *in vivo* basement membrane, which supports cellular adhesion, proliferation and extracellular matrix (ECM) production. Scaffolds are composed of porous biomaterials that enable gas, nutrition and waste exchange between seeded cells and culturing media. One type of the most widely used scaffolds are hydrogels, which contain high levels of water and can be made from naturally derived biomaterials such as Matrigel (Barletta, Ramazzotti, Fratianni, Pessani, & Degl'Innocenti, 2015), collagen (Hakkinen et al., 2011; Hogrebe & Gooch, 2016; Sung et al., 2009), gelatin (Nichol et al., 2010), fibrin (Hakkinen et al., 2011), chitosan (Ji, Khademhosseini, & Dehghani, 2011) and alginate (Gryshkov et al., 2014); or synthetic biomaterials, mainly polymers, such as poly(ethylene glycol) (PEG) (Leight, Tokuda, Jones, Lin, & Anseth, 2015; Sridhar, Doyle, Randolph, & Anseth, 2014),

poly(acrylamide) (PAAm) (Trappmann et al., 2012), and poly(2-hydroxyethyl methacrylate) (pHEMA) (Mokrý, Karbanová, Lukáš, Palečková, & Dvořánková, 2000). Naturally derived biomaterials mimic the *in vivo* ECM in many ways. They are degradable, contain adhesion ligands and growth factors, making naturally derived biomaterials readily and easily adapted for cell culturing. Furthermore, naturally derived biomaterials recapitulate *in vivo* ECM fibrous structure, porosity and pore sizes, which elicit cellular morphology and response closer to *in vivo.* Naturally derived biomaterials are widely used in fabricating scaffolds and hydrogels, and their use has contributed tremendously in understanding microenvironmental effects on cellular responses and functions. However, some naturally-derived materials stimulate unwanted cellular responses because of confounding variables such as growth factors and ECM proteins contained within their structure (Hughes, Postovit, & Lajoie, 2010; Kleinman & Martin, 2005). These variables can make it difficult to isolate cellular responses to specific microenvironment factors. Naturally derived biomaterials also suffer from batch-to-batch variability, which increases the variability of cellular responses (Hughes et al., 2010). For example, Matrigel contains collagen, laminin, nidogen (entactin), and a variety of growth factors, which may stimulate a variety of receptors that trigger unwanted signaling cascades (Hughes et al., 2010). In addition, naturally derived hydrogels have highly interdependent functional moieties and microenvironmental characteristics. For example, in most naturally derived hydrogels, stiffness of the hydrogel is modified by changing the concentration of the material. However, changing the concentration not only affects hydrogel stiffness but also affects porosity, pore size and adhesion ligand density (Annabi

et al., 2010; Caliari & Burdick, 2016). Porosity, pore sizes, and adhesion ligand density are intractably interdependent, and all have effects on cellular functions, preventing researchers from effectively isolating the effect of stiffness. In addition, collagen gelation and the resulting hydrogel structure are temperature and pH sensitive, both of which can affect fiber thickness. It was demonstrated that collagen hydrogels fiber thickness affects the viability of human mammary fibroblasts, which means studying temperature or pH effects on cells cultured in collagen hydrogels is confound by fiber thickness (Sung et al., 2009). Additionally, polymerization of naturally derived biomaterials to create hydrogels is usually slow and temperature sensitive which restricts the adaptability and scalability of such biomaterials for HT application, which requires fast polymerization and less temperature sensitivity for automated liquid handling.

To address some of the limitations of naturally derived biomaterials, a number of synthetic biomaterials have also been used to generate 3D hydrogels. Use of synthetic biomaterials enables greater control over chemical and mechanical cues, which reduces unwanted co-variability and improves isolation of cellular responses to microenvironmental variables (Baker & Chen, 2012; Lutolf & Hubbell, 2005). For example, human mesenchymal stem cells (hMSCs) differentiation fate was studied utilizing PAAm hydrogels covalently coated with collagen. Differentiation of hMSCs was correlated to collagen stiffness, which is a function of anchorage density of collagen to PAAm hydrogels. Anchorage density of collagen is correlated to porosity of PAAm hydrogels. However, by controlling PAAm hydrogel porosity as a co-variable, and only

altering the anchorage density of bonded collagen, differentiation of hMSCs as a function of collagen stiffness was isolated and studied (Trappmann et al., 2012). The ability to fine tune the environmental cues (PAAm porosity and collagen anchorage density) enabled the isolation of differentiation function to a specific environmental factor (collagen stiffness). In another example, the mechanical properties of PEG hydrogels are often controlled by varying the crosslinking density. Increasing the stiffness of the PEG hydrogels increased the shear modulus and altered MMP activity of hMSCs encapsulated in PEG-norbornene (PEG-NB) hydrogels (Leight, Alge, Maier, & Anseth, 2013). The control of mechanical stiffness by altering just the crosslinking density, without altering ligands density, isolated MMP activity of hMSCs to stiffness as a microenvironmental variable. Such examples demonstrate the ability of synthetic biomaterials to aid preventing co-variables and isolating cellular responses to microenvironmental variables.

PEG is one of the most widely used synthetic biomaterial for hydrogels due to the ease of use and flexibility to adapt to a variety of applications. PEG hydrogels, which can be easily tailored to mimic the *in vivo* extracellular matrix, has been functionalized with a number of moieties to direct cell function. RGD, RLD, and IKVAV are adhesion ligands, in which aortic valvular interstitial cells elongated more in RGD than in RLD or IKVAV (Mabry, Schroeder, Payne, & Anseth, 2016). RGD, RDL or IKVAV were added to the pre-polymerized hydrogel mixture and can be changed easily to better recapitulate *in vivo* ECM. PEG hydrogels are hydrophilic and have similar water content to *in vivo* tissue. This hydrophilicity of PEG reduces protein adsorption onto PEG surfaces, which reduces

opsonisation, a process of adsorbing proteins (antigens) onto surfaces to promote an immune response such as phagocytosis. Hydrophilicity of PEG enabled the synthesis of therapeutic stealth nanocarriers, which are less amenable to phagocytosis, by coating those nanocarriers with PEG, see review (Salmaso & Caliceti, 2013). PEG hydrogel polymerization is often photo-initiated, enabling quick, user controlled hydrogel formation, making it more amenable to HT approaches than naturally derived ECM hydrogels (i.e. collagen or Matrigel) which are slower and temperature sensitive. Therefore, utilizing PEG hydrogels enables facile automation of cell encapsulation with robotic liquid handlers, as demonstrated by others (Mabry et al., 2016). This fine control of mechanical and chemical cues, and HT scalability of PEG hydrogels make PEG a practical biomaterial for utilization in HT drug screening applications with 3D culture.

1.1.3. Role of Cell-Cell Adhesion in 3D

Cells can be cultured in 3D environments as single cells or in multi-cell structures (i.e. spheroids). Multi-cell structures can be created in several ways, including the formation of multicellular aggregates prior to seeding or allowing the cells to grow within the scaffold to form multicellular structures over time. To culture cells in scaffolds as single cells or multi-cell structures, cells are seeded either pre- or post- fabrication of the scaffold. Many pre-fabricated scaffolds are made utilizing techniques such as 3D printing, lyophilization and stereo-lithography, see review (Duval et al., 2017). Such techniques may involve non-biocompatible procedures that are harsh on cells or hazardous to work with. Therefore, cell seeding is usually performed post-fabrication by

taking advantage of cellular diffusion into scaffolds, which may suffer from poor penetration of cells and non-uniform spatial cell seeding (Duval et al., 2017). Alternatively, cells may be seeded uniformly in hydrogels pre-fabrication by mixing cells with hydrogel precursor solution then polymerizing it. Hydrogels offer the option to seed cells in a single-cell or multi-cell structures. The ability to encapsulate cells in multiple spatial organizations, recapitulates different conditions encountered *in vivo*. Culture of single cells can also be appropriate to model events *in vivo,* in such as EMT and when tumor cells invade neighboring tissue and migrate to create secondary tumors in other sites, see reviews (Friedl & Wolf, 2003; Thiery, Acloque, Huang, & Nieto, 2009). *In vitro* 3D single-cell culturing models have been utilized to study EMT and tumor cell migration. For example, single-cell encapsulation into methacrylated hyaluronic acid / gelatin hydrogels were utilized to study EMT in breast cancer cell lines in response to oxygen concentration (Wang et al., 2018). Single-cell encapsulation utilizing PEG hydrogels was used in an *in vitro* 3D culture model to study melanoma cell migration in response to chemotherapeutics (vemurafenib and sorafenib) (Leight et al., 2015). Both examples illustrated the capacity of hydrogels to provide an *in vitro* model, representing biological phenomena encountered *in vivo*, in which cells are single.

Hydrogels also enable culturing cells in a multi-cell structure (i.e. spheroids). Multi-cell structure can be found *in vivo* in most biological configurations in the body such as in tissues and organs, and in many neoplastic (cancer) and non-neoplastic diseases. *In vitro*, many assays have been developed and utilized multi-cell 3D culture models to mimic

cancerous tumors and recapitulate *in vivo* cellular responses and functions. Spheroid assays are well-established methodologies and have been designated as the gold standard for *in vitro* 3D culture to recapitulate *in vivo* tumor responses. For example, researchers have been able to recapitulate *in vivo* treatment resistance observed in several cancers, including breast, pancreatic and colon cancer using paclitaxel, gemcitabine, 5-fluorouracil and SN-38 (Anand, Fu, Teoh, & Luo, 2015; Wen et al., 2013; Kinoshita et al., 2018). Spheroids may be formed via several techniques such as hanging droplets, non-adherent surfaces, and scaffold based models, such as hydrogels (more techniques are found here (Hoarau-Véchot et al., 2018)). In a 2018 study, multi-cell tumor spheroids formed in hydrogels for 14 days were used to study EMT in breast cancer cell lines in response to oxygen concentration (Wang et al., 2018). This technique was repeated in PEG hydrogels to facilitate the formation of glioblastoma spheroids for a small molecule drug screen. The spheroids demonstrated viability in hydrogels for 14 days, proving the feasibility of utilizing PEG hydrogels as a spheroid culture platform (Imaninezhad, Hill, Kolar, Vogt, & Zustiak, 2019). Many similar studies have demonstrated the adaptability of synthetic hydrogels in controlling the chemical and mechanical features of the microenvironment while maintaining HT scalability. These features render hydrogels an excellent tool in pursuing questions related to 3D culture models and detecting cellular functions other than viability in HT applications.

1.2. *Ex Vivo* Tissue Culture Models

1.2.1. Patient Derived Xenografts (PDX) and Organotypic Slices

To more closely recapitulate cellular response *in vivo,* several *ex vivo* models have been developed and utilized, including patient derived xenografts (PDX) and organotypic slices (Meijer, Naipal, Jager, & van Gent, 2017). PDX models and organotypic slices are mainly used to maintain a closer mimic to clinical responses of many diseases, especially cancer (Hidalgo et al., 2011; Naipal et al., 2016). PDX models are tumor cells or tissue that are taken from patients then implanted and expanded in immunodeficient mice. These mice are subsequently used for treatment screening (Lai et al., 2017). Organotypic slices are tissue slices that have been precisely cut from tumor samples at microscale thickness and cultured on a porous Teflon surface that allows oxygen and nutrient exchange (Meijer et al., 2017). As opposed to 2D and 3D cultures, in which tumor samples are digested, creating homogenous cell populations lacking native microenvironment, PDX and organotypic slices models maintain the molecular characteristics, cellular heterogeneity, tumor pathology, and structural features of the microenvironment (Lai et al., 2017; Meijer et al., 2017). The preservation of these features creates a closer representation of the *in vivo* microenvironment and can be used to more reliably predict clinical responses to specific therapies.

1.2.2. Advantages and Disadvantages of Current *Ex Vivo* Models

PDX models are considered the gold standard for modeling clinical tumor drug response because they maintain the original tumor characteristics and therefore can be used as

tools to facilitate drug screening and development (Lai et al., 2017). PDX models have successfully been used to recapitulate clinical responses in patients with several forms of cancer, including pancreatic, colorectal, and gastric cancers. In these models, tumor mutations, biomarkers, and drug responses were maintained through several passages, demonstrating the stability of such model (Seol et al., 2014; Tignanelli, Herrera Loeza, & Yeh, 2014; T. Zhang et al., 2015; Zhu et al., 2015). One drawback of PDX models is the fact that they have been observed to undergo mouse-specific tumor evolution during passaging, in which the resulting tumor is genetically different than the parental tumor (Ben-David et al., 2017). Additionally, PDX models are expensive, labor intensive, and have long turnaround time to produce results, while the success rate of tumor engraftment is as low as 25% for some cancers (Naipal et al., 2016). As a result, PDX models have not been suitable for HT drug screening and development applications.

Tumor organotypic slices share advantages with PDX models. Organotypic models maintain the native tumor microenvironment, provide heterogeneous cell populations, and reflect *in vivo* tumor pathology, thus creating a closer mimic to *in vivo* conditions and more accurately predicting clinical outcomes (Meijer et al., 2017; Naipal et al., 2016). Several tumors were successfully cultured utilizing organotypic tumor slices for drug treatment studies. Head and neck squamous cell carcinoma organotypic slices that were cultured for 6 days, preserved their histopathological features and formed apoptotic fragments and increased caspase-3 activation when treated with cisplatin, docetaxel, and cetuximab (Gerlach et al., 2014). This *ex vivo* cellular response demonstrates the ability

of organotypic slices to predict cellular responses to cytotoxic drugs similar to *in vivo*. Glioblastoma multiforme derived from patients' samples, sectioned and cultured in minutes, preserving parent tumor histopathology for 16 days *in vitro*. Further, caspase 3 activation, inducing cell death, and DNA double strands breakage in response to temozolomide and irradiation were measured respectively (Merz et al., 2013). Such an example demonstrates that organotypic slices could be quickly cultured, maintaining original tumor characteristics and predict responses to environmental factors similar to *in vivo*. Organotypic slice cultures provide powerful *ex vivo* tools for drug testing with faster outcomes than PDX models (Naipal et al., 2016). However, these models are delicate, labor intensive, provide limited amount of samples, and require specialized analytical tools for data acquisition and quantification (Naipal et al., 2016). Such limitations hinder organotypic slices from being used in HT applications. Therefore, there is a need to bridge the gap between efficient HT 2D cultures, and close *in vivo* recapitulation of PDX and organotypic slices to better predict clinical responses. Table 1 summarizes, the advantages and disadvantages of each culture methodology (Meijer et al., 2017).

	2D monolayer		3D spheroid			
	Primary cultures	Cell lines	3D cell line cultures	3D organoids	PDX	Organotypic tissue slice
Ease of maintenance	+/-	+	-	-	-	+/-
Preservation of tumor morphology	-	-	-	-	+/-	+
Extended *ex vivo* cell viability	+/-	+	+	+	+	-
Nonselective cell/tumor outgrowth	+/-	-	-	-	-	+
Preservation of microenviornment/ heterogeneity	-	-	-	-	+/-	+
High-throughput drug screens	+/-	+	+/-	+/-	-	-
Success rate of model system generation	+/-	-	+/-	+/-	-	+
Short generation time	+	-	-	-	-	+
Similarity to original tumor	-	-	+/-	+/-	+/-	+
Costs	+	+	+/-	+/-	-	+

Table 1: A summary of the advantages (+) and disadvantages (-) of different culturing techniques, (Meijer et al., 2017).

1.2.3. Bridging the Gap

One potential solution to bridge the gap between *in vitro* HT 2D cultures and *ex vivo* PDX and organotypic slice models, is the *ex* vivo culture of human tissue samples in HT 3D culture models. E*x vivo* culture of tissue samples in 3D may maintains tumor heterogeneity, preserves microenvironmental structure, tumor genotype, phenotype and pathology. The significance of *ex vivo* 3D culture was realized by others who cultured undigested fine needle aspirate biopsies of feline liver tissue in Matrigel to form hepatic

organoids. Interestingly, tissue samples retained their morphology between passages in a hepatic steatosis (fatty liver) *ex vivo* model for 5 days, demonstrating the ability to maintain tissue viability in *ex vivo* culture conditions (Kruitwagen et al., 2017). Several studies have cultured *ex vivo* patient-derived organoids in 3D environments, such as hydrogels, demonstrating the suitability of such technique for HT drug screening applications. For instance, patient-derived colon cancer organoids were formed *ex vivo* in Matrigel by an automated workflow, and 384-well plate robustness and reproducibility were confirmed for HT drug screening (Boehnke et al., 2016). Moreover, two uterine malignancies and two colon cancer tissue samples were derived from patients, cultured in *ex vivo* 3D Matrigel and a HT dose-response drug screen including 160 drugs was conducted and validated with 3D culture and PDX model (Pauli et al., 2017). Nevertheless, most developed assays utilizing HT, *ex vivo,* 3D culturing methods isolate single cells by digestion before culturing. As a result, these methods lack the benefit of having heterogeneous cell populations, intact tissue structures, or a native microenvironment. Thus, there is a need for a system that cultures intact *ex vivo* tissue samples in HT 3D system for therapeutics screening and development. HT 3D culture provides tissue support that better recapitulates the *in vivo* microenvironment and satisfies HT requirements for drug screening.

1.3. High Throughput Assays

Drug development and screening utilizing HT 2D culture platforms are well-established and have contributed to the discovery of many therapeutics to treat neoplastic and non-

neoplastic diseases. 2D culture platforms adequately satisfy the requirements of HT drug development and screening assays. HT drug development and screening assays are required to be time efficient, cost effective, miniaturized, and be able to cope with multiple liquid handling steps. Further, HT assays should produce quantitative outcomes that are robust, reproducible and can be acquired automatically (Ryan et al., 2016). In HT drug development and screening assays, thousands of compounds are tested, so assay efficiency and cost effectiveness are critical determinants in study feasibility. Therefore, assays are miniaturized, processes are simplified and automated, and turnaround times are reduced to allow for greater resource efficiency. For the same reason of efficiency and cost effectiveness, automated liquid handlers and data readers are utilized (Dias, Go, Hart, & Mattheakis, 1998; Maffia, Kariv, & Oldenburg, 1999). Automation of the assay process and data acquisition creates a standard that contributes to data reproducibility, robustness and precision, which are requirements for HT assay outcomes. Indeed, 2D platforms satisfy these conditions, yet most drugs developed in 2D platforms *in vitro* do not adequately predict *in vivo* outcomes in animal models and clinical trials (Johnson et al., 2001), in which high toxicity (unwanted side effects or off-target activities) or limited efficacy were observed (Hopkins, 2008; Kola, 2008). This is mainly due to the lack of environmental cues in a 2D platform, mentioned earlier, as compared to those encountered *in vivo*, which have significant effects on cellular responses and functions.

To better recapitulate *in vivo* cellular responses and functions, there is interest in adapting 3D culture systems for HT approaches for drug screening and development applications.

For example, it was demonstrated the capability of 3D spheroid assay to be developed and utilized for drug testing, using an acid phosphatase assay to measure viability of pancreatic cancer spheroids in response to gemcitabine and 5-fluorouracil (Wen et al., 2013). Similarly, another 3D spheroid assay was developed for potential HT drug screening purposes but with breast cancer magnetic spheroids cultured in 96-well plate. However, the assay was measuring viability in response to doxorubicin utilizing similar acid phosphatase assay (Guo, Loh, Tan, Loo, & Ho, 2014). Indeed, 3D spheroids assays are suitable for drug screening applications, yet it is noticeable that these assays, similar to most 3D HT platforms, assess a limited number of cell functions, namely cell viability. This is because optimizing 3D systems for HT has been hampered by increased cost, complexity, time and effort, and the incompatibility of many standard biological assays with both 3D culturing and HT approaches (Ryan et al., 2016). It is well known that many other cell functions also contribute to disease progression and pose as potential therapeutic targets. Recent studies are utilizing HT 3D culturing platforms to measure cellular functions in addition to viability, to detect cellular response to drug screening. For example, a micromolding technique was used to successfully form 3D spheroids of cervical, breast, head and neck cancers. The viability and epidermal growth factor receptor signaling of the spheroids in response to epidermal growth factor and cetuximab treatments were measured (Singh M et al., 2015). This example emphasizes the ability of 3D tumor spheroids to be adapted to HT drug testing, and the importance of detecting other cellular functions that have a potential as a pharmacological target.

1.4. Matrix Metalloproteinases (MMP)

1.4.1. MMP Structure

Matrix Metalloproteinases (MMPs) are a family of zinc-based endoproteases that share several conserved structural features. Twenty-four MMPs have been identified to-date, of which 23 of them are found in humans. Structurally, MMPs share a signal peptide, propeptide, catalytic and hemopexin domain. The signal peptide regulates secretion from cells, while the propeptide domain preserves the protein enzyme in its latent zymogen (de-activated) form. The catalytic domain contains the active zinc-binding motif that processes the substrate, while the hemopexin domain determines substrate specificity and mediates protein-protein interactions with endogenous inhibitors, (i.e. tissue inhibitor of metalloproteinase (TIMPs)) (Cathcart, Pulkoski-Gross, & Cao, 2015; Folgueras, Pendás, Sánchez, & López-Otín, 2004; Tauro, McGuire, & Lynch, 2014; Visse & Nagase, 2003). The zinc-binding motif in the catalytic domain and cysteine switch motif in the propeptide domain distinguishes MMPs from other proteases, such as aspartic, glutamic, and serine proteases (Visse & Nagase, 2003). Figure 1 summarizes the sub-classification of different types of MMP's based on their structure and unique domains (Folgueras et al., 2004), and Table 4 in Appendix A summarizes structure, substrate specificity, unique domains, substrate interactions and functions of different subclasses of MMPs (Folgueras et al., 2004; Llano et al., 1999; Marchenko et al., 2001; Nagase, Visse, & Murphy, 2006; Nakamura, Fujii, Ohuchi, Yamamoto, & Okada, 1998; Sohail et al., 2008; Stolow et al., 1996; Uría & López-Otín, 2000; Visse & Nagase, 2003).

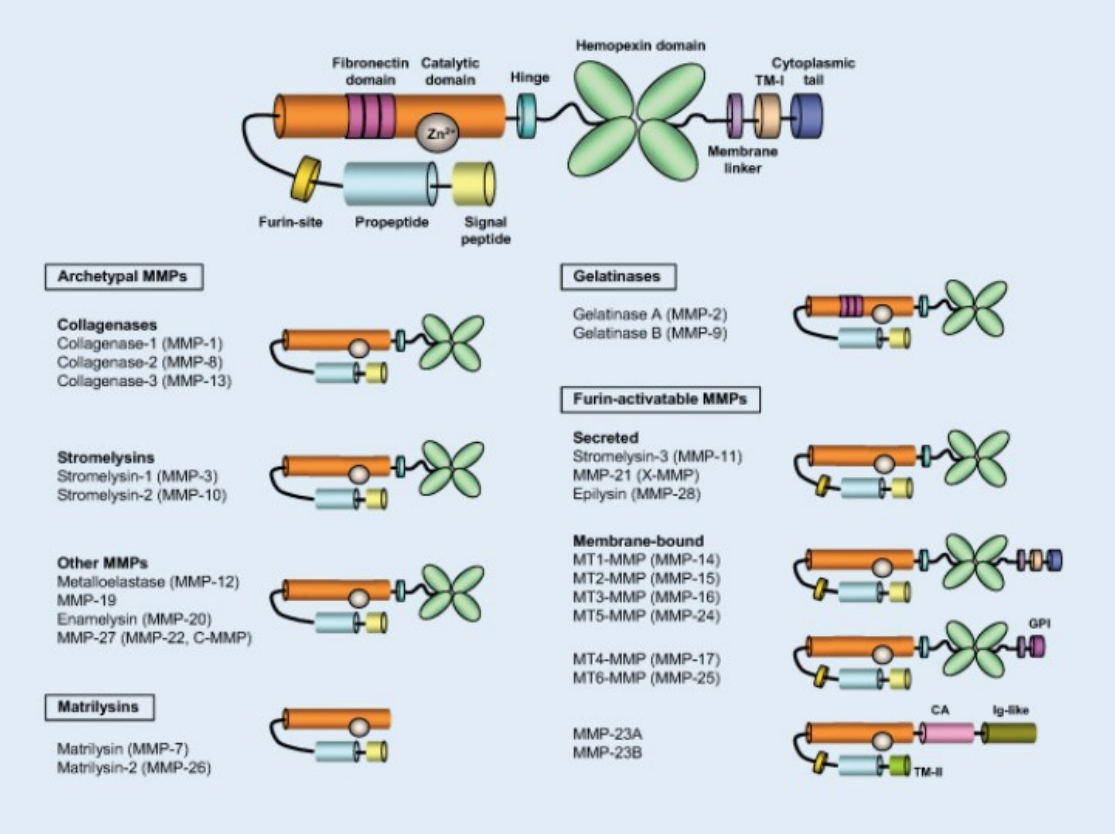

Figure 1: Sub-classification of different types of MMP's based on their structure and unique domains, from Folgueras et al., 2004.

1.4.2. MMP Functions and Biological Roles

Detection of MMPs is important because they play key roles in human physiology and pathophysiology. MMPs cleave ECM proteins as well as other bioactive molecules, including surface receptors and cytokines (Nagase et al., 2006; Tokito, Jougasaki, Tokito, & Jougasaki, 2016). Physiologically, MMPs play key roles and functions in morphogenesis and wound healing (Nagase et al., 2006; Visse & Nagase, 2003). For example, MMP-14 (MT-MMP1) is involved in the tubule formation of Madin-Darby canine kidney epithelial cells in response to hepatic growth factor (Kadono et al., 1998).

Numerous other MMPs, including MMP-1, -2, -3, -8, -9, -10, -13, and -14, regulated the degradation and deposition of ECM during wound healing and re-epithelialization (Caley, Martins, & O'Toole, 2015). Measurement of MMPs can contribute to our understanding of many physiological functions but also identify potential, treatment targets for diseases in which they are involved. MMPs have key roles in diseases such as chronic tissue ulcers and arthritis (Nagase et al., 2006; Visse & Nagase, 2003). For example, Muller and colleagues demonstrated that higher levels of MMP-1 are beneficial in healing diabetic foot ulcers, while high levels of MMP-8 and -9 are likely to exacerbate the problem (Muller et al., 2008). MMP-2 and -9 activity were observed to stimulate invasion and migration of rheumatoid arthritis synovial fibroblasts, of which MMP-9 was associated with cartilage degradation and joint destruction in rheumatoid arthritis (Xue et al., 2014). MMPs are also critical regulators of several "hallmarks of cancer", including migration, invasion, and angiogenesis (Vihinen & Kähäri, 2002). For example, when fibrosarcoma cells (HT1080) were treated with curcumin derivatives and metabolites, significant reduction in MMP-2, -9 and -14 in a dose dependent manner was observed. Consequently, cell invasion and migration, critical functions for tumor progression, were reduced in a dose dependent manner (Yodkeeree, Chaiwangyen, Garbisa, & Limtrakul, 2009; Yodkeeree, Garbisa, & Limtrakul, 2008). Angiogenesis and tumor progression of melanoma tumors in MMP-2 deficient mice were significantly lower than mice with normal MMP-2 levels (Itoh et al., 1998). Cellular invasion, migration and angiogenesis are critical functions of tumor progression mediated by MMP activity and emphasize the importance of detecting MMP activity as a treatment target.

Elevated expression of many MMPs is associated with metastasis and poor prognosis (Vihinen & Kähäri, 2002). It was demonstrated that samples of pancreatic carcinoma in patients with lymph node metastases had higher MMP-2 activity than those without metastasis (Koshiba et al., 1998). High levels of MMP-8 and TIMP-1 were associated with worse prognosis in colorectal cancer patients in comparison to patients with lower MMP-8 levels (Böckelman et al., 2018). These examples illustrate the important roles MMPs play in several pathophysiological processes and their significance as pharmacological targets.

Despite overwhelming evidence supporting the critical role of MMPs in cancer progress, direct pharmacological inhibition of MMP enzymatic activity has yet to yield clinical success. This failure has been attributed to several factors including non-specific inhibition due to high sequence overlap between MMPs and off-target adverse effects due to the pleiotropic role of MMPs in physiological processes. To overcome these limitations, an alternative strategy to inhibit MMP activity would be to target the upstream cellular signaling pathways regulating MMP activity. Small molecules developed to target upstream signaling pathways and other cell functions, such as cell viability, are not routinely screened for their effect on MMP activity due to the lack of compatible assays. However, a previous study has shown that several RAF/MEK kinase inhibitors increased MMP activity and cell migration (Leight et al., 2015). Therefore, there is a need for new technologies to perform HT measurement of MMP activity for drug development and screening purposes.

1.4.3. MMP Regulation and Measurement

MMPs must undergo multiple regulatory processes to produce a functional, active enzyme. MMPs are regulated at several stages: gene expression, translation, protein secretion, compartmentalization, zymogen activation, and inhibition by endogenous inhibitors (i.e. TIMPs) (Löffek, Schilling, & Franzke, 2011). MMPs have been detected and measured at different regulatory stages. Reverse transcription – polymerase chain reaction (RT-PCR) and western blotting measure MMPs at the gene and protein expression levels, respectively. Enzyme-linked immunosorbent assay (ELISA) detects MMPs at the protein secretion level. Although western blotting, RT-PCR, and ELISA are well-established methodologies and are highly specific to MMPs, detection at the gene or protein expression level requires intensive sample processing and a long turnaround time. More importantly, MMP expression does not necessarily correlate with functional enzymatic activity. To take into account the complex regulation of MMPs, it is necessary to detect MMPs at the activity level. The significance of detecting MMPs at the activity level was indirectly demonstrated by Muller et al., when they determined that the ratio between MMP-1 and its inhibitor TIMP-1 could be a predictive factor of diabetic foot ulcer wound healing. Although ELISA was used to find the protein concentrations of MMP-1 and TIMP-1, the ratio between the two, which reflected the net activity of MMP-1, was the significant variable in determining wound healing progression (Muller et al., 2008).

Gelatin zymography and fluorescent MMP-degradable peptides have been utilized to detect MMPs at the activity level. Gelatin zymography is a widely implemented method to measure the MMP activity of gelatinases (MMP-2 and -9). However, gelatin zymography requires intensive sample processing and is limited to gelatinase detection. This technique has been recently expanded upon by incorporating fluorescent, MMP-degradable peptides into zymography gels in place of traditional, native proteins (e.g. gelatin, collagen, casein) (Deshmukh, Weist, & Leight, 2018). MMP-degradable fluorescent peptides offer an alternative for detecting MMP activity more rapidly and with less sample processing, in spite of the intensive characterization and initial optimization needed before utilization. Fluorescent, MMP-degradable peptides enable the detection of a variety of MMPs by altering the degradable motif, which determines the specificity of MMP detection (Mucha et al., 1998; Nagase & Fields, 1996; Patterson & Hubbell, 2010). These peptides can also be used for *in situ* MMP activity detection by incorporating fluorescent MMP-degradable peptides in 3D culturing environments (Leight et al., 2013, 2015). The advantages of fluorescent MMP-degradable peptide enables their utilization in widespread applications, justifying using this technology for our further MMP activity related studies.

1.5. Summary

Currently, most assays for cancer chemotherapeutic development utilize 2D culturing systems. These 2D systems lack many aspects of the *in vivo* microenvironment significant to cellular drug response. Therefore, attempts have been made to develop 3D

culture microenvironments and tumor spheroids to recapitulate some of the *in vivo* cellular response to treatment. While these models can recapitulate certain aspects of cellular responses measured *in vivo*, 3D environments often make analysis of cellular responses more difficult. As a result, most HT 3D assays have been limited to measurements of cell viability despite the fact that many other cell functions contribute to disease progression and can pose as important pharmacological targets. Most HT 3D assays utilize isolated cell lines for drug testing. However, isolated cell lines lack the tumor heterogeneity and native microenvironment encountered *in vivo,* making them poor predictors of clinical response. To maintain tumor heterogeneity, many researchers use PDX or organotypic slices models. Such techniques offer the advantage of maintaining cellular phenotype, genotype, and molecular characteristics. Further, eliminating cellular selection and reflecting the tumor pathology, thus accurately predicting clinical responses. Nevertheless, PDX and organotypic slice models are associated with high cost, low efficiency, and prolonged experimental time to results. These disadvantages deem PDX and organotypic slices unsuitable for HT drug screening applications. There is a need for a system that enables measurement of a wider range of cellular functions, such as proteolytic activity, in a HT manner, while maintaining key biological and structural features of the tumor and its microenvironment.

1.6. Dissertation Overview

To address the need mentioned above, we developed, characterized, validated, and demonstrated the utility of a HT assay for cellular encapsulation in 3D microenvironment

to measure cellular functions such as MMP activity. We further developed an *ex vivo* 3D culture system, in which we can detect MMP and metabolic activity.

In chapter 2, we have adapted a hydrogel system that enables cells to be cultured in a 3D PEG hydrogels functionalized with an MMP-degradable fluorogenic sensor to measure MMP and metabolic activities simultaneously (Leight et al., 2013). By utilizing PEG, we could precisely tune the chemical and mechanical attributes of the hydrogel, from which the system can be optimized to more closely recapitulate the *in vivo* microenvironment of interest. Additionally, PEG hydrogel polymerization may be photo-initiated, enabling quick, user-controlled hydrogel formation, making it more amenable to HT approaches than traditional ECM hydrogels (i.e. collagen or reconstituted basement membrane) which are slower and temperature sensitive. This system was miniaturized and scaled up to facilitate HT drug screening applications. The 96-well format developed here, eliminated several steps from the previous 24 well protocol, reducing the time needed per well by approximately 50%. Further, the total hydrogel volume needed per well was reduced by 80% (50µL to 10µL) as compared to the previous 24-well format. This miniaturization also increased the number of possible conditions and replicates tested per plate from 12 duplicates utilizing the 24-well plate to 20 triplicates utilizing the 96-well plate. The reproducibility, robustness, performance and suitability for HT applications of the assay were characterized using a bacterial collagenase type I enzyme and a fibrosarcoma cell line (HT1080). The developed assay achieved a Z'-factor values above 0.9 and 0.5 for enzymatic and cellular assays respectively, intra-plate coefficients of

variation (%CV) below 10% and 12% respectively. And signal measurement was unaffected by dimethyl sulfoxide (DMSO), a common solvent of therapeutic compounds. The calculated edge effect, drift, Z'-factor, %CV, inter-plate, and inter-day fold shifts of the signals were within the acceptable range for HT applications, indicating this HT 3D MMP activity assay as reproducible and robust, designating it suitable for screening applications. Next, the assay was validated with commercially available human MMPs and encapsulation of several different cell types, utilizing different MMP-degradable sensors. Human MMP-1, -2 and -9 resulted in a significant increase in signal intensity. Encapsulation of several cell types in different MMP-degradable sensors produced robust signals above background noise and within the linear range of the assay. Finally, to demonstrate the ability of the system to measure the effect of small molecule drugs on cellular MMP activity and for future HT applications, a fibrosarcoma cell line (HT1080) was treated with several drugs, known to alter MMP activity, over a range of concentrations. Interestingly, sorafenib (SOR), a small molecule multi-kinase inhibitor utilized in clinical trials to treat fibrosarcoma, increases MMP activity in a dose-dependent manner in fibrosarcoma cell line. It would be interesting to conduct further investigation to determine if the increased MMP activity with SOR treatment observed here also regulates fibrosarcoma cell invasion and migration, cell functions critical to tumor progression and metastasis.

In chapter 3, *ex vivo* adipose fine needle aspirate biopsies (FNAB) and tissue dissections from patients who underwent breast lumpectomy or mastectomy surgeries were directly

encapsulated into our HT 3D MMP activity hydrogels, achieving similar advantages to PDX and organotypic slices models and the HT scalability of the 3D culture assay. In this chapter, optimization of FNAB and tissue dissection encapsulation is discussed. Viability of FNAB and tissue dissections were validated utilizing commercial live/dead staining showing maintenance of cellular viability after 24 hours of incubation in our 3D HT assay. Moreover, MMP and metabolic activities were detected in a volume-dependent manner for FNAB and diameter-dependent manner for tissue dissections.

Chapter 4 concludes this dissertation by summarizing important observations and implications of our work. Summary and conclusions in this chapter discuss the rationale behind this work, the needs it fulfills, and future applications of the assay. This dissertation succeeds in bridging several gaps in the body of knowledge. First, we show the ability to measure important cellular functions, other than viability, in a HT 3D cultures. Second, we successfully culture *ex vivo* tissue samples in a HT manner, overcoming limitations imposed upon PDX models and organotypic slices. The developed assay measures MMP activity alongside metabolic activity in a 3D HT assay, suitable for drug screening and development applications. Due to the key roles played by MMPs in physiological and pathophysiological processes, MMPs were pharmacological targets for direct clinical MMP inhibitors. Many of these drugs ultimately failed, largely due to non-specific inhibition and undesirable side-effects due to the pleiotropic role of MMPs in normal tissue function. Another approach would be to target the upstream cellular signaling pathways regulating MMP activity. However, small molecules

targeting other cell functions, such as cell viability, are not routinely screened for their effect on MMP activity due to the lack of compatible assays. Therefore, the assay described in this dissertation provides a solution to measure MMP activity in a HT manner for drug screening and development purposes. To illustrate the potential impact of this technique we would like to highlight one particular result in which we measured increases in MMP activity in fibrosarcoma cells treated with sorafenib in a dose dependent manner. This finding encourages us to perform further studies of fibrosarcoma migration and invasion which are cellular functions critical for tumor progression and metastasis. Finally, we would like to point out that the assay described here utilizes a modular design which can be used to survey a variety of proteolytic enzymes, thus displaying high adaptability and robustness. The HT 3D assay requires minimal personnel training, sample processing and turnaround time, and utilizes commercially available reagents and tools making it easily accessible to other users.

The other gap this dissertation aim to bridge, is the ability to culture intact tissue samples derived from patients, *ex vivo* in a 3D biomaterial that is efficient and amenable for HT applications. PDX and organotypic models provide close clinical prediction of cellular response, by closely mimicking features encountered *in vivo*. Yet, they are not suitable for HT applications, due to their high cost, labor intensity, and long turnaround time. Therefore, adipose FNAB and tissue dissections were encapsulated *ex vivo*, preserving the native microenvironment and heterogeneity of the samples. Furthermore, we demonstrate the viability of these tissues after 24 hours of culture, and the ability to

measure MMP and metabolic activity simultaneously. The results of chapter 3 provide compelling evidence for the feasibility of characterizing the histological fidelity of *ex vivo* tissue samples cultured in 3D hydrogels. MMP activity levels can be validated utilizing gelatin and in-situ zymography, well-established MMP activity assays, to confirm the preliminary results demonstrated in chapter 3. After characterization and validation, a pilot drug screen on breast cancer cell lines utilizing traditional 2D plastic and 3D spheroid cultures would be beneficial to measure chemotherapeutic effects on MMP activity in various cellular culture formats. While utilizing 3D spheroids will give us an insight of the multicellular structure effects on MMP activity in response to drugs, isolated cell lines are usually used. Isolated cells may have a different response than clinical outcomes due to their homogeneity. Thus, using patient-derived FNAB samples overcome cellular homogeneity, utilized to determine drugs effects on MMP activity in a closer mimic to a clinical response. The developed system could be utilized for many applications. Individualized treatment could be achieved by patient profiling and drug screening at point of care by culturing patient samples *ex vivo* in the HT 3D assay. Furthermore, targeted therapies could be developed based on the understanding of drug treatment effects on cellular and tissue functions, including MMP activity. Developing this HT 3D *ex vivo* culture system provides a powerful tool that enables robust and efficient study of patient tissue response to a variety of variables and applications such as treatment evaluation and precision medicine.

Chapter 2. High Throughput Three-Dimensional Hydrogel Assay for Measuring Matrix Metalloproteinases Activity: Assay Development, Characterization, Validation, and Utility Demonstration*

2.1 Abstract

Three dimensional (3D) cell culture systems more closely mimic the in vivo cellular microenvironment than traditional two dimensional (2D) cell culture methods, making them a valuable tool in drug screening assays. However, 3D environments often make analysis of cellular responses more difficult, so most high throughput 3D assays have been limited to measurements of cell viability. Yet many other cell functions contribute to disease and are important pharmacological targets. Therefore, there is a need for new technologies that enable high throughput (HT) measurements of a wider range of cell functions for drug screening. Here, we have adapted a hydrogel system that enables cells to be cultured in a 3D environment and allows for the simultaneous detection of matrix metalloproteinase (MMP) and metabolic activities. This system was then characterized for utility in HT screening approaches. MMPs are critical regulators of tissue homeostasis and are upregulated in many diseases, such as arthritis and cancer. The developed assay

* This chapter was a merge of two publications with some modifications under the following references: (1) Fakhouri, A. S., Weist, J. L., Tomusko, A. R., & Leight, J. L. (2019). High-Throughput Three-Dimensional Hydrogel Cell Encapsulation Assay for Measuring Matrix Metalloproteinase Activity. *ASSAY and Drug Development Technologies*, 17(3), 100–115. https://doi.org/10.1089/adt.2018.877. (2) Fakhouri, A. S., & Leight, J. L. (2019). Measuring Global Cellular Matrix Metalloproteinase and Metabolic Activity in 3D Hydrogels. *JoVE (Journal of Visualized Experiments)*, (143), e59123. https://doi.org/10.3791/59123.
Contributions were as following: Fakhouri, A. – Experimental design, conduction and data analysis. (effect of plate geometry, detection limits, stiffness and DMSO tolerances, MMP inhibitor dose response, enzymatic and cellular plate uniformity, purified human MMP activity, seeding density effect, cellular time course, drug screen) Publications, manuscripts, and dissertation preparation and writing. Leight, J. – Experimental design and data analysis. Publications, manuscripts, writing, and dissertation editing. Tomusko, A. – Experimental design, conduction and data analysis (effect of plate geometry, detection limits, stiffness and DMSO tolerances, and cellular time course). Weist, J.- Publication manuscript writing and editing. Experiments conduction (cellular plate uniformity and cellular time course).

achieved a Z'-factor values above 0.9 and 0.5 for enzymatic and cellular assays, respectively, intra-plate coefficients of variation (%CV) below 10% and 12%, respectively, and signal measurement was unaffected by dimethyl sulfoxide (DMSO), a common solvent of therapeutic compounds. Human MMP-1, -2 and -9 resulted in a significant increase in signal intensity. Encapsulation of several cell types, utilizing two different MMP-degradable peptides, produced robust signals above background noise and within the linear range of the assay. Multiple drugs that are known to alter MMP activity were utilized in a range of concentrations with a fibrosarcoma cell line to demonstrate the feasibility of the assay for HT applications. This assay combines 3D cellular encapsulation and MMP activity detection in a HT format, which makes it suitable for drug screening and development applications. Please see (Fakhouri & Leight, 2019; Fakhouri, Weist, Tomusko, & Leight, 2019).

2.2 Introduction

Over the past several decades, mounting evidence has demonstrated that three dimensional (3D) in vitro culture systems more closely mimic the in vivo cellular microenvironment than culture on traditional two dimensional (2D) tissue culture plastic. 3D culture provides environmental cues similar to the in vivo environment that are absent in 2D cultures, such as soluble gradients and 3D cell-cell and cell-matrix adhesion cues (Baker & Chen, 2012; Duval et al., 2017; Hoarau-Véchot et al., 2018). Such differences between 3D and 2D cultures have significant effects on cell behavior and function. For example, human mesenchymal stem cells differentiate to osteoblasts when cultured on

top of stiff gels (2D) but differentiate to chondrocytes when cultured within the same stiff gel (3D) (Hogrebe & Gooch, 2016). 3D culture can also restore the differentiation state of chondrocytes after 2D culture (Benya & Shaffer, 1982). Fibroblasts in 3D matrices are more spindle shaped and migrate faster as compared to 2D matrices (Hakkinen et al., 2011). Using 3D cell spheroid models, researchers have been able to recapitulate in vivo treatment resistance observed in several cancers, including breast, colon and pancreatic cancer, in an experimentally accessible in vitro setting (Anand et al., 2015; Kinoshita et al., 2018; Wen et al., 2013).

Because of the advantages of 3D culture systems, there is great interest in adapting these systems for HT approaches. However, optimizing 3D systems for HT has been hampered by the increased cost, complexity, time and effort, and the incompatibility of many standard biological assays with both 3D culturing and HT approaches (Ryan et al., 2016). Thus, current 3D HT platforms assess a limited number of cell functions, namely cell viability and migration (see review (Ryan et al., 2016)). However, many other cell functions also contribute to disease progression and are possible targets for therapy. Therefore, new techniques are needed that enable easy measurement of cell function within 3D environments. One way to address this need is the development of materials that not only support 3D cell culture but also incorporate sensors to measure cell function. For example, several hydrogel systems have incorporated fluorogenic protease cleavable moieties to enable visualization of protease activity within 3D environments (Chalasani et al., 2017; DeForest, Polizzotti, & Anseth, 2009; Jedeszko, Sameni, Olive,

Moin, & Sloane, 2008; Lee, Miller, Moon, & West, 2005). While these systems were originally utilized for microscopic imaging, these systems can also be adapted for use in a global matrix metalloproteinase (MMP) activity assay using a standard plate reader, enabling facile measurement of a cell function in a 3D environment (Leight et al., 2013).

In humans, MMPs are a family of 23 proteolytic enzymes that cleave extracellular matrix proteins as well as other bioactive molecules, including surface receptors and cytokines (Nagase et al., 2006; Tokito et al., 2016). MMPs play key roles in morphogenesis and wound healing, and in diseases such as chronic tissue ulcers and arthritis (Nagase et al., 2006; Visse & Nagase, 2003). MMPs are also critical regulators of several "hallmarks of cancer", including migration, invasion, and angiogenesis, processes which are inherently 3D phenomena (Vihinen & Kähäri, 2002). Elevated expression of many MMPs is associated with metastasis and poor prognosis (Vihinen & Kähäri, 2002). MMP activity is regulated at multiple levels, including expression, secretion, proenzyme cleavage, and the action of endogenous inhibitors (i.e. tissue inhibitors of metalloproteinases (TIMPs)). Therefore, activity based measurements, such as cleavage of fluorescent reporters or zymography, are critical, as mRNA and protein expression assays are not sufficient to capture and integrate these multiple layers of regulation.

Despite the overwhelming evidence supporting the critical role of MMPs in cancer progress, direct pharmacological inhibition of MMP enzymatic activity has yet to yield clinical success. This failure has been attributed to several factors including the broad

spectrum nature of the inhibitors and off target effects due to the pleiotropic role of MMPs in normal tissue function. To overcome these limitations, an alternative strategy to reduce MMP activity would be to target the upstream cellular signaling pathways regulating MMP activity. In addition, small molecules developed to target other cell functions, such as cell viability, are not routinely screened for their effect on MMP activity due to the lack of compatible assays. However, a previous study has shown that several RAF/MEK kinase inhibitors increased MMP activity and cell migration (Leight et al., 2015). Therefore, there is a need for new technologies to perform HT measurement of MMP activity. To address this need, a previously developed 3D hydrogel system functionalized with an MMP-degradable sensor to enable facile measurement of MMP activity was miniaturized and optimized for HT applications (Leight et al., 2013).

The 3D hydrogel system utilizes poly(ethylene glycol) (PEG) hydrogels functionalized with a degradable type I collagen-derived fluorogenic peptide sensor to measure MMP activity (Leight et al., 2013). PEG is a synthetic polymer that can be crosslinked to form a biocompatible hydrogel and has similar water content to in vivo tissue (Leight et al., 2013; Seliktar, 2012). By being able to precisely tune the chemical and mechanical attributes of the hydrogel, the system can be optimized to more closely recapitulate the in vivo microenvironment of interest. Additionally, PEG hydrogel polymerization is often photo-initiated, enabling quick, user controlled hydrogel formation, making it more amenable to HT approaches than traditional ECM hydrogels (i.e. collagen or reconstituted basement membrane) which are slower and temperature sensitive.

Therefore, utilizing PEG hydrogels enables the automation of cell encapsulation with robotic liquid handlers, as demonstrated by others (Mabry et al., 2016). PEG hydrogels have been functionalized with a number of moieties to direct cell function, such as cell adhesion with ECM mimetic peptides like RGD, RLD, and IKVAV, or by tethering of growth factors such as transforming growth factor-β (TGF-β) (Mabry et al., 2016; Sridhar et al., 2014). More recently, PEG hydrogels have been functionalized with sensor peptides that enable measurement of cell function as well (DeForest et al., 2009; Leight et al., 2013). Specifically, the use of a PEG hydrogel system functionalized with a fluorogenic MMP-degradable peptide enabled measurement of cellular MMP activity in 3D cultures with a standard plate reader and required no further processing. These systems are also compatible with other measurements of cellular function, including metabolic activity.

In this work, the 3D MMP hydrogel assay was miniaturized and scaled up to facilitate drug screening applications. The reproducibility and robustness of the HT assay was determined using a bacterial collagenase type I enzyme and a fibrosarcoma cell line (HT1080). The assay was validated with commercially available human MMPs and encapsulation of several different cell types in two different MMP-degradable peptides. Finally, to demonstrate the ability of the system to measure the effect of small molecule drugs on cellular MMP activity and for future HT applications, HT1080 cell line was treated with several drugs over a range of concentrations.

2.3 Materials, Methods and Assay Protocol

2.3.1 Fluorescent MMP-Degradable Peptides Synthesis

The fluorescent MMP-degradable peptides GGPQG↓IWGQK(AdOO)C (QGIW) and GPLA↓C(pMeOBzl)WARKDDK(AdOO)C (LACW) were synthesized using Fmoc solid phase peptide synthesis (Liberty Blue™ Peptide Synthesizer, CEM, Matthews, NC) with a Rink Amide MBHA resin (EMD Millipore, Burlington, MA) as described elsewhere (Leight et al., 2013) with the following modifications: Fmoc-8-amino-3,6-dioxaoctanoic acid (AdOO) (Chem-Impex International, Wood Dale, IL) was used as the small hydrophilic spacer between cysteine and the MMP degradable peptides to increase the hydrophilicity of the peptides over the previously used aminohexyl (Ahx) spacer. Dabcyl succinimidyl ester (Anaspec, Fremont, CA) and Fluorescein NHS ester (Thermo Scientific™, Pittsburgh, PA) coupling was performed as described (Leight et al., 2013) with a shortened resin cleavage time of 2.5 hr. A detailed protocol of the fluorescent MMP-degradable peptide coupling with dabcyl and fluorescein can be found in Appendix B. The peptides were purified using high-performance liquid chromatography (HPLC) (LaChrom ELITE, Hitachi, Schaumburg, IL), Peptides were dissociated from purification column and collected at %60 to %62 v/v (fraction 5) (Figure 2A) and %54 to %60 v/v (fractions 8 to 10) (Figure 2B) of acetonitrile concentration for QGIW and LACW, respectively. Theoretical molecular weight calculated by ChemSketch software (ACD/Labs, Toronto, Canada) of the fluorescent MMP-degradable peptides QGIW and LACW are 1884 and 2337 Da (Figures 3A and 3B), respectively. The molecular weights of the peptides QGIW (Figure 4A) and LACW (Figure 4B) were verified using matrix

assisted, laser desorption-ionization, time-of-flight (MALDI-TOF) mass spectrometry (UltrafleXtreme™, Bruker, Billerica, MA). Molecular weights with an additional 23 or 39 Da (±1 Da proton) more than the calculated theoretical molecular weight were likely due to monovalent cation adducts of sodium or potassium, respectively.

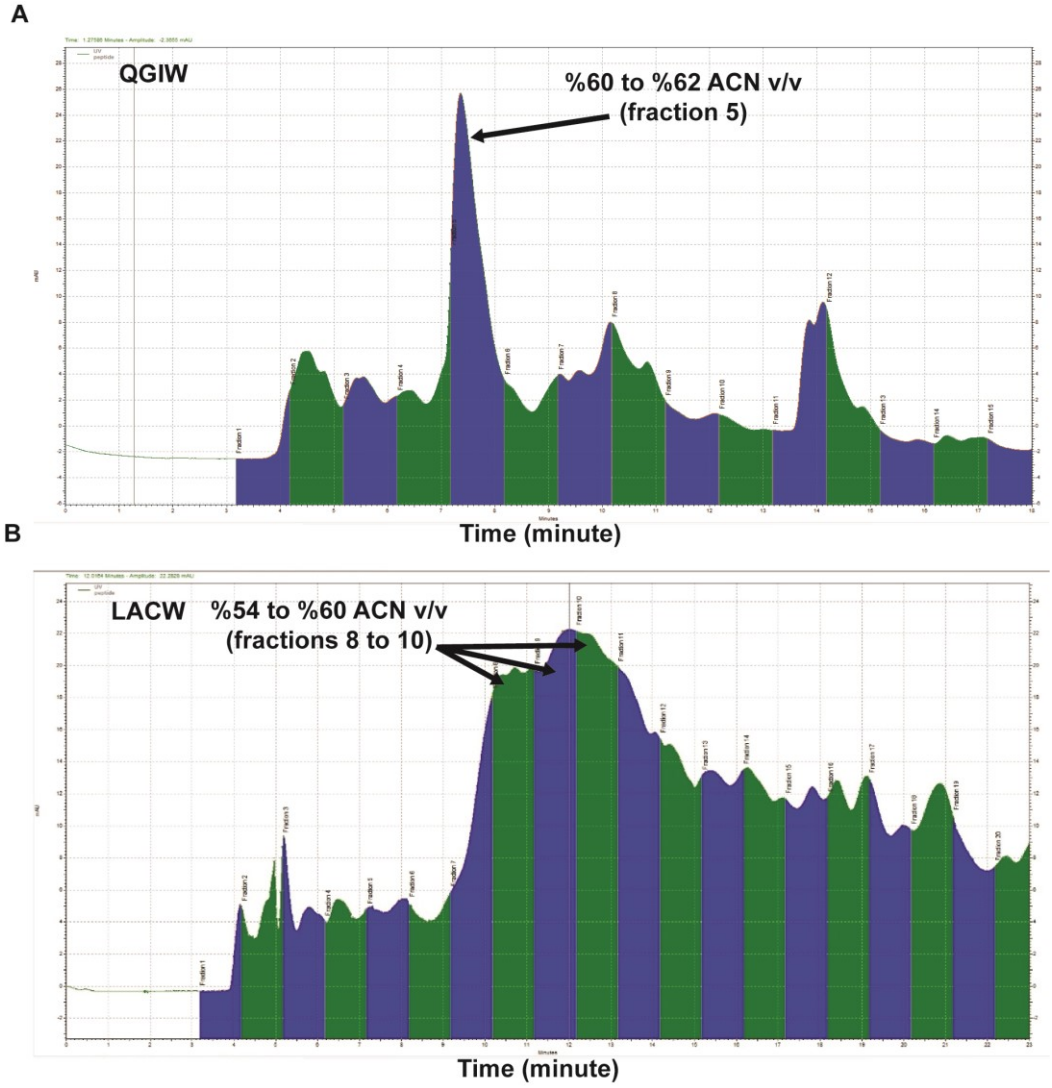

Figure 2: HPLC purification fractions. (A) QGIW fluorescent MMP-degradable peptide purification fractions start at %52 up to %72 v/v at %2 acetonitrile concentration increments per minute, which is equivalent to one fraction. (B) LACW fluorescent MMP-degradable peptide purification fractions start at %40 up to %70 v/v at %2 acetonitrile concentration increments per minute, which is equivalent to one fraction.

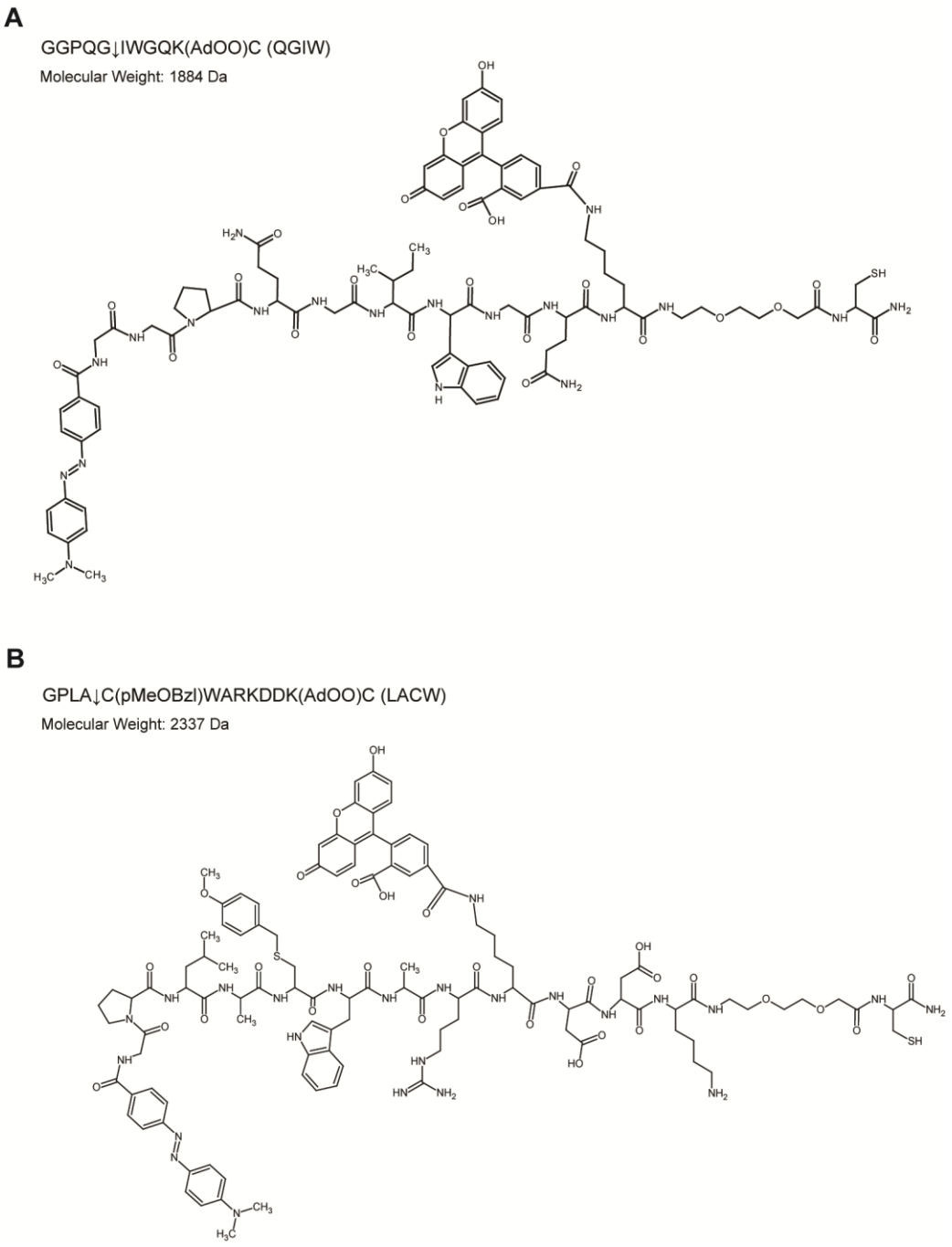

Figure 3: Chemical structure of the fluorescent MMP-degradable biosensors. Chemical structures of (A) QGIW and (B) LACW MMP-degradable peptides after functionalization with dabcyl and fluorescein. Molecular weights were calculated to be 1884 and 2337 Da for (A) QGIW and (B) LACW peptides, respectively.

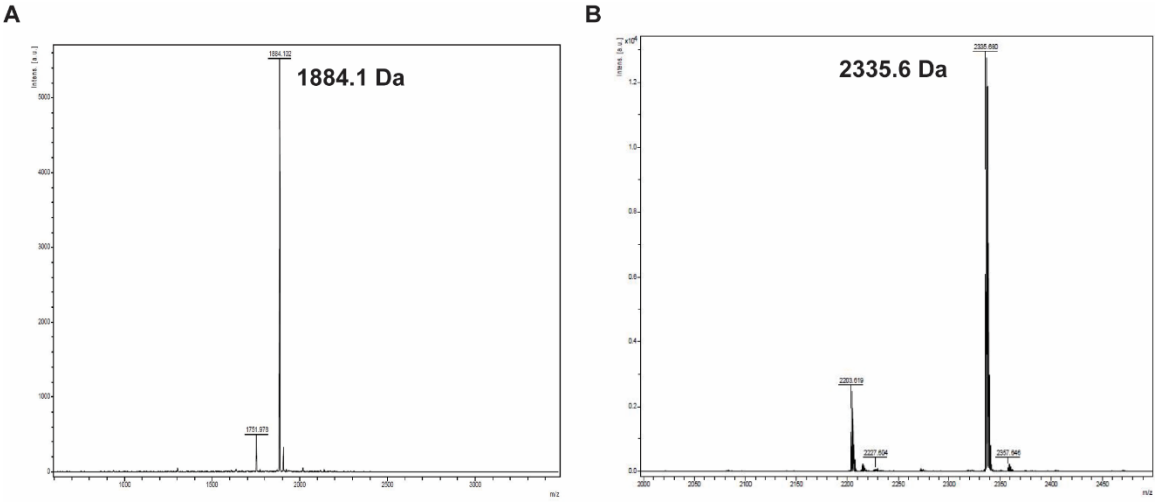

Figure 4: MALDI-TOF Molecular weight verification of the fluorescent MMP-degradable peptides. Highest intensity peaks correspond to molecular weights of 1884.1 Da and 2335.6 Da for (A) QGIW and (B) LACW respectively. Peptides are mixed with α-Cyano-4-hydroxycinnamic acid (HCCA) matrix to assist samples dissociation from test plate and detection.

2.3.2 PEG-NB Functionalization and Hydrogel Precursors

8-arm poly(ethylene glycol) amine (PEG) (MW 40,000 Da, hexaglycerol core, JenKem, Beijing, China) was functionalized with norbornene end groups as previously described (Sridhar et al., 2015) (Protocol in appendix C). End group functionalization was verified by ^{1}H NMR to be ≥90% (Figure 5). PEG functionality percentage with norbornene utilize PEG (alkyl) peak integration of the repeating motif with the knowledge of PEG molecular weight and geometry, using this formula:

$$Functionalization\ \% = \left(\frac{PEG\ molecular\ wieght}{PEG\ peak\ *\ 22\ *\ number\ of\ PEG\ arms}\right) * 100$$

With the assumption of full functionality at 1:1 ratio of PEG end groups to norbornene groups, the estimation of the actual ratio indicates functionality percentage. The photoinitiator lithium phenyl 2,4,6 trimethylbenzoylphosphinate (LAP) was synthesized

as described elsewhere (Fairbanks, Schwartz, Bowman, & Anseth, 2009). The crosslinker MMP-degradable peptide (KCGPQG↓IWGQCK) and the cell adhesion peptide (CRGDS) were purchased from American Peptide Company, Inc. (Sunnyvale, CA) and GenScript® USA Inc. (Piscataway, NJ), respectively.

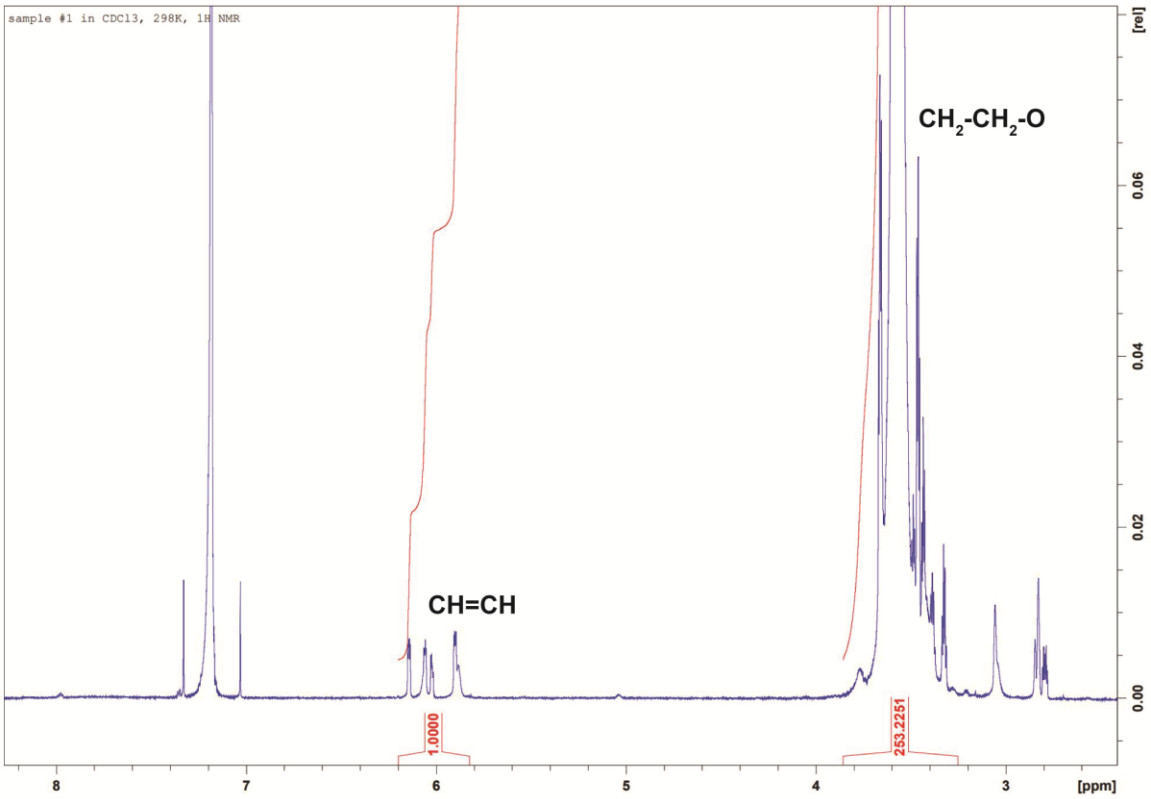

Figure 5: PEG-NB end group functionalization test utilizing ^{1}H NMR. (253.2 ppm) is the ratio of number of hydrogens in the repeating motif of PEG (alkyl peaks) to the normalized number of hydrogens of norbornene (alkene peaks) at (1.0 ppm). Red lines corresponds to the integration curves.

2.3.3 Cell Culture

Adipose-derived human mesenchymal stem cells (hMSCs, Lonza, Allendale, NJ) were cultured in low glucose DMEM (Life Technologies™, Carlsbad, CA) supplemented with

10% fetal bovine serum (FBS) (Seradigm, Radnor, PA) and 1 ng/mL human fibroblast growth factor (PeproTech®, Rocky Hill, NJ) and used within 4 passages after thawing. Primary cervical fibroblasts (CFs) were provided by Dr. Douglas Kniss (Columbus, OH) from non-malignant hysterectomy samples from pre-menopausal women. The Biomedical Institutional Review Board at The Ohio State University approved tissue collections and following informed consents were obtained (Shukla et al., 2018). CFs were cultured in phenol red free high glucose DMEM (Life Technologies) with 10% FBS and used within 2 passages after thawing. Fibrosarcoma cells (HT1080) (American Type Culture Collection (ATCC®), Manassas, VA; RRID: CVCL_0317) were cultured in 1640 RPMI media (Life Technologies) supplemented with 10% FBS and used within 20 passages after thawing. All media was supplemented with 2 mM L-glutamine, 10 U/mL penicillin and 10 µg/mL streptomycin (all from Life Technologies). All cells were maintained in a 37 °C incubator at 5% CO_2. For encapsulation experiments, cells were incubated for 24 hr in phenol red free growth media with 2 mM L-glutamine, 10 U/mL penicillin, 10 µg/mL streptomycin and 1% charcoal stripped FBS. All cells were tested for mycoplasma every 6 months with a PCR based kit (PromoKine, Heidelberg, Germany) and were determined to be free of contamination.

2.3.4 Charcoal Stripping and Heat Inactivation of FBS

FBS was first heat inactivated at 55°C for 30 minutes. In a separate beaker, 0.25% weight/ volume (w/v) (total serum volume to be processed) activated charcoal (Sigma Aldrich, Burlington, MA) and 0.025% w/v dextran (Sigma-Aldrich) were added. 1 - 2

mL of FBS was added to the activated charcoal/dextran and stirred until a homogeneous mixture formed. The rest of the serum volume was then added and stirred for 30 minutes at 55°C. The serum was centrifuged at 3000 rpm for 20 minutes at 4°C, and the supernatant was transferred to another vessel. The charcoal-dextran addition and incubation steps were repeated, but at 37 °C. The serum was centrifuged at 3000 rpm for 20 minutes at 4°C and the supernatant was sterilized by passing through a 0.45 μm then 0.2 μm filters.

2.3.5 High Throughput Assay Procedure

A hydrogel precursor solution consisting of 20 mM 8 arm 40 kDa PEG-NB, 17.8 mM NaOH, 12.75 mM crosslinker MMP-degradable peptide, 1 mM CRGDS, 2 mM LAP, and 0.25 mM fluorescent MMP-degradable peptide in PBS (Life Technologies) was briefly vortexed. Because The MMP-degradable crosslinker peptide is solubilized in an HCl solution, in experiments where the amount of crosslinker was varied, the amount of NaOH was adjusted to achieve a final pH of 7. Low, medium, and highly crosslinked gels corresponded to thiol:ene ratios of 0.5, 0.7 and 0.9 , and used 8.75 mM, 12.75 mM, and 16.75 mM crosslinker peptide and 12.2 mM, 17.8 mM, and 23.4 mM NaOH, respectively.

For cell encapsulation experiments, a thiol:ene ratio of 0.7 was used and a concentrated cell suspension in PBS was added to the hydrogel precursor solution to achieve a final cell seeding density of 3 x 10^6 cells/mL, unless otherwise noted. For hydrogels without

cells, an equivalent volume of PBS was used in lieu of suspended cells. 10 μL of the hydrogel precursor solution was pipetted into black, round bottom, 96-well plates (BrandTech® Scientific Inc., Essex, CT) using a single or multi-channel pipette. Hydrogel polymerization was photoinitiated by exposure to 365 nm UV light (UVP, model UVL-56, Cambridge, UK) at 4 mW/cm^2 for 3 minutes. After polymerization, 150 μL of assay media was added to each sample well. PBS was added to the outermost and empty wells, and the moat between wells to reduce sample evaporation.

For drug screening assays, encapsulated cells were treated with sorafenib (SOR) (Selleck Chemicals, Houston, TX), paclitaxel (PAC) (Invitrogen™, Grand Island, NY), or gemcitabine (GEM) (Selleck Chemicals), which were reconstituted in dimethyl sulfoxide (DMSO) then diluted in assay media in a range of concentrations (0.01 to 50 μM), or 0.5% (v/v) DMSO as a vehicle control. For all assays, plates were incubated (at 37 °C and 5% CO_2) for 24 hr. 1:10 v/v of resazurin (alamarBlue™, Life Technologies) was added to the wells containing encapsulated cells 6 hr prior to the final fluorescence well scan reading. A detailed protocol (mentioned below) and a video illustrating the HT assay procedure can be found in this publication (Fakhouri & Leight, 2019).

2.3.6 Fluorescence Measurements

Fluorescence measurements were conducted using a SPECTRA Max M2 microplate reader (Molecular Devices, San Jose, CA) at 494 nm / 521 nm (excitation/emission) for the fluorogenic peptide and 560 nm / 590 nm for the metabolic reagent, alamarBlue™.

An area scan was performed using the opaque 96-well plate setting with a 3x3 matrix, and the average of each matrix was calculated (Fakhouri & Leight, 2019).

2.3.7 Enzymatic Hydrogel Degradation

Fluorescent functionalized hydrogels were made utilizing 20 mM 8 arm 40 kDa PEG-NB, 17.8 mM NaOH, 12.75 mM crosslinker MMP-degradable peptide, 1 mM CRGDS, 2 mM LAP, and 0.25 mM fluorescent MMP-degradable peptide in PBS. A stock concentration of 10 mg/mL collagenase type I enzyme (Life Technologies) was made by reconstituting in PBS, and further dilutions were made as indicated. MMP-1, -2 and -9 (EMD Millipore) were activated following the manufacturer's protocols, and used at a final concentration of 1 μg/mL. 150 μL of assay buffer with or without MMP-1, -2, or -9 was added to each well. Assay buffer consisted of 50 mM Tris-HCl (Sigma-Aldrich), 10 mM $CaCl_2$ (Fisher Scientific™, Pittsburgh, PA), 150 mM NaCl (Fisher Scientific), 0.5% v/v sodium azide (Fisher Scientific) and 0.05% v/v Triton-X100 (Sigma-Aldrich). For MMP inhibition, 20 μM of the broad spectrum MMP inhibitor GM6001 (Abcam, Cambridge, MA) or an equivalent volume (0.02% v/v) of DMSO vehicle control was added.

2.3.8 Statistical Analysis

Each high throughput assay was completed three independent times with three replicates per condition. All other experiments were repeated at least three independent times. Data was analyzed using GraphPad Prism 7 software (GraphPad Software, Inc, San Diego,

CA) using one-way ANOVA with Tukey multiple comparisons posttest, with a significance level set at $p < 0.05$.

2.3.9 Protocol

2.3.9.1 Hydrogel Components Preparation

2.3.9.1.1 Synthesize the fluorescent protease-degradable peptides as described elsewhere (Leight et al., 2013), utilizing fluorescein as the fluorescent molecule and dabcyl as the quencher. Dissolve the peptide in DMSO to a concentration of 10 mM and store in a -80 °C freezer in small (~30 µL) aliquots to avoid repeated freeze-thaw cycles. NOTE: These peptides can also be purchased commercially. However, for a faster experimental turnaround time, fluorescent protease-degradable peptides were synthesized. This protocol requires a C-terminal cysteine in the peptide sequence to enable covalent incorporation into the hydrogel polymer network.

2.3.9.1.2 Prepare 8 arm 40 kDa poly(ethylene glycol) amine (PEG)-norbornene (NB) as described (Sridhar et al., 2015). Verify end group functionalization of greater than 90% using ^{1}H NMR. Dissolve PEG-NB in sterile phosphate buffer saline (PBS) at 25% w/v and store in -80 °C freezer in (~300 µL) aliquots. NOTE: PEG functionalized with norbornene can also be purchased commercially.

2.3.9.1.3 Synthesize the photo-initiator lithium phenyl 2,4,6 trimethylbenzoylphosphinate (LAP) as described elsewhere (Fairbanks, Schwartz, Bowman, et al., 2009). Dissolve LAP in sterile water to a concentration of 68 mM and store in a -80 °C freezer in (~300 µL) aliquots. NOTE: As an alternative, Irgacure (2-Hydroxy-4′-(2-hydroxyethoxy)-2-methylpropiophenone) can be used as the photo-initiator. LAP and Irgacure can be purchased commercially.

2.3.9.1.4 Dissolve the MMP-degradable peptide crosslinker (KCGPQG↓IWGQCK) and the cell adhesion peptide (CRGDS) in sterile water to a concentration of 200 mM and 100 mM respectively, and store them in a -80 °C freezer in (~300 µL and ~30 µL) aliquots, respectively.

2.3.9.2 Assay Media Preparation

2.3.9.2.1 Prepare the heat-inactivated, charcoal stripped fetal bovine serum (FBS) for the MMP assay. NOTE: Proteases in FBS can produce a high background signal with the MMP assay; therefore, it is recommended to heat-inactivate and charcoal strip the FBS for the assay media.

2.3.9.2.1.1 Inactivate 100 mL of FBS by heating for 30 min at 55 °C. NOTE: 100 mL of FBS was utilized here for aliquoting and storage at -20 °C for future use. Smaller volumes can be used as needed.

2.3.9.2.1.2 Add 0.25% of activated charcoal and 0.025% of dextran to a small amount of FBS (approximately 5 mL) and stir until a slurry is formed. Then, add the rest of the FBS and stir for 30 min at 55 °C.

2.3.9.2.1.3 Centrifuge at 3000 *rpm* for 20 min at 4 °C. Then transfer the supernatant to another vessel.

2.3.9.2.1.4 Repeat step 2.3.9.2.1.2 but at 37 °C followed by step 2.3.9.2.1.3. Sterilize the supernatant using a 0.45 µm filter and then a 0.2 µm filter.

2.3.9.2.2 Prepare assay media using media supplemented with 1% charcoal stripped FBS, 2 mM L-glutamine, 10 U/mL penicillin, 10 µg/mL streptomycin. NOTE: Media without phenol red is recommended because it has less fluorescence interference. Other additions to the assay media such as insulin, growth factors, etc. may be added as long as the absorbance and fluorescence spectrum peaks do not overlap with the sensor (494 nm/521 nm).

2.3.9.2.3 Dilute bacterial collagenase enzyme type I at 10 and 1000 µg/mL in the assay media as a positive control.

2.3.9.3 Hydrogel Preparation and Cell Encapsulation

2.3.9.3.1 Prepare the hydrogel precursor solution.

2.3.9.3.1.1 Add the reagents to a 1.5 mL tube in the following order, vortexing after addition of each component: 20 mM 8 arm 40 kDa PEG-NB, 12.75 mM crosslinker MMP-degradable peptide, 17.8 mM NaOH, 1 mM CRGDS, 2 mM LAP, and 0.25 mM fluorogenic MMP-degradable peptide.

NOTE: Table 2 shows hydrogel precursor solution contents, stock concentrations, working concentrations, volume calculation formulas and the required volumes needed to make 120 µL of hydrogel precursor solution, which is sufficient to conduct an experiment with 10 hydrogels. To account for loss of the hydrogel solution due to pipetting, increase the total volume by 20%. The commercial peptides are often supplied in an acidic hydrogen chloride solution; therefore, NaOH is added to achieve a final pH of 7. pH of the final solution should be confirmed by the user.

Precursor Solution Contents	**Stock Conc.**	**Working Conc.**	**Volume Formula**	**Example volume for 10 hydrogels (µL)**
PEG-NB (wt%)	25	10	working conc.*total volume / stock conc.	48.00
Crosslinker MMP-degradable peptide (mM)	200	8. 75 to 18.75	Stoichiometry (thiols:enes) (0.5 to 1)	5.25 to 7.65
NaOH (M)	1	-	28% of the crosslinker volume	1.47 to 3.14
RGD pendant peptide (mM)	100	1	working conc.*total volume / stock conc.	1.20
LAP (mM)	68	2	working conc.*total volume / stock conc.	3.53
Fluorescent MMP-degradable peptide (mM)	10	0.25	working conc.*total volume / stock conc.	3.00
1X PBS (for all conditions)	-	-	total volume - sum of all precursor components	57.56 to 49.88
Total Volume =			number of hydrogels (10 hydrogels) * hydrogel volume (10 µL) * 20% extra	120.00

Table 2: Hydrogel Precursor Solution Preparation.

2.3.9.3.1.2 Divide the hydrogel precursor solution into multiple 1.5 mL tubes, one tube per condition being tested. NOTE: Several control conditions in which hydrogels are prepared without the addition of cells are suggested. For a negative control, to account for non-specific degradation of the fluorogenic sensor, one hydrogel condition can be incubated with the vehicle control or the experimental media alone if there are no treatment conditions. For a positive control and for calibration between experiments, hydrogels can be incubated with a protease known to cleave the fluorogenic sensor. For example, two concentrations of bacterial collagenase were used here.

2.3.9.3.2 Encapsulate cells in hydrogels.

2.3.9.3.2.1 Prepare a single cell suspension as appropriate for the cell type being used. For example, wash cells with 10 mL of PBS. Trypsinize cells using 0.05% trypsin and incubate at 37 °C and 5% CO_2 for 3 min. Count cells with a hemocytometer to determine total cell number.

2.3.9.3.2.2 Centrifuge the cell solution at 1200 *rpm* for 3 min, aspirate culture media, then re-suspend cells in PBS at approximately three times the highest required seeding density for the experiment. For example, a cell suspension with a density of 21 x 10^6 cells was used to achieve a final encapsulated density of 7 x 10^6 cells/mL.

2.3.9.3.2.3 Count the cells again to ensure an accurate cell concentration.

2.3.9.3.2.4 Add suspended cells and PBS to each tube of hydrogel precursor solution according to the required seeding density. Add PBS to conditions with no cells in lieu of suspended cells. NOTE: All conditions should have the same final hydrogel precursor solution volume to ensure the ratio between the hydrogel components and PBS is constant. Do not vortex tubes that have cells in them, pipette up and down vigorously without creating bubbles in order to mix the precursor solution.

2.3.9.3.2.5 Dispense 10 µL of the hydrogel precursor solution into a sterile black round bottom 96-well plate, ensuring that the tip is centered in the middle of the each well while dispensing.

2.3.9.3.2.6 Polymerize hydrogel precursor solution by exposing the plate to ultra violet (UV) light at 4 mW/cm^2 for 3 min. NOTE: The UV lamp (UVL-56 Handheld UV Lamp, UVP, Upland, CA) produces UV-A light at a long UV wavelength (365 nm), which does not affect cellular viability.

2.3.9.3.2.7 Add 150 µL of assay media to all wells except for the positive control conditions without encapsulated cells. To the positive controls, add 150 µL of collagenase enzyme solution.

2.3.9.3.2.8 Add 150 µL of PBS to the outer wells of the plate to reduce evaporation during incubation.

2.3.9.4 MMP and Metabolic Activity Measurement

2.3.9.4.1 Measure fluorescence immediately post-encapsulation to establish a baseline fluorescence measurement and ensure uniformity in hydrogel polymerization. Read the plate using a fluorescence microplate reader utilizing an opaque 96-well plate protocol with an area scan setting at 494 nm/521 nm (excitation/emission). This will be the 0 hr read.

2.3.9.4.2 Incubate plate in a humidified incubator at 37 °C and 5% CO_2 for 18 hr.

2.3.9.4.3 Add metabolic activity reagent (resazurin) at 1:10 (v/v) for each well.

2.3.9.4.4 Incubate plate in a humidified incubator at 37 °C and 5% CO_2 for an additional 6 hr. NOTE: This incubation time may vary depending on cell type.

2.3.9.4.5 Measure fluorescence at 24 hr post-encapsulation. Read the plate using a fluorescence microplate reader utilizing an opaque 96-well plate protocol with an area scan setting at 494 nm/521 nm (excitation/emission) for MMP activity and 560 nm/590 nm (excitation/emission) for metabolic activity.

2.4 Results and Discussion

2.4.1 High Throughput Assay Development

3D microenvironments can be synthetically generated to more closely mimic the in vivo tumor microenvironment, making them a valuable tool in drug screening assays (Baker & Chen, 2012; Ryan et al., 2016; Seliktar, 2012). However, 3D culture often makes analysis of cellular responses to drug treatment more difficult; hence most 3D drug screening assays have been limited to measurements of cell viability. However, many other cell

functions contribute to disease. For example, MMP activity is upregulated during tumor progression and this increased MMP activity can promote cancer cell invasion and migration (Yodkeeree et al., 2009, 2008). Therefore, there is a need for new technologies that enable HT measurements of a wider range of cell functions.

To begin to address this need, we have adapted and characterized a hydrogel culture system that enables the culturing of single cells in a 3D microenvironment and detection of MMP activity simultaneously. Previously, we developed a low throughput 3D fluorescent hydrogel system for measuring global MMP activity (Leight et al., 2013). Briefly, this system measures MMP proteolysis through the use of quenched fluorescent MMP-degradable peptides covalently incorporated into a PEG hydrogel network during polymerization. Cleavage of the peptide sensor by cell secreted MMPs resulted in increased fluorescence that was directly detected using a standard microplate reader. Figure 6 illustrates the basic design of the fluorescent MMP-degradable peptide.

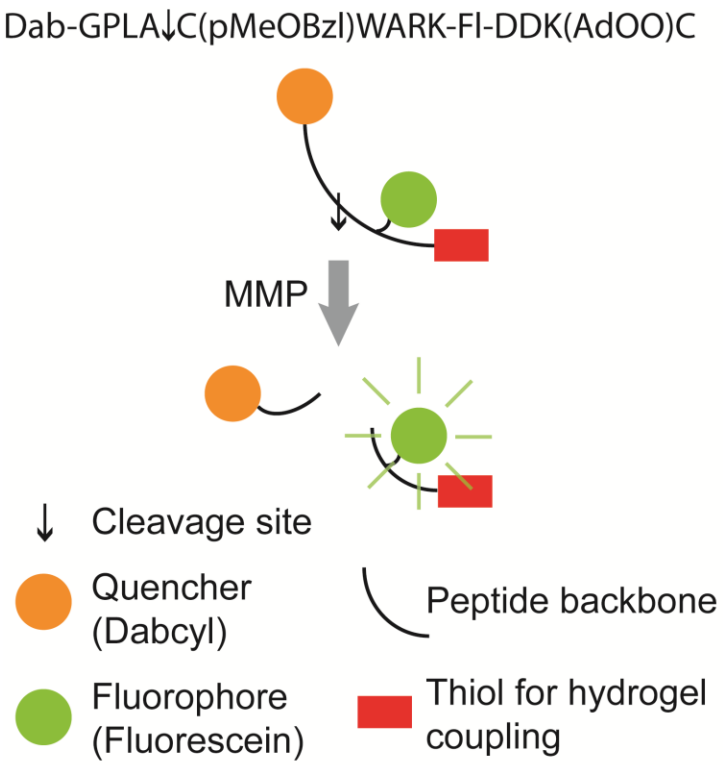

Figure 6: The fluorogenic MMP-degradable peptide design. The fluorogenic MMP-degradable peptide consists of a backbone peptide GPLA↓C(pMeOBzl)WARKDDK(AdOO)C (↓ indicates the cleavage site), LACW as an example here, that determines the specificity of the sensor. The peptide is labeled with a quencher (dabcyl) and a fluorophore (fluorescein), which is unquenched (fluoresces) when the backbone peptide is cleaved by MMP. A thiol group is conjugated to the backbone peptide to enable covalent reaction with norbornene functional groups in the PEG molecule, coupling the sensor to the hydrogel.

To adapt this system for HT screening, the MMP sensor hydrogel system was miniaturized to a 96-well format. First, a hydrogel precursor solution, consisting of a PEG 8-arm macromer, a MMP-degradable peptide crosslinker, a cell adhesion peptide (CRGDS), photo-initiator, and the fluorescent MMP-degradable peptide were combined

with a concentrated cell suspension in phosphate buffered saline (PBS). The cell-hydrogel precursor solution was then pipetted into each well, and hydrogel polymerization was photo-initiated by exposure to long wavelength UV light (365 nm, 4 mW/cm2 for 3 min). Photo-initiated polymerization is a well-established technique for cell encapsulation that does not significantly affect cell viability (DeForest et al., 2009; Fairbanks, Schwartz, Halevi, et al., 2009; Leight et al., 2013; Mabry et al., 2016). Cell culture media was added, and the encapsulated cells were incubated (37 °C, 5% CO_2) for 24 hr.

As an internal control for differences in cell number, cellular metabolic activity was measured using resazurin, a non-fluorescent dye that is converted into a fluorescent molecule by a reduction reaction in metabolically active cells. The excitation and emission spectrum of resazurin is sufficiently separated from the fluorogenic MMP sensor spectrum, enabling measurement of both MMP activity and metabolic activity in the same well. However, the overall intensity of the fluorophore was reduced in comparison to conditions without resazurin dye, because resazurin opaqueness partially absorbs emitted light from the excited fluorophore (Figure 7A). Nevertheless, the reduction in signal intensity was consistent, around 50-60%, across all conditions (Figure 7B).

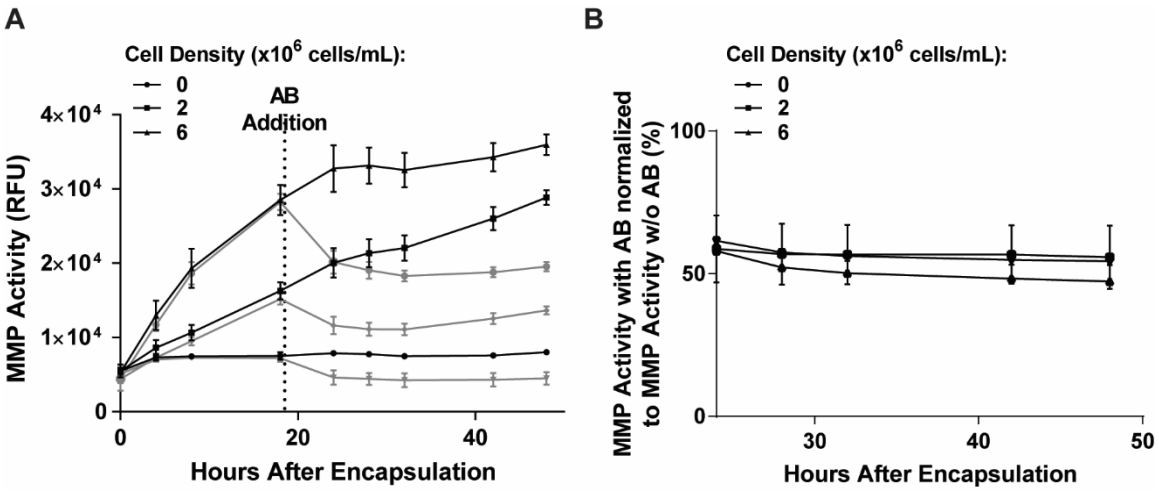

Figure 7: Resazurin dye effect on fluorogenic MMP sensor signal. (A) 6, 2 x 10^6 cells/mL and no cells were incubated in functionalized hydrogels for 18 hr, then resazurin was added (gray lines) and MMP activity was measured for a total of 48 hr, n=3 ± SD. (B) MMP activity of conditions with resazurin (Alamar Blue (AB)) was normalized to MMP activity of conditions without AB to reflect signal intensity reduction rate, n=3 ± SD.

Resazurin was added to the wells 6 hr before the final plate read at 24 hr. Fluorescence intensity was measured using a microplate reader with an area well scan. A schematic of the process is illustrated in Figure 8. The 96-well format eliminated several steps from the previous 24 well protocol, reducing the time needed per well by approximately 50%. Further, the total hydrogel volume needed per well was reduced by 80% (50µL to 10µL) as compared to the previous 24-well format. This miniaturization also increased the number of possible conditions tested per plate from 12 conditions in duplicates utilizing the 24-well plate to 20 conditions in triplicates utilizing the 96-well plate.

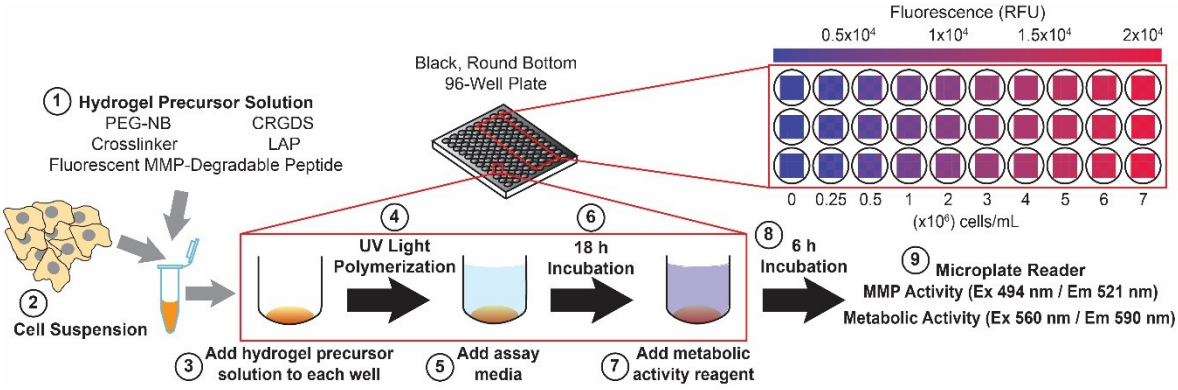

Figure 8: Assay schematic. The hydrogel precursor solution components are mixed with cells suspended in PBS. The precursor solution is then pipetted into black, round bottom, 96-well plates and polymerized by exposure to UV light for 3 min. Assay media is added, and plates are incubated for 18 hr (37 °C, 5% CO_2). The metabolic activity reagent resazurin is then added, and plates are incubated for an additional 6 hr. MMP and metabolic activity are measured using a fluorescent microplate reader with a well scan protocol at the indicated excitation/emission wavelengths.

For consistent fluorescence measurements using a plate reader, it is essential that the hydrogels are centered within the culture well, and have geometrically reproducible shape. The importance of centering and having a reproducible geometrical hydrogel shape has also been observed by others (Mabry et al., 2016). However, centering the gels proved to be difficult and highly variable using standard flat bottom 96-well plates, due to the liquid precursor solution being drawn up the side of the well by surface tension and the resulting hydrogels not evenly covering the bottom of the well. In the system developed by Leight et al. (Leight et al., 2013), the hydrogel shape and centered position was determined by the use of silicone gaskets acting as a mold, whereas the 96-well system relies upon surface tension for maintaining hydrogel shape until the polymerization process is complete. In flat bottom plates, the hydrogel precursor solution

incompletely covered the bottom of the well and formed a meniscus with the side wall in 46% ± 7.3% (mean ± SD, n=3) of the wells. This caused irregularly shaped hydrogels that were not centered within the well, which increased the variability of the fluorescent measurements. Fluorescent measurements of functionalized hydrogels in flat bottom plates incubated for 24 hr with collagenase type I enzyme concentrations (0 - 1000 μg/mL) had high coefficients of variation (%CV) (the ratio of the standard deviation to the mean) between triplicates (Figure 9A). To overcome this variability, round bottom 96-well plates were used, where the curvature of the well centered the hydrogel by facilitating the placement of the dispensing tip in the center of the well.

Hydrogels in round bottom plates were observed to have a uniform shape. This uniformity was reflected by a reduction in the %CV for fluorescent measurements of hydrogels exposed to collagenase concentrations at or below 10 μg/mL compared to the flat bottom plates, and more consistent readings across all concentrations (Figure 9A). Low variability between triplicates is a critical factor in the development of HT assays and can affect the working range and sensitivity of the assay. The working range is defined as 3 standard deviations above the minimum detected signal (background), while the maximum limit of the working range is 3 standard deviations below the maximum detected signal. Because conditions in round bottom plates had a lower %CV, the working range in the round bottom plates was 15% larger than the flat bottom plates (Figure 9B). Therefore, black round bottom 96-well plates were utilized for all subsequent assays due to the ease of pipetting consistently centered gels, the increased

working range of detection, and reduced overall variability between triplicates. It is worth noting that the curvature of the wells in round bottom plates would also aid in future use of automated liquid handlers. Round bottom plates would decrease the amount of time spent calibrating placement of the dispensing tip in the center of wells and offer an alternative solution for automated liquid handlers that are not equipped with self-calibrating features.

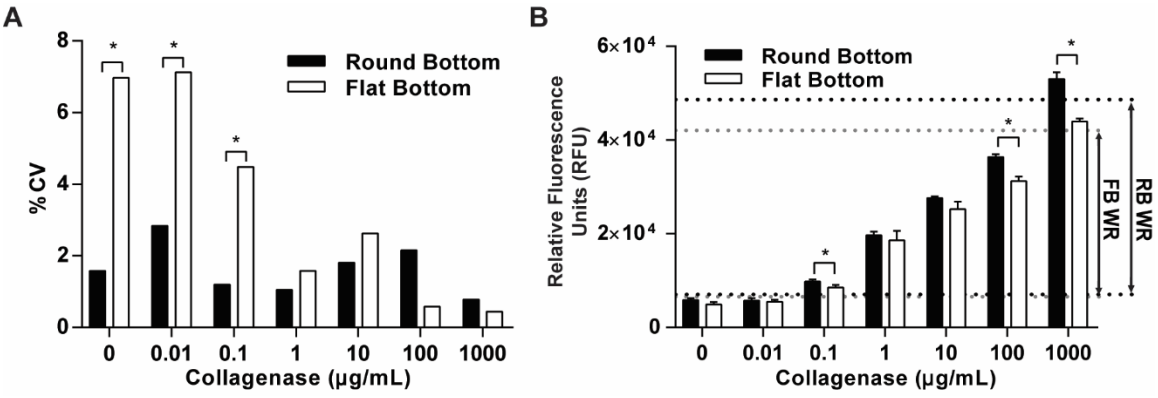

Figure 9: Effect of plate geometry on fluorescent measurements. (A) Coefficient of variation percentage (%CV) of round bottom (RB) and flat bottom (FB) plates. n=3, *p<0.05. (B) Working ranges (WR) based on the fluorescence intensity (RFU, relative fluorescence units) of the MMP fluorogenic peptide in RB and FB plates after incubation for 24 hr with a range of collagenase type I enzyme concentrations. n=3 ± SD, *p<0.05.

2.4.2 High Throughput Assay Characterization

To characterize the assay and determine its suitability for HT applications, the detection limits and signal range were determined. Hydrogels were incubated in a range of collagenase type I enzyme concentrations (0 to 2000 µg/mL) at 37 °C for 24 hr to establish the dynamic range (maximum and minimum detected intensities) of the fluorescent sensor functionalized hydrogels. The upper limit of detection was observed

with collagenase concentrations at or above 1000 μg/mL, while background noise levels were established by negative control hydrogels with no collagenase (Figure 10A). From this dynamic range, the working range was calculated to be between ≈ 0.02 μg/mL and ≈ 575 μg/mL of collagenase (Figure 10A). This large working range over four orders of magnitude gives this HT assay the flexibility to detect a wide range of MMP concentrations, which is important since different cell types can produce varying concentrations of MMPs.

Mechanical properties of the cellular microenvironment have been shown to regulate a number of cell functions, including cell morphology, migration, and MMP activity (Ehrbar et al., 2011; Leight et al., 2013; Mabry et al., 2016). The mechanical properties of synthetic hydrogels, including PEG, can be precisely tuned by varying the crosslinking density (i.e the ratio of thiol groups in the crosslinking peptide to the norbornene groups on the PEG macromer (thiols:enes)) (Mabry et al., 2016), or the structure of the polymer building blocks (i.e the number or length of macromer arms) to recapitulate in vivo tissue properties without affecting ligand density. However, changing the underlying structure of the hydrogel may affect the porosity and diffusion of molecules within the hydrogel. Therefore, to determine if changes in mechanical properties of the hydrogel affect the measurement of enzyme activity the crosslinking density was varied with three thiol:ene ratios (0.5, 0.7 and 0.9) corresponding to low, medium and high stiffness respectively and the hydrogels were exposed to a range of collagenase type I enzyme concentrations (0 – 2000 μg/mL) (Figure 10B). No significant difference between the three ratios for each

collagenase concentration from 0.01 – 2000 μg/mL, indicating that varying the mechanical properties of the hydrogel did not affect the performance of the assay.

An important attribute of HT assays is their tolerance to dimethyl sulfoxide (DMSO), a common organic solvent used for reconstituting therapeutic compounds. High concentrations of DMSO have been observed to affect signal detection methods and enzyme kinetics (Williams & Scott, 2009). To investigate the effect of DMSO in this assay, we incubated the hydrogels with a range of concentrations of DMSO (0 to 2% v/v) with or without collagenase (10 μg/mL), or with encapsulated cells (HT1080 at 3 x 10^6 cells/mL). This range of DMSO concentrations was selected due to most cellular applications limiting DMSO to 1% of the total volume in order to avoid cellular toxicity, which has been observed with higher concentrations. There was no significant difference between signals with or without collagenase for any of the DMSO concentrations (Figure 10C). Similarly, there was no significant difference between signals of encapsulated cells for MMP Activity (Figure 10C). Moreover, metabolic activity was not significantly different than control at DMSO concentrations of 1.5% (v/v) or less (Figure 10D). Therefore, this assay can be utilized to measure the effects of a wide variety of chemotherapeutic agents on cellular MMP and metabolic activity without DMSO affecting signal detection.

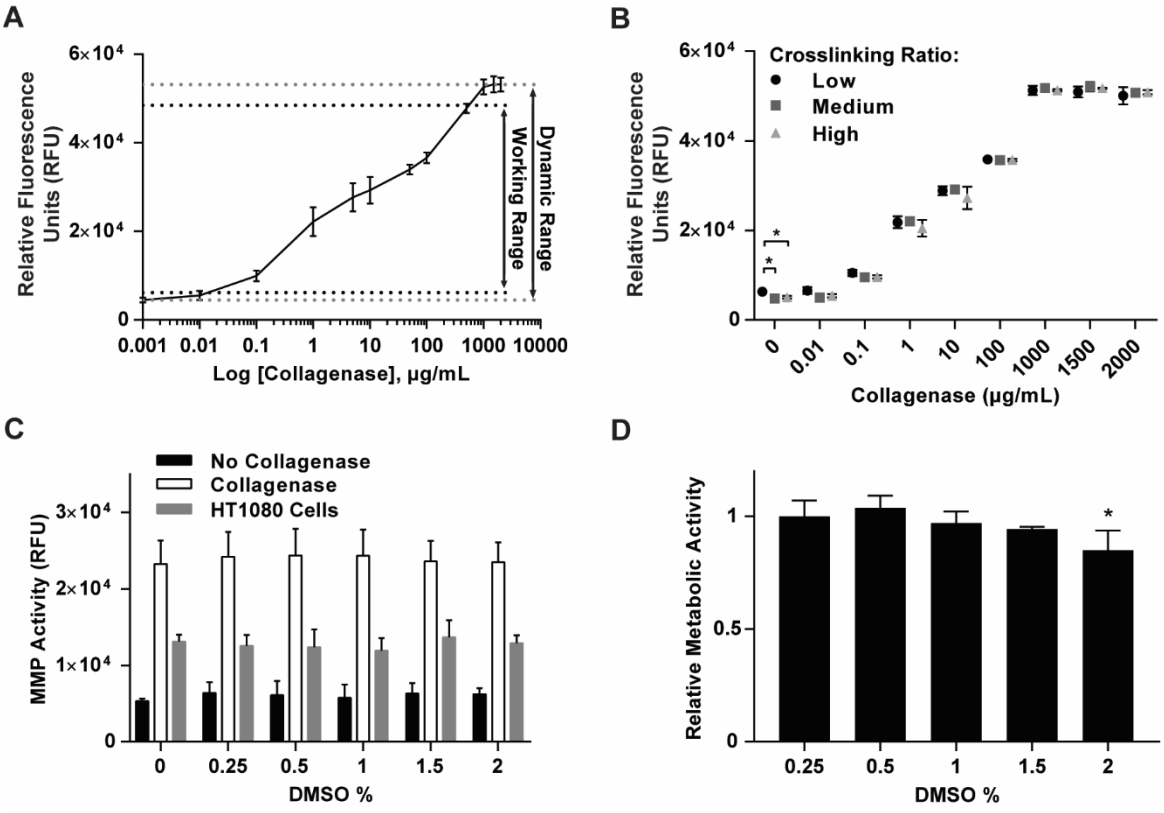

Figure 10: Assay characterization: detection limits, stiffness and DMSO tolerances. (A) Dynamic and working range of the assay. Functionalized hydrogels were incubated with a range of collagenase enzyme concentrations for 24 hr and fluorescence intensities were measured n=3 ± SD. (B) Fluorescence intensities of the functionalized hydrogels with low, medium, and high crosslinking ratios incubated in a range of collagenase concentrations for 24 hr. n=3 ± SD, *p<0.05. (C) Fluorescence intensity of the functionalized hydrogels incubated with a range of DMSO concentrations for 24 hr with or without collagenase, or with encapsulated cells (HT1080). n=3 ± SD. (D) Metabolic activity of HT1080 cells encapsulated in the functionalized hydrogels and incubated with a range of DMSO concentrations for 24 hr, normalized to metabolic activity at 0% DMSO. n=3 ± SD, *p<0.05.

To determine the assay robustness and reproducibility, standard plate uniformity tests were performed to determine the variability across multiple plates and multiple days. Uniformity tests were also used to determine the separation of each signal level (Z'-

factor) and the suitability of the assay for HT applications. The uniformity test determines spatial intra-plate and inter-plate uniformity and variability within the same day and across different days of experimentation. The uniformity tests were performed with collagenase enzyme or with HT1080 cells by producing high, medium (med) (approximately half the intensity of high) and low (background) fluorescence signals arranged in an interleaved format, as described elsewhere (Chai, Goktug, & Chen, 2015; Iversen et al., 2004).

For the uniformity test with the collagenase enzyme, functionalized hydrogels were incubated with 1000, 10, and 0 µg/mL collagenase type I enzyme, for 24 hr (37 °C, 5% CO2). For the encapsulated cell uniformity test, cell seeding density was utilized to produce the three fluorescent signal levels (low, med and high). HT1080 cells were encapsulated for 24 hr in functionalized hydrogels at 0 (no cells), 3 and 6 x 10^6 cells/mL to produce low, med and high signals, respectively. However, due to the small Hill slope value of 0.186, calculated from the HT1080 cell seeding density MMP activity curve (Figure 15A), tolerance of the assay to plate-to-plate and day-to-day variability was dramatically reduced. Consequently, some inter-plate and inter-day fold shifts calculated from formulas in Table 3 were above 2 (ranged from 1.1 to 2.5 for inter-plate and 1.3 to 4.8 for inter-day fold shifts). A single occurrence of inter-plate or inter-day fold shift greater than 2 means that the HT assay does not meet the acceptance threshold, which results in rejecting the HT cellular assay uniformity test utilizing producing signal levels as a function of cell seeding density. Another approach was conducted to overcome this

rejection. Cells were treated with the broad spectrum MMP inhibitor GM6001 to identify conditions that produce high, med, and low signals. HT1080 cells were encapsulated in the functionalized hydrogels at 3 x 10^6 cells/mL, and incubated for 24 hr with GM6001 over a range of concentrations from 0.01 μM to 500 μM (Figure 11A). The highest signal was observed in the control cells treated with (0.5% v/v) DMSO vehicle control. From the dose response curve (Figure 11A), the concentration of GM6001 that resulted in 50% inhibition (IC_{50}) of MMP activity was determined to be 0.29 μM. MMP activity was completely inhibited, with a fluorescence signal similar to background, with concentrations greater than 5 μM of GM6001. At concentrations greater than 100 μM of GM6001, metabolic activity was significantly reduced (Figure 11B). Therefore, a concentration of 10 μM was used to produce the low signal in the uniformity tests. The Hill slope was calculated to be 1.1, and this value was used to calculate the inter-plate and inter-day fold shifts for the uniformity tests (Table 3).

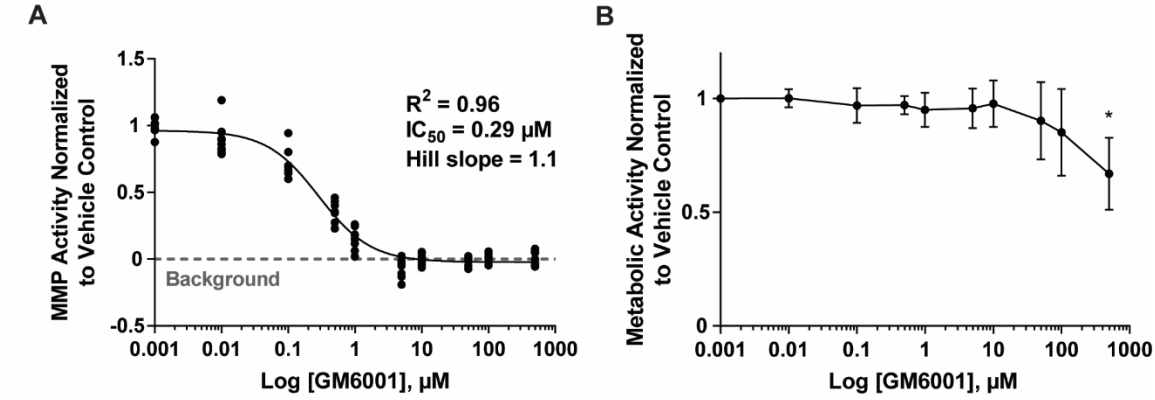

Figure 11: MMP and metabolic activity of fibrosarcoma cells in response to MMP inhibitor (GM6001). (A) MMP activity of HT1080 cells, encapsulated in the functionalized hydrogels at 3 x 10^6 cells/mL, and incubated for 24 hr (37 °C, 5% CO_2) with GM6001 in a concentration range from 0.01 µM to 500 µM. Triplicates of n=3 experiments were fit with a nonlinear regression curve fit with variable slope. (B) Measurement of metabolic activity normalized to the vehicle control for encapsulated cells treated with GM6001. n=3 ± SD, *p<0.05, compared to the vehicle control.

To test the uniformity of the assay for measuring cell secreted enzymes, HT1080 cells were encapsulated in the functionalized hydrogels at 3 x 10^6 cells/mL, and incubated for 24 hr (37 °C, 5% CO2) with a broad spectrum MMP inhibitor (GM6001) at 0.4 µM and 10 µM, or (0.01% v/v) DMSO control (Figure 12B). The uniformity tests were performed on three different days (Day A, B, and C) utilizing three separate plates each day (Figure 12 A, B). Each plate was incubated for 24 hr with a total of 32 wells for each signal level, as described previously (Chai et al., 2015; Iversen et al., 2004). Variability in average signal level, even in the DMSO treated control, was observed to be higher between days with the encapsulated cells as compared to the enzyme uniformity test (Figure 12A and 12B). Cell-based assays often have higher variability (Shelper, Lovitt, & Avery, 2016) similar to the results observed here, and can be more sensitive to batch-to-batch

variability (Chai et al., 2015). Therefore, the results of the uniformity test were normalized to the average high signal level per day to give a relative decrease in MMP activity due to the MMP inhibitor, which resulted in a similar decrease in signal across days (Figure 12B). Cellular uniformity test data without normalization can be found in Figure 13.

To assess the HT assay performance, both the Z'-factor and %CV of all the plates were calculated (Figure 12C and 12D). Unlike signal-to-background or signal-to-noise ratios, Z'-factor calculations account for the variability in the controls and the samples and is therefore a more accurate indicator of the measurement quality of an assay (J.-H. Zhang, Chung, & Oldenburg, 1999). The Z'-factor is a ratio between the working range and dynamic range to determine the overlap between signal bands of the positive and negative controls. Z'-factor can be calculated using the following formula:

$$\frac{(Mean_{high} - 3 * SD_{high}/\sqrt{n}) - (Mean_{low} + 3 * SD_{low}/\sqrt{n})}{Mean_{high} - Mean_{low}}$$

Z'-factor values closer to 1 indicate large separation between signal bands and values closer to zero indicate little separation between signal bands. Values below zero indicate the assay is unsuitable for screening applications due to overlapping signal bands (J.-H. Zhang et al., 1999).

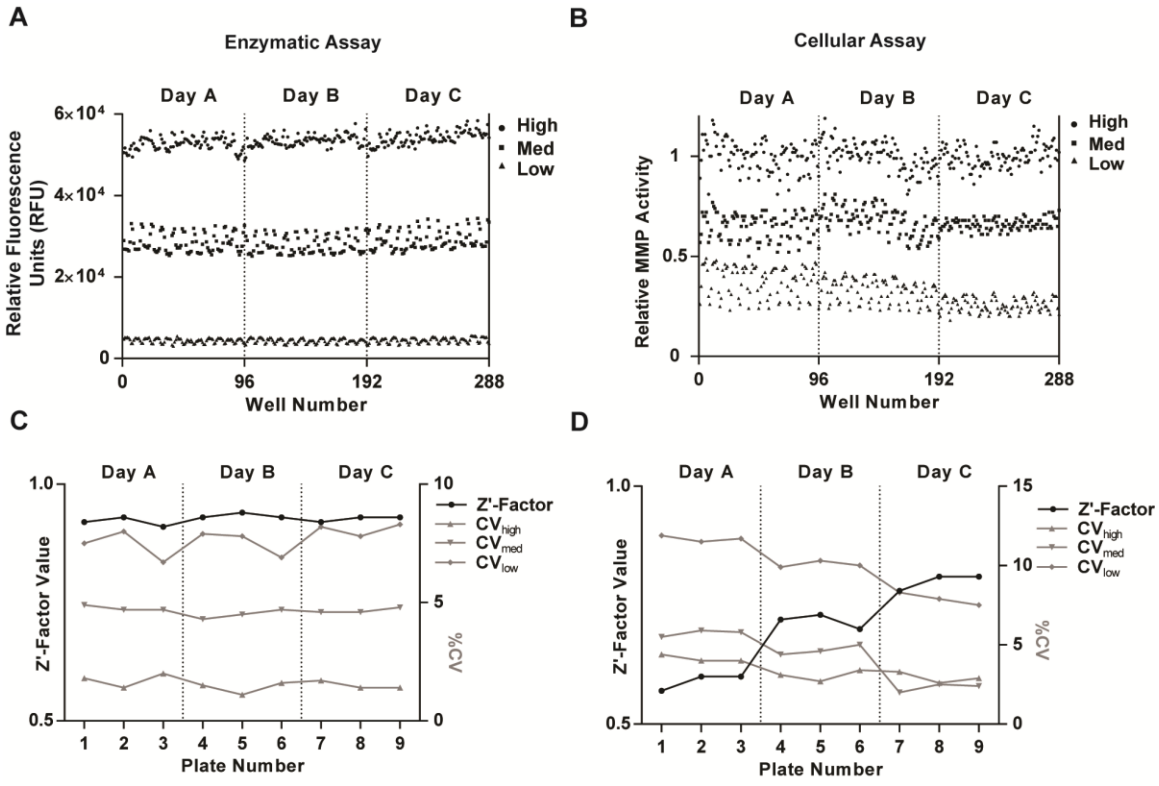

Figure 12: Plate uniformity with collagenase enzyme and HT1080 cells. (A) 96-well plate uniformity test using high, medium (approximately half the intensity of high) and low (background) fluorescence signals arranged in an interleaved format by adding 1000, 10, and 0 µg/mL collagenase type I enzyme to the functionalized hydrogels, respectively. Each plate was incubated for 24 hr with a total of 32 wells for each signal level. (B) Normalized 96-well plate uniformity test was performed by utilizing low, medium and high fluorescence signals arranged in an interleaved format by culturing HT1080 cells at 3 x 10^6 cells/ mL with 10 µM, 0.4 µM and DMSO control of the broad spectrum MMP inhibitor GM6001, respectively. Each plate was incubated for 24 hr with a total of 32 wells for each signal level. Signal levels were normalized to the mean of the high signal for each day. (C) Z'-factor for high signals and %CV for all three signal levels (high, medium and low) were calculated from the enzymatic plate uniformity test. (D) Z'-factor for high signals and %CV for all three signal levels (high, medium and low) were calculated from the cellular plate uniformity test.

Based on previous values reported in the literature, we chose a Z'-factor value of 0.5 or greater as the acceptance threshold for the enzymatic assay and 0.4 or greater for the

cellular assay (Chai et al., 2015; Iversen et al., 2004; Williams & Scott, 2009; J.-H. Zhang et al., 1999). The Z'-factor was calculated from the high signal control, produced by collagenase enzyme and HT1080 cells. The Z'-factor values for the high signals for the 9 plates incubated with collagenase enzyme were above 0.9 and the %CV of all three signal levels were below 10% (Figure 12C). The Z'-factor values for the high signals for the 9 plates with encapsulated cells were above 0.5 and the %CV of all three signal levels were below 12% (Figure 12D). These Z'-factor and %CV indicates that the variability of this assay is suitable and within the acceptable range for high throughput applications (Chai et al., 2015; Iversen et al., 2004; J.-H. Zhang et al., 1999).

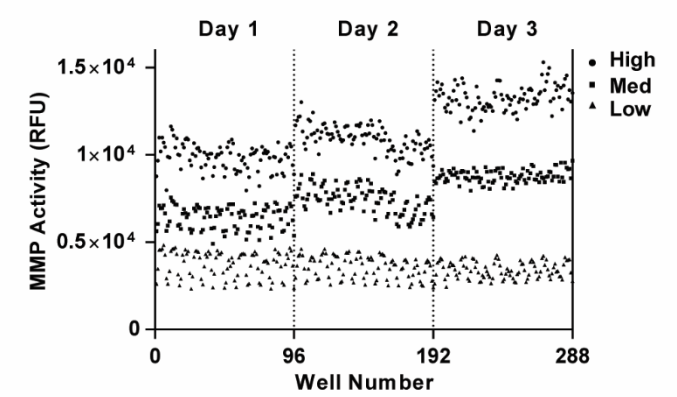

Figure 13: Cellular assay uniformity test without normalization. 96-well plate uniformity test was performed by utilizing low, medium and high fluorescence signals arranged in an interleaved format by culturing HT1080 cell line at 3 x 10^6 cells/ mL with 10 μM, 0.4 μM and DMSO control of the broad spectrum MMP inhibitor GM6001, respectively. Each plate was incubated for 24 hr with a total of 32 wells for each signal level.

Uniformity test results include edge effect, drift, Z'-factor, $\%CV_{high}$, $\%CV_{med}$, $\%CV_{low}$, and inter-plate and inter-day fold shifts of the med signals, and are summarized in Table 3 for both enzymatic and cellular assays. The spatial intra-plate uniformity, evaluated by calculating the edge effect and drift within the same plate, achieved values ranged from 16% to 22% and 3% to 8%, respectively for the enzymatic assay and 7% to 28% and 3% to 7%, respectively for the cellular assay (Chai et al., 2015; Iversen et al., 2004). Within the uniformity test, the edge effects were more than 20% for some plates, with a mean ± SD of 19.5% ± 1.74% for the enzymatic assay and 17.8% ± 7.77% for the cellular assay. Therefore, wells on the edges of the plate (36 wells total) were not used for further studies. Eliminating the edge wells reduces the edge effect to 14.95 ± 5.12 for the enzymatic assay and 13.47 ± 4.70 for the cellular assay. Other methods, such as sealing membranes could also be used to reduce the edge effect further (Boehnke et al., 2016).

Z'-factor values for the high signals were above 0.5, with a Z'-factor range from 0.91 to 0.94 for the enzymatic assay and from 0.57 to 0.81 for the cellular assay, indicating that the assays measurement quality are within the excellent range. The range of %CV for the high, med and low (background) signals were from 1.1% to 2.0%, from 4.3% to 4.9%, and from 6.9% to 8.3%, respectively, for the enzymatic assay, and from 2.6% to 4.4%, from 2.0% to 5.9% and from 7.5% to 11.9%, respectively, for the cellular assay, all of which are below the acceptance threshold of 15% and 20%, respectively (Chai et al., 2015; Iversen et al., 2004). For the enzymatic assay, the inter-plate and inter-day fold shifts were all below the acceptance threshold of 2 (ranged from 1.0 to 1.6 and from 1.1

to 1.7, respectively). For the cellular assay, the inter-plate and inter-day fold shifts ranged from 1.0 to 1.1 and from 1.1 to 1.5, respectively. The metrics described above indicate this HT 3D MMP activity assay is reproducible and robust, making it well suited for screening applications.

Parameter	Enzymatic		Cellular		Formula
	Min - Max	Threshold	Min - Max	Threshold	
Intraplate					
Edge effect (%)					$\frac{Max.row\ mean_{med} - Min.row\ mean_{med}}{Overall\ mean_{med}} * 100$
With edge wells	16 - 22	≤ 20	7 – 28	≤ 20	
Without edge wells	11 - 22		6 - 19		
Drift (%)					$\frac{Max.column\ mean_{med} - Min.column\ mean_{med}}{Overall\ mean_{med}} * 100$
With edge wells	3 - 8	≤ 20	3 - 7	≤ 20	
Without edge wells	2 - 7		2 - 9		
Z'-Factor*	0.91 - 0.94	≥ 0.5	0.57 - 0.81	≥ 0.4	$\frac{(Mean_{high} - 3 * SD_{high}/\sqrt{n}) - (Mean_{low} + 3 * SD_{low}/\sqrt{n})}{Mean_{high} - Mean_{low}}$
CV_{high} (%)	1.1 - 2.0	≤ 15	2.6 - 4.4	≤ 20	$\frac{SD/\sqrt{n}}{Mean} * 100$
CV_{med} (%)	4.3 - 4.9		2.0 - 5.9		
CV_{low} (%)	6.9 - 8.3		7.5 - 11.9		
$SD_{med\ activity}$ (%)	4.2 - 5.1	≤ 15	3.1 - 10.8	≤ 20	$Med\ activity = \frac{S_{med} - Mean_{low}}{Mean_{high} - Mean_{low}} * 100$
Interplate, interday					
Fold shift between plates	1.0 - 1.6	≤ 2	1.0 - 1.1	≤ 2 For all plates	$(\frac{(100 - Med\ activity_{plate\ a}) * Med\ activity_{plate\ b}}{(100 - Med\ activity_{plate\ b}) * Med\ activity_{plate\ a}})^{\frac{1}{Slope}}$
Fold shift between days	1.1 - 1.7	≤ 2	1.1 - 1.5	≤ 2 For all days	$(\frac{(100 - Mean_{med\ activity\ day\ a}) * Mean_{med\ activity\ day\ b}}{(100 - Mean_{med\ activity\ day\ b}) * Mean_{med\ activity\ day\ a}})^{\frac{1}{Slope}}$

* n is number of replicates per concentration to be used in the application assay (triplicates here).
Three black round bottom 96-well plates were used each day for three consecutive days in an interleaved signal manner. For low, med and high signals in the enzymatic uniformity test, our functionalized hydrogels were incubated for 24 hr (37°C, 5% CO_2) in 0, 10 and 1000 µg/mL collagenase type I enzyme, respectively. n=32 for each signal level in each plate for a total of nine plates. For low, med and high signals in the cellular uniformity test, HT1080 cells (3 x 10^6 cells/mL) were encapsulated in the functionalized hydrogels and incubated for 24 hr (37°C, 5% CO_2) in 10 µM, 0.4 µM and DMSO control of broad spectrum MMP inhibitor GM6001, respectively. n=32 for each signal level in each plate for a total of nine plates.
CV, coefficient of variation; SD, standard deviation; Med, medium; Min, minimum; Max, maximum.

Table 3: High Throughput Assay Robustness, Reproducibility and Performance.

2.4.3 Assay Validation with Human MMPs and Encapsulated Cells

Bacterial collagenase was used in the characterization studies as a model enzyme due to its ease of use, requiring no activation step, and low cost. Collagenase is also often used for digestion assays since it is known to degrade ECM components such as type I collagen, from which the fluorescent MMP-degradable peptide and the crosslinker MMP-degradable peptide sequences (GPQG↓IWGQ) were derived from (Koblinski et al., 2002; Nagase & Fields, 1996; Nakatani, Tsuboyama-Kasaoka, Takahashi, Miura, & Ezaki, 2002).

To validate the ability of the assay to detect MMP activity, we utilized commercially available purified human MMPs. The fluorescent MMP-degradable peptide sequence (QGIW) has been characterized for specificity elsewhere, and was found to be cleaved by MMP-1, -2, -3, -7, -8, and -9 (Lutolf et al., 2003; Nagase & Fields, 1996; Patterson & Hubbell, 2010). Here, MMP-1, -2 and -9 were used for validation in the HT MMP assay. After enzyme activation, the functionalized hydrogels were incubated for 24 hr (37 °C, 5% CO_2) with each MMP and a broad spectrum MMP inhibitor (GM6001) or DMSO vehicle control. Fluorescence intensity of conditions incubated with MMPs were significantly higher than the controls containing no MMPs, and all conditions treated with GM6001 were significantly lower than those that were not treated with the inhibitor. Furthermore, treatment with GM6001 completely abrogated the increase in fluorescence induced by treatment with each MMP (Figure 14). The cleavage of the utilized fluorescent MMP-degradable peptide sequence here with MMP-1, -2 and -9 is consistent

with what has been reported in literature (Lutolf et al., 2003; Nagase & Fields, 1996; Patterson & Hubbell, 2010), and validates the detection of a variety of MMPs by the degradation of the fluorescent MMP-degradable peptide. The measured fluorescent intensity of the peptide incubated with human MMPs was greater than the background noise and within the working range of the assay (Figure 14). These results demonstrate that human MMPs produce signals that are detectable in the HT MMP assay.

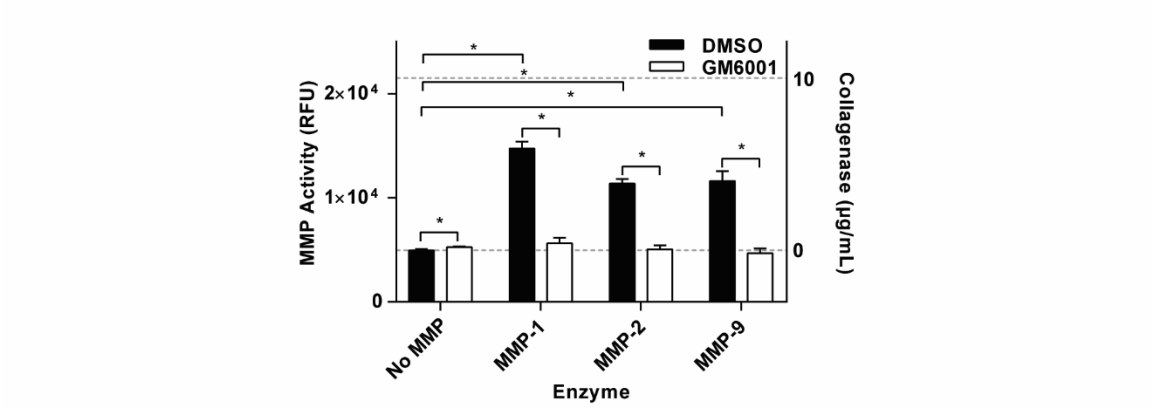

Figure 14: Functionalized hydrogel degradation with human MMPs. Fluorescent intensity of the functionalized hydrogels incubated with human MMP-1, -2 and -9 for 24 hr, with the broad spectrum MMP inhibitor GM6001 or DMSO vehicle control. Background and medium fluorescence intensities are represented with 0 μg/mL and 10 μg/mL of collagenase, respectively, and are plotted on the right Y axis of the graph, represented by dashed lines. n=3 ± SD, *$p<0.05$.

The assay was then characterized for measurement of MMP activity produced by encapsulated cells. Primary cells are often more sensitive to in vitro culture conditions than immortalized cell lines, therefore, two primary cell types, human mesenchymal stem cells (hMSCs) and human cervical fibroblasts (CFs), and one immortalized cell line, HT1080, were chosen to highlight the range of cell types compatible with this assay.

hMSCs are non-tumorigenic primary stem cells that play an important role in tissue regeneration and can be derived from a variety of tissues including bone marrow and adipose tissue. hMSCs are highly motile through ECM and basement membranes and are known to express a number of MMPs, including MMP-2 (Ries et al., 2007). hMSCs have also been observed to degrade PEG hydrogels crosslinked with the same peptide sequence used here, and to cleave a similar fluorescent MMP-degradable peptide to the one utilized in this work (Anderson, Lin, Kuntzler, & Anseth, 2011; Fairbanks, Schwartz, Halevi, et al., 2009; Leight et al., 2013). CFs are non-tumorigenic primary cells derived from human patients undergoing a hysterectomy. Cervical tissue is highly fibrous and undergoes extensive remodeling processes associated with pregnancy and birth, which involve MMP-2 and -9 production (Stygar et al., 2002). Finally, HT1080 cells are immortalized, highly metastatic fibrosarcoma cell line that have been observed to produce a high level of MMP activity (Bremer, Bredow, Mahmood, Weissleder, & Tung, 2001; Yodkeeree et al., 2008).

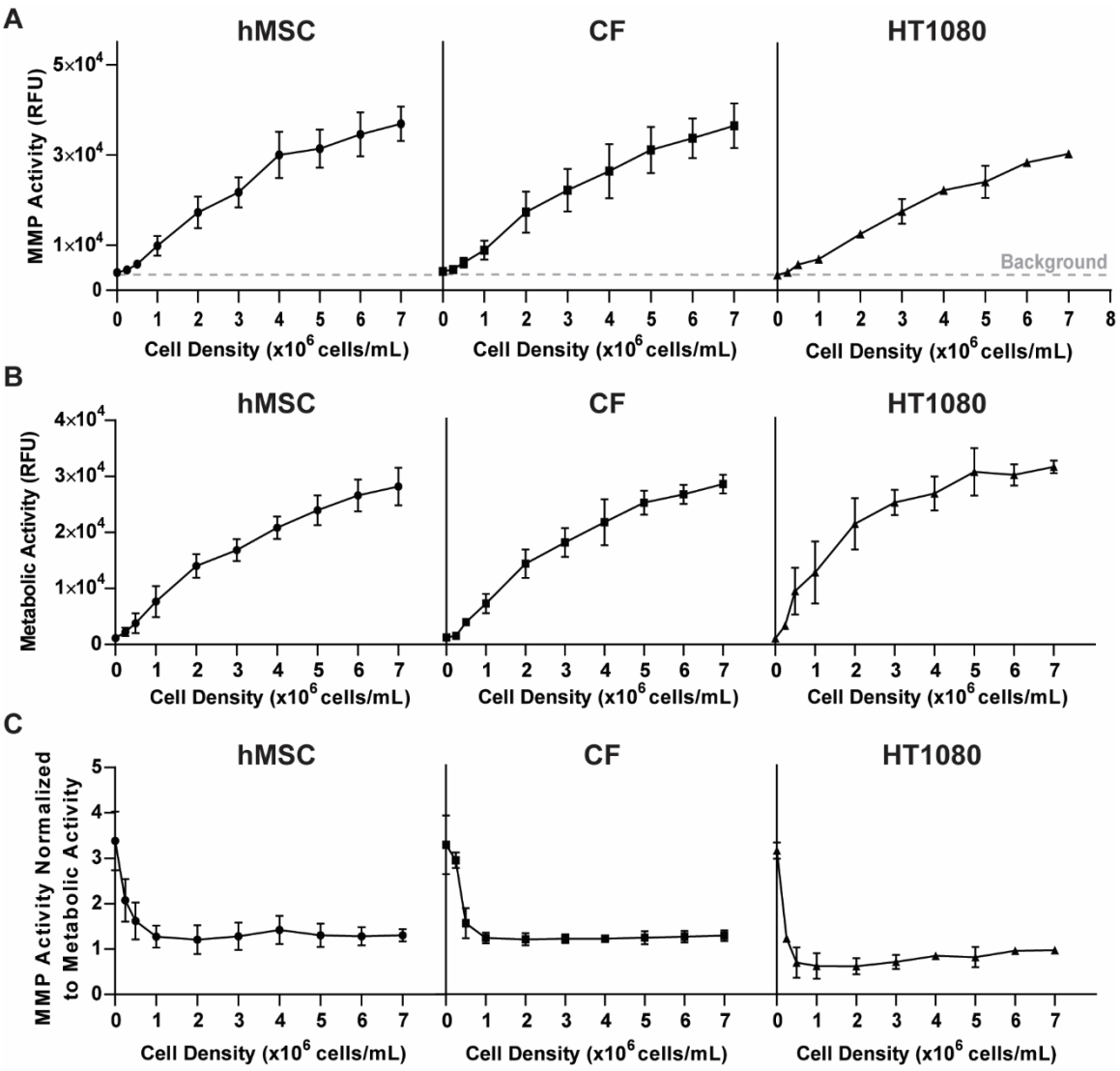

Figure 15: Effect of seeding density on MMP activity measurements for several cell types. (A) MMP activity of hMSCs, CFs, and HT1080 cells encapsulated over a range of seeding densities and incubated for 24 hr. Background noise represented by dashed lines. n=3 ± SD. (B) Metabolic activity of hMSCs, CFs, and HT1080 cells encapsulated over a range of seeding densities and cultured for 24 hr. n=3 ± SD. (C) hMSCs, CFs, and HT1080 MMP activity normalized to metabolic activity. n=3 ± SD.

To determine the seeding densities that are within the linear range of the assay and produce a signal greater than background noise, hMSCs, CFs and HT1080 cells were encapsulated over a range of densities (0.25 to 7 x 10^6 cells/mL), and MMP activity and

metabolic activity were measured (Figure 15A and 15B). The background noise was measured from control hydrogels without cells and is represented with a dashed line (Figure 15A). For hMSCs, CFs and HT1080 cells, the minimum seeding density which produced a detectable signal greater than the background noise of the assay was 0.5 x 10^6 cells/mL. MMP activity increased linearly with increasing the cell seeding density above 0.5 x 10^6 cells/mL. The end point of the assay is also important to determine if the selected seeding density is within the linear range of the assay. For example, encapsulating HT1080 cells at a seeding density of 2 x 10^6 cells/mL, the MMP activity signal was observed to increase linearly until 48 hr (the last time point measured) (Figure 16). However, the MMP activity signal began to plateau at 24 hr for HT1080 cells seeded at 6 x 10^6 cells/mL.

Metabolic activity was also proportional to the number of encapsulated cells within the range of cell seeding densities tested (Figure 15B). Previously, metabolic activity has been used as an internal control to determine MMP activity on a "per cell" basis (Leight et al., 2013). Normalizing MMP activity to metabolic activity resulted in no change across seeding density at densities greater than 0.5 x 10^6 cells/mL (Figure 15C). This is important to define the appropriate seeding densities for the assay, which are the densities that are above the minimal detectable density (0.5 x 10^6 cells/mL) yet are also within the linear portion of the normalization curve (Figure 15C). For the cell types tested here, seeding densities between 2 and 6 x 10^6 cells/mL would be appropriate. Each condition was plated in in triplicate and repeated for n=3 experiments. As illustrated here (Figure

15C), the appropriate cell density required to be within the linear range of the assay can vary by cell type, therefore, to have a signal within the linear range of the assay, cell type, cell seeding density, and time point of the final measurement need to be determined experimentally.

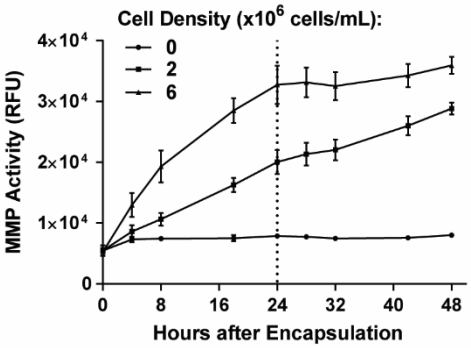

Figure 16: Time course of HT1080 cells. Measurement of MMP activity for HT1080 cells encapsulated in two seeding densities (2 and 6 x 10^6 cells/mL) and incubated for 48 hr. n=3 ± SD.

2.4.4 High Throughput Assay Biosensor Modularity

While one fluorescent MMP-degradable peptide was used in the preceding sections, the assay and methodology are not sensor specific and are amenable to other fluorescent reporter molecules. The use of other degradable substrates would enable the detection of other MMPs or proteolytic sub-groups beyond MMPs, such as serine, threonine, or cysteine proteases. The HT assay described above was developed, characterized and validated, utilizing (QGIW) MMP-degradable peptide, which is cleaved by MMP-1, -2, -3, -7, -8, and -9 (Lutolf et al., 2003; Nagase & Fields, 1996; Patterson & Hubbell, 2010). The assay was also characterized using a different degradable peptide sequence, GPLA↓C(pMeOBzl)WARKDDK(AdOO)C (↓ indicates the cleavage site) (abbreviated

as LACW) that was previously optimized for cleavage by MMP-14 and MMP-11 (Mucha et al., 1998). The exchange of the MMP-degradable peptide, which is a replacement of a single reagent in the hydrogel precursor solution, offers an easy alteration of the detection specificity of the 3D HT assay, demonstrating the flexibility of the developed 3D HT assay for other applications. To establish the detection limits and signal range of the LACW assay fluorescent MMP-degradable peptide, the functionalized hydrogels were incubated with a range of concentrations (0 to 2000 μg/mL) of bacterial collagenase enzyme type I. After 24 hr of incubation at 37 °C, a plate reader was used to measure the fluorescence (Figure 17). From these measurements, the dynamic and working range were determined. After 24 hr of incubation, it was observed that the lowest detected signal was produced by negative controls (background noise) at 0 μg/mL collagenase, while the highest detected signal was produced by 1000 μg/mL collagenase or above, where the signal begins to plateau (Figure 17). From the dynamic range, the working range was calculated to be between ≈0.16 μg/mL and ≈474 μg/mL of collagenase, a wide signal range across three orders of magnitude. While QGIW and LACW had very similar wide signal detection range ≈ 0.02 to ≈ 575 μg/mL and ≈ 0.16 to ≈ 474 μg/mL of collagenase enzyme, respectively, QGIW is more sensitive by detecting less amount of collagenase and had wider working range. Such an example highlights the importance of establishing the detection limits and signal range for every biosensor replacement.

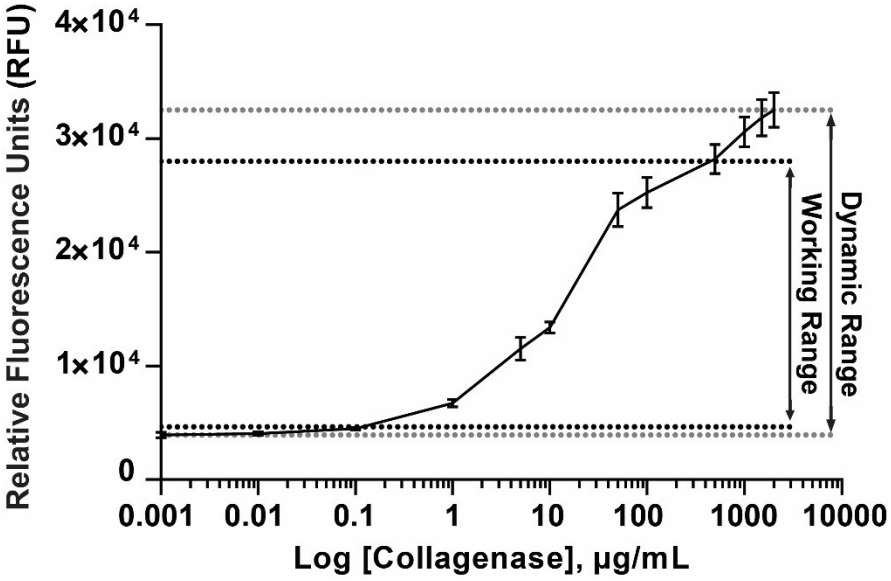

Figure 17: Dynamic and working range of the assay with LACW fluorescent MMP-degradable peptide. Hydrogels functionalized with LACW fluorogenic MMP-degradable peptide were incubated with a range of concentrations of collagenase enzyme type I for 24 h at 37 °C and fluorescence intensity was measured. Dotted lines represent the dynamic and working range. n = 3, mean ± SD.

For cell culture assays, we utilized the melanoma cell line A375s, and conducted a cell density experiment to determine the seeding densities within the working range of the assay. A375s were encapsulated across a range of densities from 0.25 to 7 x 10^6 cells/mL. Fluorescence intensity was acquired utilizing a standard microplate reader at two different time points: 1) directly after encapsulation (0 hr) and 2) after 24 hr of encapsulation. At 0 hr, fluorescence readings were low across seeding densities (Figure 18A), as expected. After 24 hr of culture (Figure 18B), MMP activity was proportional to the seeding density, in which more cells resulted in more cleavage of the LACW fluorogenic MMP cleavable sensor and higher fluorescence intensity. As internal controls, hydrogels containing no cells were incubated with 0, 10, and 1,000 µg/mL of

collagenase type I enzyme to indicate the low, medium and high levels of the signal respectively (as determined by the collagenase signal range characterization in Figure 17) and represented by dashed lines in Figure 18B. Further, the working range limits were calculated from the 0 and 1000 µg/mL signals and represented by dotted lines in Figure 18B. Seeding densities at or greater than 1 x 10^6 cells/mL fall within the limits of the working range. Metabolic activity measurements of the A375 cell line were also proportional to the cell seeding density (Figure 18C). Previously, MMP activity has been normalized to metabolic activity as an internal control to determine MMP activity on a per cell basis (Leight et al., 2013). Normalizing MMP activity to metabolic activity across seeding densities resulted in no significant difference in MMP activity at seeding densities greater than 2 x 10^6 cells/mL (Figure 18D).

The cell density that results in fluorescence readings within the working range of the assay will be peptide and cell type dependent, therefore the linear portion of the normalization curve must be determined for each new combination by conducting an encapsulation density optimization experiment as demonstrated here. Additionally, the timing of the fluorescent measurements can affect the signal range. In the above experiments, after 24 hr of encapsulation, MMP and metabolic activity were directly proportional to cell seeding density. However, at longer times the fluorescent signal can plateau, therefore the timing of the assay may have to be optimized by the user (Leight et al., 2013). The specific protease sensor can also affect the working range and timing of the assay. The working range of the assay can be determined by conducting a signal

range experiment with no cells and a proteolytic enzyme over a wide concentration. Inclusion of several no cell hydrogel conditions incubated with enzyme controls enables establishment of the low (background noise), medium and high levels of signal within each assay (0, 10 and 1000 μg/mL of collagenase here). This gives an indication of where the signals produced by cells fall within the working range of the assay. This assay is also compatible with other fluorescent sensors that do not have overlapping excitation and emission spectra, such as the metabolic activity assay used here as an internal control to calculate MMP activity on per cell basis, as previously reported (Leight et al., 2013). MMP activity normalized to metabolic activity demonstrated the validity of this approach for seeding densities at or above 2 x 10^6 cells/mL, in which there was no significant change across seeding densities. This normalization is crucial to identify the appropriate seeding densities that are within the working range of the MMP activity curve and within the linear portion of the normalization curve.

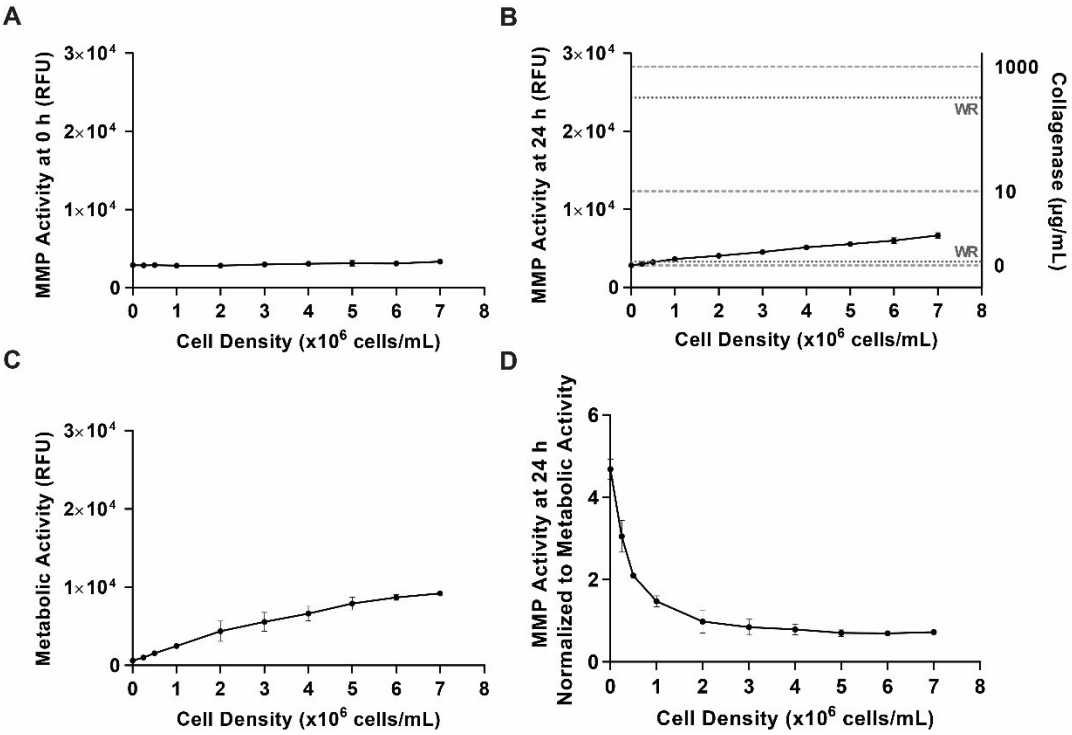

Figure 18: Effect of seeding density of melanoma cell line A375 on MMP activity. (A) Initial measurement (0 hr) of MMP activity for A375 cell line encapsulated over a range of seeding densities. n = 3 mean ± SD. (B) Measurement of MMP activity at 24 h. 0, 10 and 1000 µg/mL of collagenase are represented by dashed lines. Dotted lines represent the working range (WR) calculated from collagenase controls. n = 3, mean ± SD. (C) Measurement of metabolic activity for A375 cell line encapsulated for 24 h over a range of seeding densities and incubated with resazurin for 6 hr. n = 3, mean ± SD. (D) A375 MMP activity normalized to metabolic activity. n = 3, mean ± SD.

2.4.5 Effect of Drug Treatment on MMP Activity of the Fibrosarcoma Cell Line HT1080

To determine the feasibility of the newly developed assay for drug screening applications and to observe the effects of chemotherapeutics on MMP activity, we treated HT1080 cells with several drugs over a range of concentrations. While HT1080 cells have been

previously shown to express high levels of MMPs, it is not known how drug treatment affects MMP activity in fibrosarcoma cells.

Here, several clinically used drugs with different mechanisms of action were chosen to investigate their effect on MMP activity. SOR, which has been used in clinical trials to treat fibrosarcoma ("Sorafenib in Treating Patients With Metastatic, Locally Advanced, or Recurrent Sarcoma - Study Results - ClinicalTrials.gov," n.d.), is a small molecule multi-kinase inhibitor that arrests cancer cell growth, invasion and migration (Ha et al., 2015). SOR targets RAS/RAF kinases (Boespflug, Caramel, Dalle, & Thomas, 2017), and therefore may have an effect on the HT1080 cell line which is known to have an N-RAS mutation (Geiser, Anderson, & Stanbridge, 1989; Hall, Marshall, Spurr, & Weiss, 1983). SOR has also been found to decrease the expression of MMPs in hepatocellular carcinoma cells (Chiang et al., 2012; Ha et al., 2015). PAC inhibits mitosis through depolymerization of microtubules and has been shown to decrease HT1080 tumor growth in mice (Grant, Williams, Zahaczewsky, & Dicker, n.d.; Vanhoefer, Cao, Harstrick, Seeber, & Rustum, 1997; Weaver, 2014). In human melanoma cells, PAC has previously been found to decrease the secretion of MMP-2 and -9 (Schnaeker et al., 2004). GEM is a fluorinated nucleoside analogue that replaces deoxycytidine to arrest DNA replication and induce apoptosis (Maki, 2007). However, in contrast to the increased MMP activity observed with SOR and PAC, no significant changes in MMP-2 expression levels were observed in pancreatic cell lines treated with GEM (Yang & Kurkinen, 1998). PAC and

GEM have been used in the clinic to treat soft tissue sarcomas ("Treatment of Soft Tissue Sarcomas, by Stage," n.d.).

HT1080 cells were encapsulated in hydrogels, functionalized with the QGIW MMP-degradable peptide, at a density of 3 x 10^6 cells/mL and treated with SOR, PAC, GEM or DMSO vehicle control at 0.5% (v/v), over a range of concentrations (0.01 – 50 μM dissolved in DMSO then diluted in assay media) for 24 hr, for a total of 25 conditions and 75 wells. To replicate the same number of wells in the previous 24-well plate format, it would have required 3 plates and two additional hours for the experimental set up. Overall MMP activity was not significantly different than the vehicle controls throughout the range of concentrations used for each drug (Figure 19A).

Drug treatment can also affect cell viability and cell number, therefore a metabolic activity assay was performed simultaneously in the same wells with the MMP activity assay. Metabolic activity, while not a direct measurement of cell number or cell viability, is commonly measured in drug screening assays as an overall indicator of cellular health as these assays are easy to use and inexpensive. Tetrazolium salts assays (3-(4,5-dimethylthiazol-2-yl)-2,5-diphenyltetrazolium bromide) (MTT) and (3-(4,5dimethylthiazol-2-yl)-5-(3-carboxymethoxyphenyl)-2-(4-sulfophenyl)-2H-tetrazolium) (MTS) are the most common metabolic activity assay used to detect cellular viability, cytotoxicity and proliferation in HT drug screenings (Haas et al., 2017; Sekhon, Roubin, Tan, Chan, & Sze, 2008). Here, resazurin, which fluoresces when oxidized by

cellular mitochondria, was chosen to measure metabolic activity because the excitation (560 nm) and emission wavelength (590 nm) are sufficiently separated from the fluorescein signal of the MMP sensor to enable measurement of both MMP activity and metabolic activity within the same well using a standard plate reader (Leight et al., 2013, 2015). In addition, previous work with pancreatic cancer cells and a panel of chemotherapeutics has demonstrated that resazurin produces comparable results to viability staining using calcein AM with no significant difference in the 50% inhibition concentration (IC_{50}) between both methods (Shelper et al., 2016). Metabolic activity of HT1080 cells was significantly reduced as compared to vehicle controls with SOR at 5, 10 and 50 μM and PAC at 50 μM (Figure 19B). No significant effect on metabolic activity was observed with GEM. For SOR treatment, metabolic activity was reduced in a dose dependent manner, and a similar trend is observed with PAC treatment for concentrations above 10 μM.

To control for changes in cell viability with drug treatment and determine cellular MMP activity on a "per cell" basis, the MMP activity of each sample was normalized to its metabolic activity (Figure 19C). HT1080 cells treated with high concentrations of SOR (10 and 50 μM) had significantly higher MMP activity per cell compared to vehicle controls, but not cells treated with PAC or GEM. Although the metabolic activity was significantly less than vehicle control at 5 μM of SOR (Figure 19B), MMP activity was not significantly different than vehicle control on a per cell basis (Figure 19C). Similarly, with PAC treatment at 50 μM, metabolic activity was significantly less than vehicle

control (Figure 19B), but there was no significant difference in MMP activity on a per cell basis (Figure 19C). In previous studies with melanoma cells, utilizing a similar fluorescent MMP-degradable hydrogel system, conditions in which drug treatment upregulated MMP activity also increased 3D cell migration (Leight et al., 2015). Further investigation will be needed to determine if the increased MMP activity with SOR treatment observed here also regulates fibrosarcoma cell invasion and migration, cell functions critical to tumor progression and metastasis.

The system developed here measures global MMP activity and metabolic activity simultaneously in response to variety of compounds. To follow up on promising leads, these measurements could be complemented by further studies, such as cell viability experiments or to explore the mechanisms of action by which the drugs affect MMP or metabolic activity. A metabolic activity reagent (resazurin) was utilized here as an overall cell health indicator, other assays could be used to directly measure cellular viability such as live/dead staining assays with calcein AM and ethidium homodimer. MMP activity is regulated at multiple levels (i.e. expression, secretion, pro-enzyme cleavage and endogenous inhibitors), and future explorations could be targeted at determining which of these levels are modulated to affect final MMP activity.

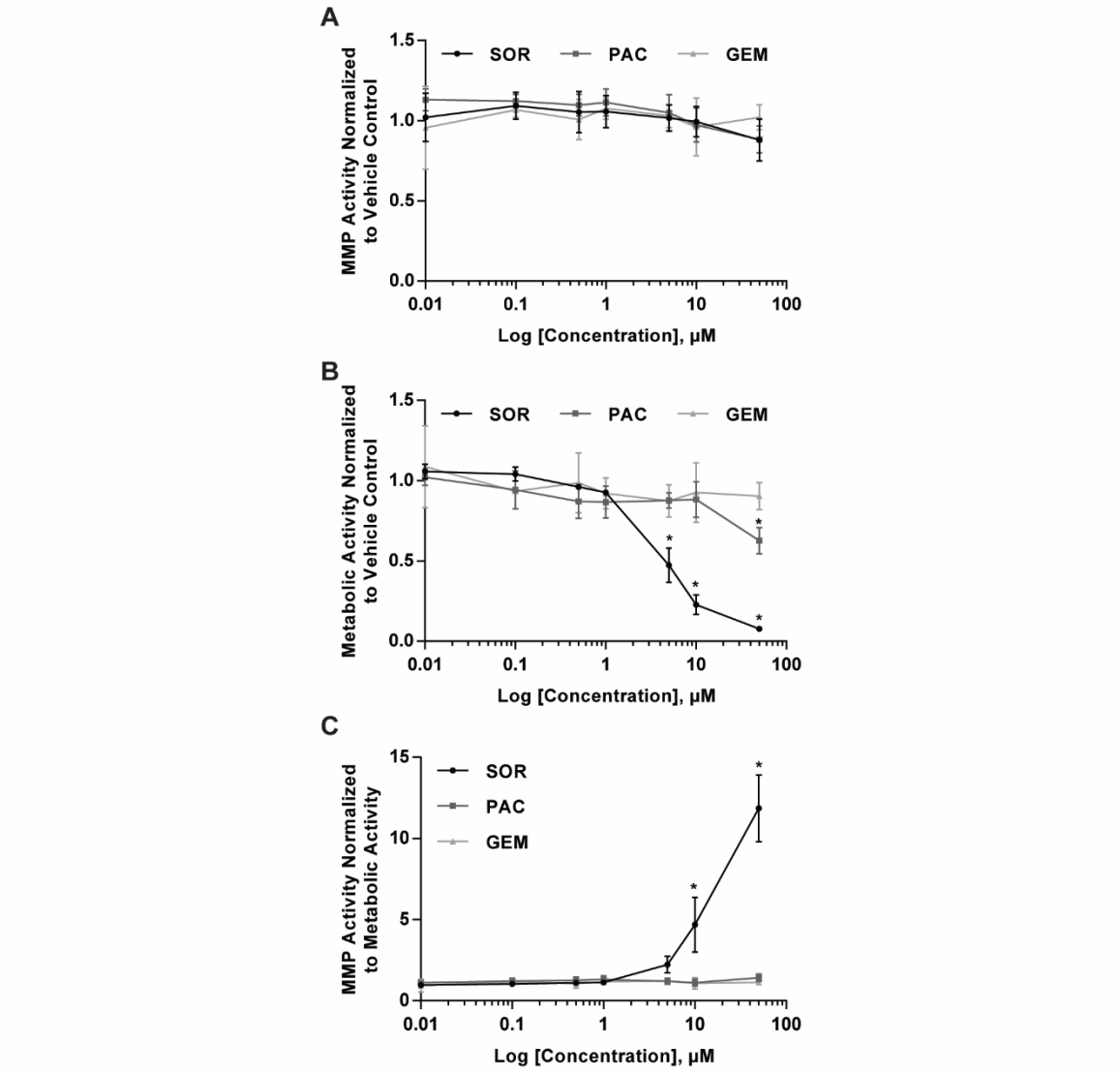

Figure 19: Effect of drug treatment on MMP activity of the fibrosarcoma cell line. HT1080 cells were encapsulated and treated with a range of concentrations (0.01 to 50 µM) of each drug and incubated for 24 hr. Resazurin was added 6 hr prior to the 24 hr read. (A) Measurement of MMP activity normalized to the vehicle control of encapsulated cells treated with SOR, PAC and GEM. n=3 ± SD, no significance compared to the vehicle control. (B) Measurement of metabolic activity normalized to the vehicle control for encapsulated cells treated with SOR, PAC and GEM. n=3 ± SD, *$p<0.05$, compared to the vehicle control. (C) MMP activity normalized to metabolic activity for encapsulated cells treated with SOR, PAC and GEM. n=3 ± SD, *$p<0.05$, compared to the vehicle control.

While the assay can be adapted for several purposes, there are several limitations and critical aspects the user should consider, specifically regarding interference with the fluorescent signal and preparation of the hydrogels. First, care must be taken with the choice of culture media and additional treatments, as these can have an overlapping absorbance spectrum or opaqueness that may interfere with the detection of fluorescence or quench the signal. It is recommended to use culture media that does not contain phenol red. Also, some drug treatments are fluorescent (e.g., doxorubicin) (Figure 20A), or have absorbance spectrum that overlaps with the excitation/emission spectrum of the fluorophore (e.g., curcuminoids) (Figure 20B). A second aspect that can affect the performance of the assay is the hydrogel preparation. Because of the high viscosity of the hydrogel precursor solution, care needs to be taken to ensure thorough mixing of the hydrogel solution and careful pipetting practices to prevent unequal fluorophore content or hydrogel solution volume in each well. Pre-wetting of the pipette tips and using low-retention tips can help reduce variability. Another important aspect of hydrogel preparation is the hydrogel shape and location in wells. The hydrogel should be centered within the well and of a uniform shape to enable accurate fluorescence measurements with less variability (Mabry et al., 2016). Here, the use of round bottom plates aids in centering the pipette tip in each well and the production of semi-spherical hydrogels consistently across all wells.

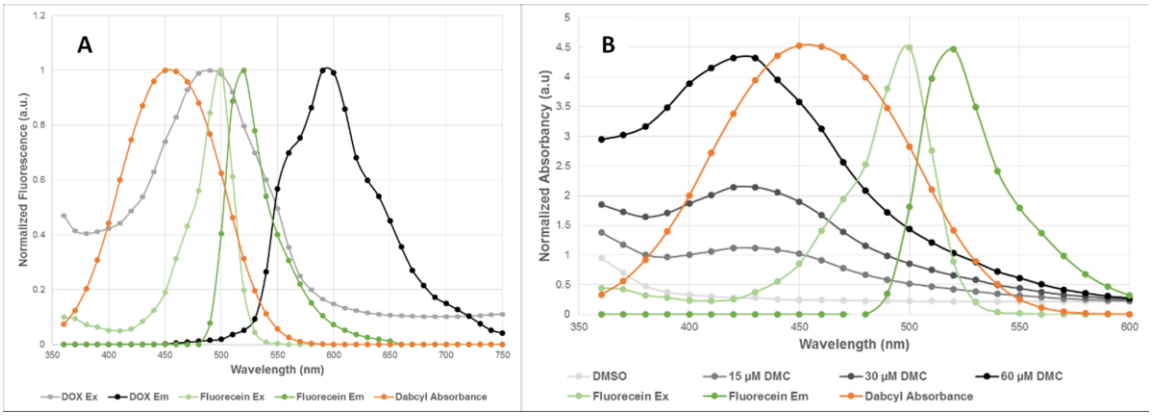

Figure 20: Fluorescence interference. (A) Fluorescence spectrum of doxorubicin (DOX) at 100 µM and (B) absorbance spectrum of demethoxycurcumin (DMC), a curcumin derivative, in a dosage dependent manner compared to fluorescein Ex/Em and dabcyl absorbance, which are utilized as the fluorophore / quencher pair in our peptides. Fluorescein Ex/Em and dabcyl absorbance data points were exported from Fluorescence SpectraViewer at https://www.thermofisher.com/us/en/home/life-science/cell-analysis/labeling-chemistry/fluorescence-spectraviewer.html.

Utilizing synthetic PEG as a hydrogel biomaterial offer several advantages. PEG hydrogel reduces the batch-to-batch variability observed with naturally derived ECM hydrogels. Furthermore, using PEG hydrogels enables precise independent tuning of the cellular microenvironment, including the mechanical properties, the degradability, and the matrix adhesion moieties within the hydrogel. The adhesion molecule RGD used in this work is a fibronectin-derived sequence and enables integrin-mediated adhesion. Other adhesion molecules such as (RLD) and (IKVAV) that are derived from fibrinogen and laminin respectively could be utilized to activate other types of integrin receptors. For example, it was demonstrated that altering the adhesion molecules changed the elongation of aortic valvular interstitial cells (VIC), which may have an effect on aortic

valve stenosis (Mabry et al., 2016). The hydrogel crosslinker sequence tunes the degradability of the hydrogel and encapsulated cellular behavior within the hydrogel. For example, it was demonstrated that fibroblasts had increased proliferation and cell spreading when cultured in faster degrading hydrogels, which may expedite the healing process *in vivo* (Patterson & Hubbell, 2010). Mechanical properties of the microenvironment can also regulate cell function, and hydrogel stiffness can be modified by altering the number of arms in the PEG macromer, PEG molecular weight and the ratio between PEG and crosslinker. Moreover, the PEG hydrogel polymerization described here is a photo-initiated process, making it quick and more amenable to high throughput methodologies than classic natural ECM hydrogels (i.e*.,* collagen or Matrigel), which are slower and temperature sensitive. This quick, user-controlled polymerization allows the scaling-up of the system to be further automated using robotic liquid handlers, as demonstrated by others (Mabry et al., 2016).

2.5 Conclusion

MMPs are critical regulators of cancer progression, and assays that can measure MMP activity will be critical in the development of new therapeutic strategies. While MMP activity detection systems such as gelatin zymography are well established and widely used, these systems have not been compatible with HT approaches. Therefore, developing an MMP activity detection system that is suitable for HT, and combines simplicity, adaptability and ease of access to other researchers will be valuable. To this end, a 3D low throughput MMP activity assay was miniaturized to a 96-well plate format

and characterized for reproducibility and robustness. The assay was validated with human MMPs and several cell types. A fibrosarcoma cell line was treated with several chemotherapeutic drugs in a range of concentrations to demonstrate the ability of this assay to measure MMP activity in response to drug treatment. Interestingly, it was found that SOR increased MMP activity per cell in a dose dependent manner. While a specific fluorescent metalloproteinase-degradable peptide was used here, the assay and methodology are not sensor specific and would be amenable to the incorporation of other fluorescent reporter molecules. The use of other degradable substrates would enable the detection of other MMPs, as demonstrated earlier with LACW MMP-degradable peptide, or proteolytic sub-groups beyond MMPs, such as serine, threonine, or cysteine proteases. In addition, although, the system was demonstrated here for single cell encapsulation, the system could likely also be adapted for the encapsulation of 3D spheroids, such as those produced by the hanging drop method or with low attachment plates.

2.6 Acknowledgment

The authors would like to acknowledge Ohio Cancer Research (OCR), OH, USA for funding this work as well as King Saud University (KSU), Riyadh, KSA for sponsoring the first author. Molecular weight of the fluorescent peptide sensor was measured using matrix assisted, laser desorption-ionization, time-of-flight (MALDI-TOF) mass spectrometry with assistance from the Campus Chemical Instrument Center Mass Spectrometry and Proteomics Facility at The Ohio State University.

Chapter 3. High Throughput Assay Utilization: *Ex Vivo* Tissue Samples Encapsulation**

3.1 Introduction

Since the early 1900s, 2D culture platforms (glass or plastic dishes) have been the standard culturing platform for cells and tissue. 2D culturing platforms are economical and well-established and enabled the study of cellular responses and functions. 2D culturing platforms are simple, efficient and scalable, therefore, they are widely used in HT drug development. However, 2D systems lack critical cues of the *in vivo* microenvironment, such as soluble gradients, 3D cell-cell and cell-matrix interaction (Baker & Chen, 2012; Duval et al., 2017; Hoarau-Véchot et al., 2018), which may have significant effects on cellular responses to treatments. Therefore, a number of 3D culturing microenvironments and tumor spheroids have been developed to recapitulate some of the *in vivo* cellular response to treatment. Indeed, they have been able to recapitulate some of the encountered cellular responses *in vivo* such as drug resistance (Anand et al., 2015; Kinoshita et al., 2018; Wen et al., 2013). However, isolated cell lines were used that lack tumor heterogeneity and natural microenvironment encountered *in vivo*.

** Contributions to this chapter were as following: Fakhouri, A. – Experimental design, conduction and data analysis (tissue samples encapsulation optimization, viability assessment, and MMP and metabolic activity measurements). Dissertation preparation and writing. Leight, J. – Experimental design and data analysis. Dissertation editing. Weist, J.- Experimental design, conduction and data analysis (tissue samples encapsulation optimization, viability assessment, and MMP and metabolic activity measurements). Yee, L. – provided FNAB and tissue dissections samples from patients undergoing surgeries.

To maintain the tumor heterogeneity observed *in vivo*, patient derived xenografts (PDX) models are utilized. Patient derived xenografts are cancerous tissue that is taken from patients then implanted and expanded in immunodeficient mice, in which treatments are tested *ex vivo* to better recapitulate the complexity and heterogeneity of the disease (Lai et al., 2017). PDX models have many advantages, such as maintaining phenotype, genotype, and molecular characteristics, eliminating cellular selection, and reflecting the tumor pathology. Researchers were able to maintain biological stability, molecular characteristics, genetic mutations and treatment responses of pancreatic, colorectal and gastric cancers in PDX models similar to their parental patient-derived tumors (Seol et al., 2014; Tignanelli et al., 2014; T. Zhang et al., 2015; Zhu et al., 2015). However, PDX models have some limitations. It was observed that PDX tumor cells undergo mouse-specific tumor evolution during passaging, in which PDX tumor cells were genetically different than their parental tumors across 24 cancer types (Ben-David et al., 2017). Add to this, the success rate of tumor engraftment is as low as 25% for some cancers such as breast cancer (Naipal et al., 2016). PDX models are expensive, time consuming, labor intensive and have long turnaround time (months) to produce results. Although, PDX models provide superior mimic, improving the prediction of clinical responses, PDX models are not practical to be utilized for HT drug testing applications.

An alternative relatively faster approach known as organotypic slice culture is utilized. Organotypic slices are tissue slices that have been precisely cut from tumor samples at microscale thickness and cultured on a porous surfaces that allows oxygen and nutrient

exchange (Meijer et al., 2017). Organotypic slice culture have similar advantages to PDX models, such as preserving parental tumor heterogeneity, pathology, microenvironment and treatment response, but in a cheaper and shorter turn-around time (days) (Meijer et al., 2017; Naipal et al., 2016). For example, *ex vivo* organotypic culture of non-malignant human prostate maintained viability of glandular epithelial, stromal and endothelial cells. Further, architecture and differentiated phenotype were preserved similar to human *in vivo* prostatic tissue (Bläuer, Tammela, & Ylikomi, 2008). To demonstrate organotypic culture compatibility with drug testing studies and similar treatment response to *in vivo*, several tumors were successfully cultured in a relatively fast process, producing outcomes similar to *in vivo*. For example, head and neck squamous cell carcinoma organotypic culture, cultured for 6 days, preserved their histopathological features, formed apoptotic fragments, and caspase 3 was activated when treated with cisplatin, docetaxel and cetuximab (Gerlach et al., 2014). Additionally, glioblastoma multiforme were derived from patients' samples, sectioned and cultured in minutes, preserving native tumor histopathology for 16 days *in vitro*. Further, caspase 3 was activated, and DNA double strands were damaged in response to temozolomide and irradiation, respectively (Merz et al., 2013). Such examples demonstrate the ability of organotypic slices to live in culture *in vitro*, and to produce measurable outcomes for individual tumors. Indeed, organotypic slices provide an alternative *ex vivo* model to measure cellular functions in a relatively fast manner, while maintaining native tumor heterogeneity, architecture and pathology (Naipal et al., 2016). However, organotypic slices suffer from several limitations, such as hypoxia and low throughput outcomes. Due to lack of intact

vascularity and relatively thick slices, oxygen depends on diffusion to reach inner portions of the slice. Hypoxia usually develops in inner portions, making long time culturing a challenge (Meijer et al., 2017). Organotypic slices provide limited number of samples, are delicate, labor intensive, and require non-automated specialized analytical tools for data acquisition and quantification (Naipal et al., 2016). Such drawbacks make this technology a low throughput model not suitable for drug screening and development. Therefore, there is a need for a technology that combines HT 2D culture advantages, such as efficiency and having large number of samples, and close recapitulation of *in vivo* responses similar to PDX and organotypic slices.

Another approach to closely represent *in vivo* responses is known as patient-derived organoids, a simpler and more efficient approach, which is more amenable to HT applications than PDX models or organotypic slices. In patient-derived organoids, patient samples are digested with proteases such as collagenase, dispase or trypsin, then single cells are cultured to form organoids (multicellular structure) after incubation for couple of days (Boehnke et al., 2016; Kruitwagen et al., 2017; Pauli et al., 2017). *Ex vivo* cultured patient-derived organoids from human, mouse, cat and dog accumulated lipids, similar to *in vivo*, modeling diseases such as hepatic steatosis (fatty liver). Tissue samples, retained their morphology between passages *ex vivo* for 5 days, demonstrating the ability of organoids to maintain tissue viability in *ex vivo* culture conditions. Additionally, organoids demonstrated the ability to represent *in vivo* diseases for *ex vivo* studies, such as β-oxidation effects on lipid accumulation in feline liver organoids (Kruitwagen et al.,

2017). Several studies have cultured *ex vivo* patient-derived organoids in 3D environments, such as hydrogels, demonstrating the suitability of such technique for HT drug screening applications. For instance, patient-derived colon cancer organoids were formed *ex vivo* in Matrigel by an automated workflow, and 384-well plate robustness and reproducibility were confirmed for HT drug screening (Boehnke et al., 2016). Moreover, two uterine malignancies and two colon cancer tissue samples were derived from patients, cultured in *ex vivo* 3D Matrigel and a HT dose-response drug screen including 160 drugs was conducted and validated with 3D culture and PDX model (Pauli et al., 2017). Clearly, patient-derived organoid assays are amenable to HT applications, yet, cells were initially isolated and native tissue structure was disturbed, which are factors that may affect cellular responses.

To this end, we aimed to bridge the gap between efficient HT 2D drug screening platforms and the closer representation of PDX and organotypic slices models to *in vivo*, by optimizing the previously developed HT 3D hydrogel assay as a culturing platform for patient-derived tissue samples without sample processing or digestion. As a proof of concept, healthy adipose fine needle aspirate biopsies (FNAB) and tissue dissections were derived from breast cancer patients undergoing lumpectomy or mastectomy surgeries for cancer treatment and cultured in the MMP sensitive HT 3D hydrogel assay. Viability of FNAB and tissue dissections utilizing commercial viability/cytotoxicity staining was determined after minimal sample processing and 24 hr of encapsulation.

Finally, MMP and metabolic activity of FNAB and tissue dissections were measured in relation to encapsulated tissue size.

3.2 Materials and Methods

3.2.1 Human Adipose FNAB and Tissue Dissections Preparation

FNAB and larger tissue dissections (~2 cm^3) samples of healthy breast adipose tissue were obtained from consented patients (IRB #1999C0262) undergoing breast lumpectomy or mastectomy surgeries. FNAB (aspirated using 21 or 25 gauge needle) and tissue dissection samples were received immersed in PBS. FNAB tissue samples were rinsed with PBS 1 to 2 times then ~100 to 400 µL of PBS was added to suspend FNAB tissue samples. Tissue dissections were bluntly dissected from the bulk sample with a pair of tweezers into small (~1.5 mm), medium (~2.5 mm) and large (~4.0 mm) diameter tissue dissections.

3.2.2 FNAB and Tissue Dissections 3D Encapsulation

A hydrogel precursor solution consisting of 20 mM 8 arm 40 kDa PEG-NB (PEG-NB functionalization mentioned in chapter 2), 17.8 mM NaOH, 12.75 mM crosslinker MMP-degradable peptide (thiol:ene ratio of 0.7), 1 mM CRGDS, 2 mM LAP, and 0.25 mM fluorescent MMP-degradable peptide (GGPQG↓IWGQK(AdOO)C) (QGIW) (fluorescent MMP-degradable peptide synthesis mentioned in chapter 2) in PBS (Life Technologies™, Carlsbad, CA) was briefly vortexed. For FNAB encapsulation, 5.46 µL of the hydrogel precursor solution, without PBS addition, was pipetted into clear, round

bottom, 96-well plates using a pipette. Pre-washed FNAB tissue samples supernatant was pipetted over the hydrogel precursor solution utilizing a wide mouth tip at 1.14, 2.27 and 4.54 µL, and pipetted up and down to have a homogenous mixture. PBS was added to complement the volume of the final hydrogel precursor solution to 10 µL/well. For tissue dissections encapsulation, 10 µL/well of the hydrogel precursor solution, with PBS added, was pipetted into clear, round bottom, 96-well plates using a pipette. Tissue dissections were immersed in the 50 µL hydrogel precursor solution utilizing previously developed protocol (Leight et al., 2013). For hydrogels without tissue (controls), 10 µL of the hydrogel precursor solution, with PBS added, was pipetted into each well. For viability test, tissue samples were encapsulated in hydrogels without the addition of the fluorescent MMP-degradable peptide. Hydrogel polymerization was photoinitiated by exposure to 365 nm UV light (UVP, model UVL-56, Cambridge, UK) at 4 mW/cm^2 for 3 minutes. After polymerization, 150 µL of assay media (high glucose DMEM) (Life Technologies™) supplemented with 1% charcoal stripped FBS (charcoal stripping and heat inactivation of FBS mentioned in chapter 2) (Seradigm, Radnor, PA), 2 mM L-glutamine, 10 U/mL penicillin and 10 µg/mL streptomycin (Life Technologies)) was added to each sample well. PBS was added to the outermost and empty wells, and the moat between wells to reduce sample evaporation. Plates were incubated (at 37 °C and 5% CO_2) for 24 hr. 1:10 v/v of resazurin (alamarBlue™, Life Technologies) was added to the wells containing encapsulated tissue 6 hr prior to the final fluorescence well scan reading.

3.2.3 MMP and Metabolic Activity Measurement

Fluorescence measurements of MMP and metabolic activity were acquired using a SPECTRA Max M2 microplate reader (Molecular Devices, San Jose, CA) at 494 nm / 521 nm (excitation/emission) for the fluorogenic peptide and 560 nm / 590 nm for the metabolic reagent, alamarBlue™. An area scan was performed using the clear 96-well plate setting with a 3x3 matrix, and the average of each matrix was calculated (Fakhouri & Leight, 2019).

3.2.4 Nuclei Staining and Viability Assay Preparation

Tissue samples at different time points were tested, after encapsulation and sample processing, and after 24 hr of incubation in non-fluorescent hydrogels. To stain tissue samples nuclei, Hoechst 33342 (Invitrogen, Eugene, OR) was added to samples at 8 µM and incubated for 15 minutes. Commercial fluorescent viability/cytotoxicity staining with calcein AM (live) and ethidium homodimer (EthD-1) (dead) (Invitrogen™, Grand Island, NY) was utilized. Samples were washed with 200 µL of PBS 3 times. Stains were added at 2 µM for calcein AM and at 0.2 µM for EthD-1. Plates were incubated at 37 °C and 5% CO_2 for 20 minutes. Samples were washed with 150 µL of PBS 3 times before imaging.

3.2.5 Fluorescence Imaging

Fluorescence imaging of calcein AM, EthD-1, and Hoechst were acquired using a Nikon ECLIPSE E800 (Nikon Inc., Melville, NY) at 480 nm excitation wavelength for the calcein AM, 560 nm for the ethidium homodimer, and 350 nm for the Hoechst.

3.2.6 Statistical Analysis

Each assay was completed four independent times using triplicates for each FNAB and duplicates for tissue dissections. Data was analyzed using GraphPad Prism 7 software (GraphPad Software, Inc., San Diego, CA) using one-way ANOVA with Tukey multiple comparisons posttest, with a significance level set at $p < 0.05$.

3.3 Results and Discussion

3.3.1 FNAB and Tissue Dissections Encapsulation Optimization

Currently, most HT 3D culturing assays for cancer treatment studies utilize isolated cells from immortalized cell lines or primary cancer cells, by digesting tissue samples. Isolated cells are invaluable resource for basic and translational studies, enabling the development of many drugs. Primary cancer cells recapitulate parental tumor features closely, yet they don't have the capacity of unlimited proliferation. Cancer cell lines are easier to maintain, generate reproducible results and are immortalized. Therefore, cancer cell lines are almost exclusively used for HT drug screening (Meijer et al., 2017). However, isolated cells lack tumor heterogeneity and natural microenvironment encountered *in vivo*, which have significant effects on cellular responses to treatments. Consequently, reducing the

accuracy of predicting clinical outcomes. To overcome this dilemma, PDX and organotypic slices are developed to maintain a closer mimic to clinical responses (Hidalgo et al., 2011; Naipal et al., 2016). Yet, PDX and organotypic slices are low in throughput and impractical for HT drug screening development. Patient-derived organoids are more practical for HT applications and reflect *in vivo* pathology. However, sample processing by digestion disturbs tissue sample heterogeneity, cell-cell contact and tissue structure, which are factors that may affect cellular responses. There is a need for a system that offers a closer representation of *in vivo* tumor similar to PDX and organotypic slices, while having the capacity to adapt to HT drug screening applications similar to organoids assays.

To begin to address this need, healthy adipose tissue samples from breast cancer patients undergoing surgery for breast cancer treatment were obtained and cultured *ex vivo* in the HT 3D hydrogel assay. Received samples were either FNAB suspended in bodily fluids and blood, or grossly dissected adipose tissue, with a size of approximately 2 cm^3. First, hydrogel precursor solution without PBS was prepared. Briefly, PEG 8-arm macromer, MMP-degradable peptide crosslinker, cell adhesion peptide (CRGDS), photo-initiator, and the fluorescent MMP-degradable peptide were combined and vortexed. The hydrogel precursor solution was then pipetted into each well at around half the volume (5.45 µL) of the final hydrogel volume (10 µL). Second, tissue samples were processed and added to the hydrogel precursor solution. For FNAB, a PBS wash was done to rinse tissue from bodily fluids and blood, then suspended in sterile PBS. Afterwards, FNAB tissue samples

were dispensed, utilizing wide mouth tips, on top of the hydrogel precursor solution, in 3 different volumes (1.14, 2.27 and 4.54 µL). PBS was added to the hydrogel precursor solution with FNAB to reach a final volume of 10 µL/well, and pipetted up and down 2-3 times to create a homogenous mixture. For tissue dissections, a pair of tweezers were utilized to mechanically and bluntly dissect the large adipose tissue samples, then samples were immersed into the 50 µL precursor hydrogel solution that has been developed previously elsewhere (Leight et al., 2013). Tissue dissections were also encapsulated in 10 µL hydrogels (Figure 21B). Hydrogel polymerization was photo-initiated by exposure to long wavelength UV light (365 nm, 4 mW/cm2 for 3 min). Cell culture media was added, and the encapsulated tissue samples were incubated (37 °C, 5% CO_2) for 24 hr. Total ischemic time from receiving tissue samples to encapsulation and media addition was around 60 - 90 minutes. Cell metabolic activity was measured using resazurin, which was added to the wells 6 hr before the final plate read at 24 hr. Fluorescence intensity was measured using a microplate reader with an area well scan. The HT MMP assay requires a black plate because of the fluorogenic MMP sensor. However, we wanted to be able to visualize the tissue samples encapsulated in the hydrogels during the optimization process, so clear round bottom 96-well plates were used to visualize the distribution of the sample within each hydrogel and consistency across different hydrogels from the same condition (Figure 21). Use of the FNAB samples offered an advantage over tissue dissections as the FNAB samples could be pipetted using manual pipetters or automated liquid handlers, allowing the scale up of the encapsulation process to suit HT applications.

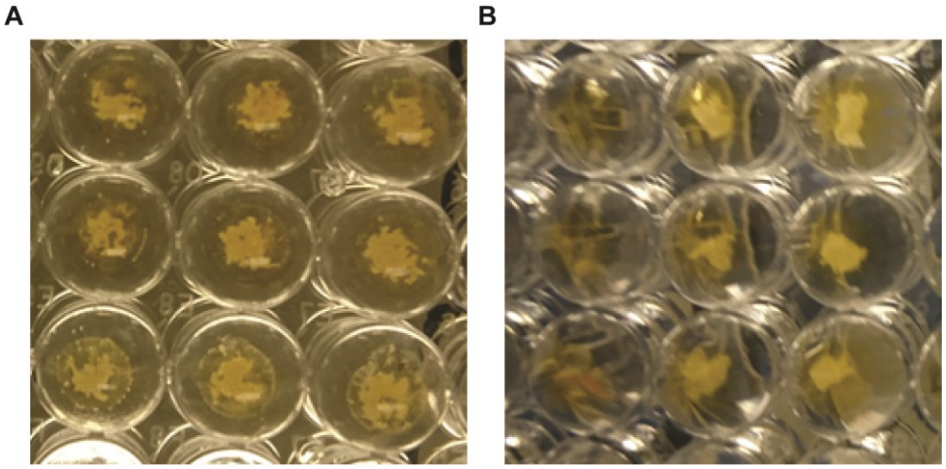

Figure 21: Clear plate bottom view of tissue samples encapsulated in hydrogels. Bottom view of (A) FNAB and (B) tissue dissections after encapsulation, polymerization of hydrogels, and assay media addition. (A) FNAB are encapsulated in three different volumes (1.14, 2.27 and 4.54 µL) left to right, respectively. (B) Tissue dissections encapsulated in 10 µL hydrogels in three different diameters (~1.5, 2.5 and 4.0 mm) left to right, respectively.

3.3.2 Viability of Tissue Samples

To evaluate the viability of the FNAB and tissue dissections, encapsulated tissue samples were stained with a commercial viability kit at two different time points. The first time point (0 hr) was after minimal sample processing and encapsulation and before incubation. This time point determines the viability after tissue processing to identify cell death due to processing or ischemic time. The second time point was after 24 hr of incubation in the assay, this time point confirms that cells were mostly viable after the experiment was completed in full. The commercial viability/cytotoxicity kit was used to visualize cellular viability, utilizing calcein AM to stain viable cells and EthD-1 to stain dead cells. Calcein AM labels viable cells with green fluorescent dye utilizing

intracellular esterase activity, while EthD-1 indicates cellular membrane integrity loss of dead cells by staining nucleic acids with fluorescent red dye. At the first time point (0 hr), tissue samples were processed and encapsulated in non-fluorescent hydrogels, then stained with the viability/cytotoxicity kit. Although some cells were dead, mainly on the edges of tissue sample (Figure 22B), the majority of cells were alive when live and dead images are merged (Figure 22D). After 24 hr of encapsulation, cells of encapsulated tissue samples were still mostly viable. Similar to the 0 hr, there was dead cells at the edges of the tissue samples (Figure 22F). Nevertheless, by comparing the total number of cells (blue nuclei stain) (Figure 22G) to the number of dead cells (red) (Figure 22F), it is apparent that most of the cells were alive (Figure 22H). The viability of encapsulated tissue after 24 hr of incubation in hydrogels suggested that the assay was able to maintain the viability of cultured samples for 24 hr *ex vivo*. Moreover, from viability/cytotoxicity images, it is noticeable that most cells in FNAB samples were intact in clusters of tissue, which indicates that FNAB tissue samples were not just viable after 24 hr of encapsulation, but also structurally preserved. Further characterization and quantification of the encapsulated samples viability, utilizing the viability/cytotoxicity assay, is required to confirm preliminary results demonstrated here. Additionally, structural integrity should be further investigated by evaluating histological fidelity of tissue samples utilizing hematoxylin and eosin (H&E) staining.

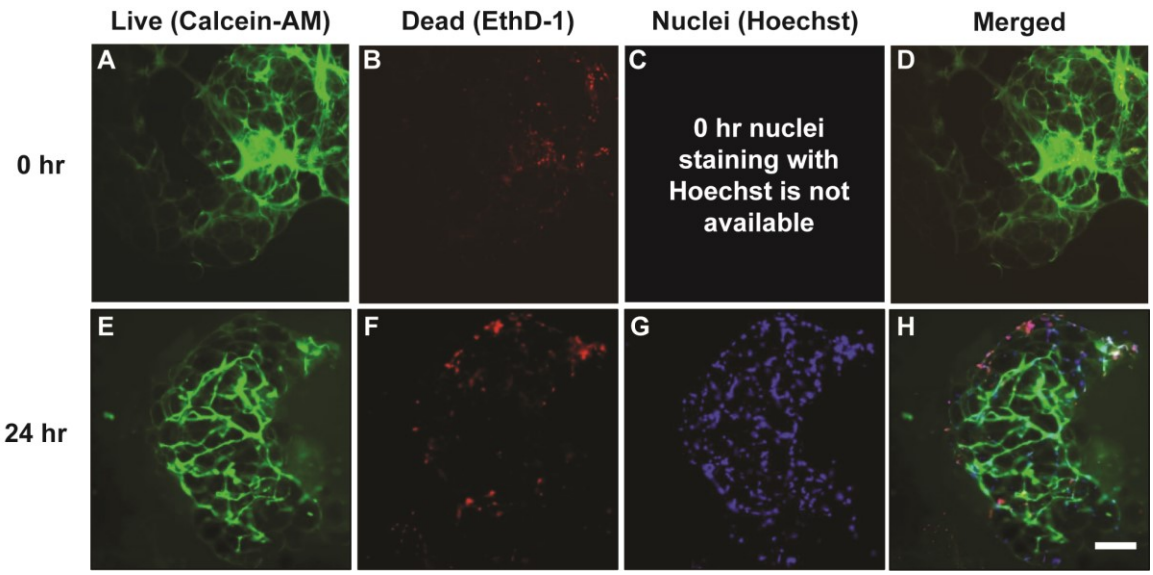

Figure 22: Viability/cytotoxicity of FNAB at 0 hr after encapsulation and sample processing, and after 24 hr of encapsulation. (A and E) Live cells stained with fluorescent green calcein AM dye. (B and F) Dead cells stained with fluorescent red EthD-1 dye. (G) Nuclei of cells stained with fluorescent blue Hoechst dye. (D and H) Merged images. Scale bar = 150 μm, 10x magnification. (C) It was thought of staining nuclei with Hoechst after 0 hr staining was done, and there were no enough tissue samples.

3.3.3 Metabolic and MMP Activity of Tissue Samples

While live/dead staining gives a more accurate account of the viability of the tissue samples, enabling an absolute quantification of the total number of cells, this assay is not compatible with HT applications. Therefore, to simplify and expedite the process of determining the overall health of encapsulated tissue, resazurin dye was used to measure metabolic activity. Metabolic activity measurements are often used in HT drug screening applications, similar to MTT and MTS assays. After 24 hours of encapsulating tissue samples in the MMP-degradable hydrogels, a microplate reader was used to acquire a fluorescence well scan for metabolic and MMP activity. FNAB samples had metabolic

activity that is significantly higher than background control in a volume dependent manner (Figure 23A). Similarly, metabolic activity of adipose tissue dissections were also significantly higher than background controls in a diameter dependent manner (Figure 23B). MMP activity was also measured for FNAB and tissue dissections simultaneously with metabolic activity. Measuring MMP activity is an example of assessing other important cellular functions that might be potential pharmacological targets. MMP activity was significantly higher than background control for FNAB samples (Figure 23C). Likewise, MMP activity of tissue dissections were significantly higher than control in a diameter dependent manner (Figure 23D). Detecting metabolic and MMP activity in a size dependent manner provides sufficient preliminary data for the assay to be utilized for further characterization and development. However, an internal control should be established considering the variability caused by tissue sample sizes due to human error in pipetting or dissection.

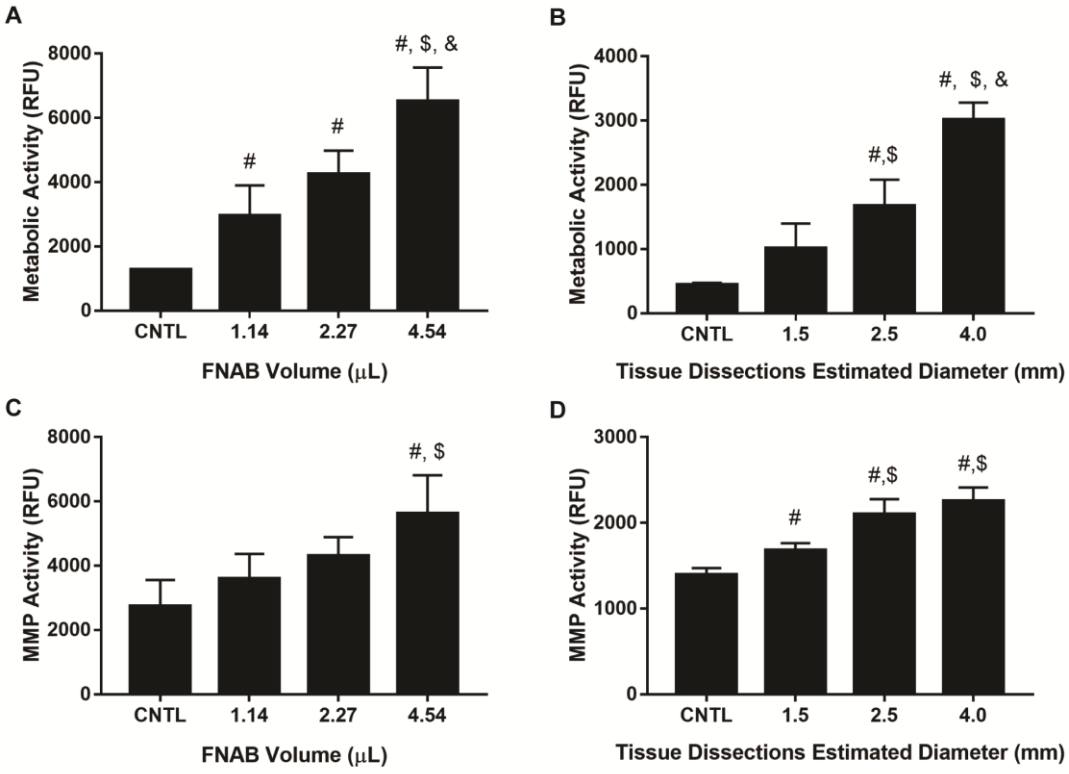

Figure 23: Metabolic and MMP activity of FNAB and tissue dissections. After 24 hr of incubation of tissue samples in the MMP-degradable hydrogel, metabolic and MMP activity were measured for (A and C) FNAB and (B and D) tissue dissections. n=4 ± SD, $p<0.05$, significantly different than: (#) control (CNTL), ($) 1.14 μL or 1.5 mm, and (&) 2.27 μL or 2.5 mm tissue samples.

To identify an internal control for encapsulated tissue size variability, several normalization methods were investigated. MMP and metabolic activity signals were normalized to FNAB volume, tissue dissections mass, or their metabolic activity. Normalized metabolic activity of FNAB sample volume (Figure 24A) resulted in no statistically significant differences between different volumes. Likewise, MMP activity of FNAB was normalized to samples volume, and no significant differences were observed (Figure 24C). This insignificant difference of normalized metabolic and MMP activity

indicates that normalizing signals to sample volume is suitable as an internal control for sample size variability. Interestingly, the variability at higher FNAB volumes (4.54 μL) was less than the variability at lower volumes (1.14 and 2.27 μL) (Figures 24A and 24C), which indicates that pipetting higher volumes of FNAB may contribute to more reproducible outcomes. On the other hand, tissue dissections do not show a trend across different sample diameters when metabolic and MMP activity were normalized to samples masses (Figures 24B and 24D), which were measured prior to the experiment. Although, there was no significant differences for normalized metabolic and MMP activity across different conditions, normalizing metabolic and MMP activity to masses of tissue dissections may not be a suitable internal control to tissue size variability. Measuring masses of tissue dissections prior to encapsulation was not practical or accurate due to the very small masses of tissue dissections (ranged from ~2 to 40 mg), which increased the overall variability in produced signals. Also, measuring the mass of every tissue sample may create a limitation for developing an efficient HT assay. Another internal control was investigated which is normalizing MMP activity to metabolic activity, similar to what was done before with cell lines in chapter 2. Normalized MMP activity to metabolic activity for FNAB and tissue dissections yielded no statistical significance (Figures 24E and 24F). However, FNAB showed large variability across different conditions when MMP activity was normalized to metabolic activity (Figure 24E). This variability means that normalizing MMP activity to metabolic activity for FNAB may not be a suitable internal control for encapsulated tissue sample size. In general, normalizing metabolic or MMP activities to FNAB high volumes (4.54 μL)

produced less variable internal control than normalizing MMP activity to metabolic activity. On the other hand, by normalizing MMP activity to metabolic activity of tissue dissections, variability was clearly less with higher tissue dissections diameters (4 mm) than lower ones (1.5 and 2.5 mm). Normalizing MMP activity to metabolic activity of tissue dissections produces generally lower variability as an internal control than normalizing metabolic or MMP activity to measured mass. To this end, optimizing a suitable internal control is necessary, considering co-variables that could affect signal produced by the assay. Here, it was demonstrated that normalizing metabolic and MMP activities to FNAB sample volumes may serve a better internal control for high volumes than normalizing MMP activity over metabolic activity, due to variability. In contrast, it was demonstrated that normalizing MMP activity to metabolic activity of larger tissue dissections could be a better internal control than normalizing metabolic or MMP activities to tissue mass, also due to variability.

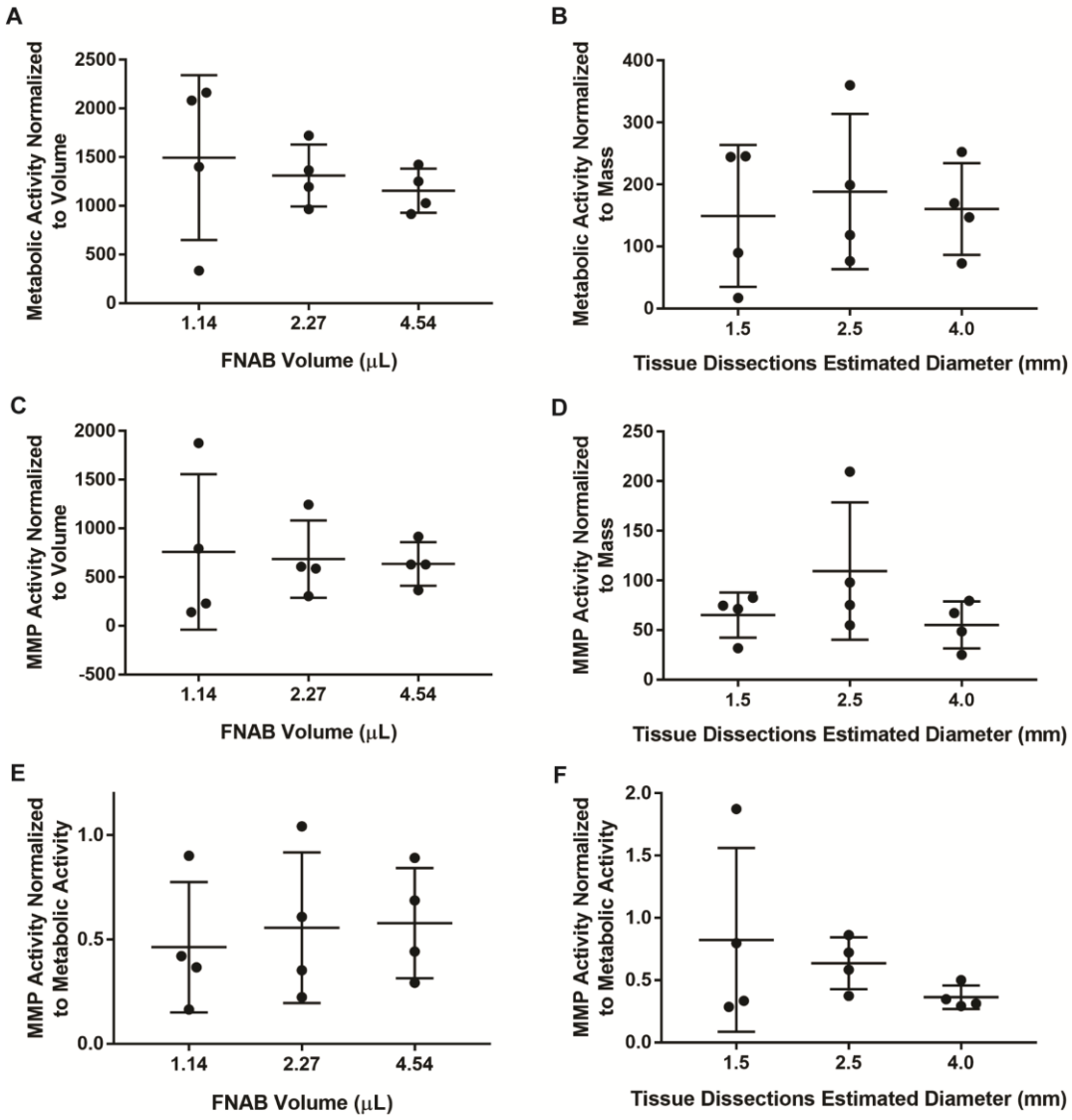

Figure 24: Normalization of MMP and Metabolic activity of FNAB and tissue dissections. (A) Metabolic activity of FNAB normalized to samples volume. (B) Metabolic activity of tissue dissections normalized to samples mass. (C) MMP activity of FNAB normalized to samples volume. (D) MMP activity of tissue dissections normalized to samples mass. (E) MMP activity of FNAB normalized to metabolic activity. (F) MMP activity of tissue dissections normalized to metabolic activity. n=4 ± SD.

FNAB offers several advantages and has some limitations in comparison to tissue dissections. FNAB were acquired from patients utilizing 21 or 25 gauge needles, which

does not require a surgery or anesthesia compared to core biopsy needles or tissue dissections. Such minimally invasive technique enables taking samples in less-equipped point of care sites, facilitating further *ex vivo* studies for individualized treatment and patient stratification applications. Because FNAB tissue size is small (less than 1 mm) they were suspended in fluid, facilitating pipetting of tissue samples and future automation using HT automated liquid handlers. Moreover, small tissue size of FNAB enables miniaturizing the assay even further to increase efficiency. Tissue dissections cannot be pipetted, and smallest tissue size achieved is dependent on the user dissection skills, which makes the assay with tissue dissections lower in throughput. Breast tissue is rich with a variety tissue types (adipose, epithelial, glandular, etc.). Since the FNAB are acquired blindly, aspirated tissue types may vary across experiments, which might increase the overall variability of results. Additionally, the total amount of aspirated tissue highly varies across different patients, making planning of experiments more difficult. In contrast, utilizing tissue dissections produced a greater amount of tissue sample, facilitating testing more conditions. FNAB and tissue dissections acquisition may disturb the architecture and structure of the tissue samples due to shear forces of suction and blunt dissection, respectively. Therefore, it is recommended to evaluate tissue samples structure with histological staining before the utilization of samples.

The developed *ex vivo* assay has a modular design, in which the specificity and methodology could be adapted to a variety of applications. While a specific fluorescent metalloproteinase-degradable peptide was used here, the assay and methodology are not

sensor specific and would be amenable to the incorporation of other fluorescent reporter molecules. The use of other degradable substrates would enable the detection of other MMPs, as demonstrated earlier with LACW MMP-degradable peptide (chapter 2), or proteolytic sub-groups beyond MMPs, such as serine, threonine, or cysteine proteases. The assay methodology is not tissue type (adipose tissue) specific. Other types of tissue samples such as skin, muscle, brain, etc. could be encapsulated to obtain quick snapshot of their proteolytic activity. This adaptability of the assay widens the spectrum of applications it could be utilized for. Potential applications may include measuring MMP activity before and after surgeries, therapeutic development by drug screenings, development of new biosensors to detect other molecules, and stratifying patients to individualize treatment.

3.4 Conclusion

Currently, most assays to develop cancer chemotherapeutics utilizes 2D culturing systems. These 2D systems lack critical cues of the *in vivo* microenvironment, which has significant effects on cellular responses to treatment. Therefore, researchers utilized 3D culturing microenvironments and tumor spheroids to recapitulate some of the *in vivo* cellular response to treatment. Indeed, they have been able to recapitulate some of the encountered cellular responses *in vivo* such as drug resistance, yet, they are using isolated cell lines that lack tumor architecture and heterogeneity encountered *in vivo*. To maintain that tumor architecture and heterogeneity, many researchers are utilizing PDX models and organotypic slices. PDX models and organotypic slices maintain molecular

characteristics, eliminate cellular selection, and reflect the tumor pathology. However, they are expensive, time consuming, labor intensive and have long turnaround time to produce results. To overcome such limitations, *ex vivo* FNAB and tissue dissections from patients undergoing lumpectomy or mastectomy surgeries were directly encapsulated into our HT 3D MMP-degradable hydrogel assay. The system maintained viability of encapsulated tissue samples for 24 hours. Furthermore, metabolic and MMP activity were detected in a sample size dependent manner. The developed *ex vivo* culture system promotes further characterization of viability, utilizing commercial viability/cytotoxicity assays, and histological integrity utilizing H & E staining. In addition, validating MMP activity utilizing well established MMP activity assays such as gelatin and *in situ* zymography.

Chapter 4. Summary, Future Work and Conclusion

4.1 Summary

2D culture systems are invaluable tools, which contributed significantly to fundamental biology research and drug development. However, 2D culture systems lack important environmental cues that have significant effects on cellular functions and responses to treatments. Therefore, 3D culture systems have been developed to provide a better *in vitro* representation of the *in vivo* cellular responses. While a number of HT 3D culture systems have been developed, these systems are often more complex, expensive and labor intensive compared to 2D culture systems. Thus, most HT 3D culturing systems measure only cellular viability and are limited in the number of cell functions that can be assessed in response to drugs. A number of cellular functions contribute to disease progression and treatment response beyond viability, and therefore are important targets for drug development purposes. For instance, MMP detection is crucial due to the significant role MMPs play in human physiology and pathophysiology, making them important pharmacological targets. There is a need for a HT 3D culture platform that measure other cellular functions. To address this need, we adapted a 3D low throughput system that enabled facile measurement of MMP activity alongside of metabolic activity of encapsulated cells in fluorescent PEG hydrogels (Leight et al., 2013). The system was developed to handle more samples by miniaturizing it from 24-well format to 96-well format, which reduced reagents used by 80% and time of experiment preparation by 50%. The system was then characterized to assess its suitability for HT applications, such as

drug screening. The HT 3D MMP activity assay had a wide range of signal detection, of approximately 4 orders of magnitude of enzyme concentration, was not affected by DMSO, a common drug solvent, or by altering mechanical properties, such as stiffness. Furthermore, the developed assay passed HT standard test, known as uniformity test, from which edge effect, drift, coefficient of variation (%CV), Z'-factor, inter-plate and inter-day fold shifts were calculated and within the acceptable range for HT applications. The system was validated using purified human MMPs and encapsulating a variety of cell types. Human MMP-1, -2 and -9 resulted in a significant increase in signal intensity. Encapsulation of several cell types, utilizing two different MMP-degradable peptides, produced robust signals above background noise and within the linear range of the assay. Finally, a small drug screen on a fibrosarcoma cells (HT1080) was performed to demonstrate the utility of the HT 3D MMP activity assay. Sorafenib, paclitaxel and gemcitabine were used, from which sorafenib was observed to increase MMP activity in a dose dependent manner.

The small drug screen mentioned above utilized an immortalized cell line that is homogenous and isolated from its native microenvironment, similar to most drug screening assays. However, tumor cells *in vivo* are heterogeneous and within their native microenvironment, which may have a significant effect on cellular responses to drugs. To improve the prediction of clinical responses, researchers utilized PDX models and organotypic slices for drug testing. Indeed, PDX models and organotypic slices maintain tumor heterogeneity, molecular characteristics, and pathology, which was reflected on the

close representation of clinical outcomes. However, PDX models and organotypic slices are expensive, complex and need long time to produce results. These disadvantages hinder PDX models and organotypic slices of being used in HT applications. To this end, we envisioned using our HT 3D MMP activity assay to encapsulate tissue samples from patients having lumpectomy or mastectomy surgeries. Encapsulating tissue samples in our HT 3D MMP activity assay with the goal to maintain cell population heterogeneity and native microenvironment, while offering the advantages of a 3D HT assay for drug screening purposes. As a proof of concept, adipose FNAB and tissue dissections were encapsulated in our HT 3D MMP activity assay, which maintained viability of tissue for 24 hr. Furthermore, metabolic and MMP activity were detected in a tissue size dependent manner. Maintaining tissue viability and detecting MMP and metabolic activity provide sufficient preliminary results to further pursue viability and histology characterization. Additionally, MMP activity could be validated utilizing well established MMP activity assays such as gelatin and in situ zymography. The developed assay has potential in many applications such as measuring MMP activity before and after surgeries, therapeutic development by drug screenings, development of new biosensors to detect other molecules, and stratifying patients to individualize treatment.

4.2 Future Work

4.2.1 Validating Effect of Drug Treatment on Cellular Viability

In HT drug screening, metabolic activity is commonly utilized as an indicator of overall cellular health because metabolic activity assays are easy to use and inexpensive.

Tetrazolium salts assays (MTT and MTS) are metabolic activity assays, which are commonly used in HT drug screening assays as cellular viability, cytotoxicity and proliferation indicator (Haas et al., 2017; Sekhon et al., 2008). Although metabolic activity correlates to cellular viability (Shelper et al., 2016), metabolic activity is not a direct measurement of cellular viability. Therefore, after completing a HT drug screen with metabolic activity measurement, effect of candidate drugs on viability should be investigated to confirm screening results. For example, sorafenib reduced metabolic activity of fibrosarcoma cells in a dose dependent manner in the mini drug screen (Figure 19B), the next step would be determining fibrosarcoma viability in response to sorafenib using live/ dead staining such as calcein AM and EthD-1. Investigating cellular metabolic activity only is not enough due to some drugs may alter metabolic activity but not cellular viability, contributing to false conclusions.

4.2.2 Validating Effect of Drug Treatment on MMP Activity per Cell

It was demonstrated earlier in chapter 2 that MMP and metabolic activities were affected by drug treatments (SOR, PAC, and GEM). However, other conclusions from the same results may be inferred. Since MMP activity was normalized to metabolic activity, leading to the conclusion of MMP activity increased on a 'per-cell' basis, metabolic activity with SOR, might be affected by drug treatment while viability was not affected. Therefore, testing viability utilizing a live/dead staining or signaling pathways, such as caspase-3 expression, would give a better indication of cellular viability in response to drugs. Also, it might be beneficial to utilize a negative control inhibiting cell death

(apoptosis) such as caspase-3 inhibitor, to evaluate the effect of the drug on cells' MMP activity without their death. Add to this, inducing cell death through cytotoxic reagents, such as ethanol, as a positive control to study the effect of cell death on MMP activity without drugs.

Another aspect of the assay that may need further analysis is related to the time frame in which the MMP and metabolic activity reads were taken, in here 24 hours after encapsulation. The fluorescence reads serves as snapshots of MMP and metabolic activity after 24 hours of encapsulation. Yet, it does not answer questions like, when did the cells die during the 24 hours? What is the effect of drug incubation duration on MMP activity? Such questions might be answered by doing a time course study varying the timing of drug addition and overall duration of the assay. Another probable explanation for PAC and GEM not affecting MMP or metabolic activity could be due to the time frame of the assay (24 hours) being too short for the drug to take effect. Hence, longer assay duration should be tested to determine these drugs effects on MMP and metabolic activity. This also encourages us to test cellular viability with faster assays, such as Cell Titer Glow, at different time points to determine the timing of cellular death in relation to drug addition.

In regards to overall MMP activity in response to treatments, other experimental approaches to measure MMP activity such as gelatin or *in situ* zymographies, would confirm results obtained from our developed assay. *In situ* zymography enables the microscopic visualization of MMP activity within tissue which also could be utilized

alongside cell death staining (such as EthD-1) to visualize MMP activity in relation to cell viability. Results of drug screen obtained in chapter 2 may have many other interpretations pertaining MMP and metabolic activities. More experimentation and characterization would add another layer of confidence to reach accurate conclusions.

4.2.3 Effect of Drug Treatment on Cellular Invasion and Migration

It is well-established that MMPs are secreted in higher levels in cancers than in normal tissue. MMPs play major roles in cancer hallmarks, for instance high MMP activity is well-correlated to cancer invasion and migration (Vihinen & Kähäri, 2002), which are critical steps for tumor metastasis. However, an increase in MMP activity level may not mean an increase in invasion and migration. Further analysis of drug effects on invasion and migration should be performed. As demonstrated in chapter 2 (Figure 19C), MMP activity was increased on a per cell basis with the treatment of fibrosarcoma cells with sorafenib, a drug utilized in clinical trials. This increase in MMP activity encourages us to further investigate if it is correlated to an increase in other critical tumor progression functions such as invasion and migration. It was demonstrated elsewhere, with a melanoma cell line (A375) that small molecule inhibitor (vemurafenib) increased MMP activity and single cell migration, while sorafenib did not alter MMP activity or cell motility (Leight et al., 2015). This example emphasizes the importance of directly testing functions such as invasion and migration in response to drug treatments. Moreover, it demonstrates that responses vary between different cell lines with the same drug, where sorafenib increased MMP activity in fibrosarcoma but not melanoma. Therefore, it is

necessary to investigate cellular functions such as MMP activity, invasion, and migration, if other cell types were utilized.

4.2.4 Characterization of Encapsulated Tissue Samples

It was demonstrated in chapter 3 (Figure 22E to 22H) that our developed *ex vivo* culturing system maintained viability of healthy adipose tissue for 24 hr. Viability was determined using live/dead staining kit (calcein AM and EthD-1), which fluoresces depending on cellular esterase activity (calcein AM) and cell membrane integrity (EthD-1) to differentiate between live or dead cells. However, viability test performed is not sufficient and should be repeated. Further viability tests, utilizing live dead staining, should be performed while altering culturing conditions such as ischemic time, encapsulation technique, hydrogels properties and media contents. Viability at three different time points of the encapsulation process should be tested. One as soon as tissue sample are acquired to determine maximum viability, one after sample processing and encapsulation to investigate process effect on viability, and the last one after 24 hours of incubation in the hydrogel assay to determine the assay ability to maintain a healthy culture. As a control for FNAB acquiring process, which might damage FNAB tissue due to shear force, tissue dissections could be utilized to determine maximum viability. Such viability testing determines optimal culturing conditions and the robustness of our assay to cope with subtle changes that are lab and user dependent. Further viability characterization could be performed utilizing the same kit or other commercially available kits such as CellTiter-Glo® luminescent cell viability assay. CellTiter-Glo®

depends on ATP presence in cells and produce a luminescence signal. Using other viability test, confirms results found with live/dead staining by using other biomarker, and may enable measuring MMP activity and viability simultaneously from the same well. Viability of adipose tissue was demonstrated in chapter 3 after 24 hr of incubation. Yet, when drugs are tested, adipose or other types of tissue might need more time to respond to drug treatment. Therefore, testing viability for periods of incubation more than 24 hr will demonstrate the assay capability of maintaining viability for longer culture periods, and determine the maximum viability duration of the encapsulated tissue. Tissue viability in *ex vivo* culture is tissue type dependent. Therefore, it is important to test and characterize the viability of different tissue types before conducting an experiment. Pushing the assay to its boundaries during characterization enables a better understanding of the developed assay capabilities and limitations.

One of the main reasons of encapsulating tissue samples *ex vivo* is to maintain native tissue structure, which has an effect on cellular responses. Therefore, it is important to characterize tissue structure, cell aggregate size and cell type proportions within a sample at different culturing conditions, mentioned above. Tissue histological structure should be tested at different steps of encapsulation, when first tissue received, after minimal processing and encapsulation, and after incubation in the hydrogel for the duration of the assay. Validating histological structure of tissue samples at different encapsulation steps confirms the suitability of the system to preserve tissue sample structure for the duration of the assay. Immunohistochemical staining such as hematoxylin and eosin (H&E) stains

could be utilized to validate tissue structure. As demonstrated in chapter 2 and 3, MMP and metabolic activity signal intensity are directly proportional to encapsulated cell quantity (Figures 15A and 15B) and tissue size (Figures 23B and 23D). Therefore, it is necessary to determine cell cluster size of encapsulated tissue samples by quantifying cell number and area of tissue sample. Determining cell cluster size may provide a suitable internal control for variability caused by tissue size, especially for FNAB as demonstrated earlier in chapter 3 (Figures 24A and 24C). Different cell types have different MMP and metabolic activity, which was demonstrated when multiple cell types were encapsulated in the MMP-degradable hydrogel, having different MMP and metabolic activity signal intensity (Figures 15A and 15B). Thus, proportions of different cell types within a tissue sample should be evaluated to determine dominant cell type and correlate cell type to MMP and metabolic activity. Different cell types can be recognized by staining a variety of biomarkers such as lipids or PPAR-gamma in adipocytes, fibroblast specific protein-1 (FSP-1) or proteoglycans in fibroblasts, pan-cytokeratin or epithelial membrane antigen (EMA) in epithelial cells and CD68 or F4/80 in macrophages.

4.2.5 Validation of MMP Activity measurements of *Ex Vivo* Tissue Samples

To validate MMP activity detected from tissue samples, our MMP activity assay could be compared to standard MMP activity assays, such as gelatin and *in situ* zymography (ISZ). In gelatin zymography, media of cells encapsulated in hydrogels is collected then run via electrophoresis through gelatin gels that segregate gelatinases (MMP-2 and -9) by their

molecular weight. Then, through a process of protein renaturing and denaturing with an SDS-PAGE zymogram, active and non-active gelatinases form bands proportional to amount of enzymes. To visualize MMP activity within tissue samples, ISZ is utilized by incubating fluorescent MMP degradable peptides on tissue slices, in which MMP activity are localized. ISZ enables visual and quantitative comparison of MMP activity within and across tissue slices highlighting MMP activity differences, such as the difference between MMP activity in normal and cancerous tissue.

4.2.6 Drug Treatment Effects on MMP Activity of Breast Tissue Samples

Many studies have demonstrated effects of chemotherapeutics on MMP expression and activity of a variety of cancers (Chiang et al., 2012; Ha et al., 2015; Leight et al., 2015; Schnaeker et al., 2004). However, isolated cell lines, which lack tumor heterogeneity, were cultured in 2D or 3D systems that may not adequately represent clinical outcomes. Therefore, testing drugs utilizing our HT *ex vivo* culturing system may bridge the gap between HT 2D and 3D models and PDX models, which are known for their excellent representation of clinical responses. Bridging the gap may be done in steps, starting with testing drug effects on MMP activity between 2D and 3D cultures (spheroids). Next, comparing results with FNAB MMP activity in response to the same drugs. Then, comparing MMP activity of FNAB to PDX models in response to drugs that altered MMP activity in the previous step. In breast cancer, similar to many other cancers, MMP activity is not usually considered in drug screening. Therefore, breast cancer cell lines could be cultured on 2D plastic and 3D spheroids to measure MMP activity in response

to several drugs. Several drugs that are used to treat breast cancer in clinics could be utilized, such as cisplatin, paclitaxel, gemcitabine, and doxorubicin. Comparing MMP activity of 2D culture to 3D spheroids in response to chemotherapeutics will determine how multicellular culture affects MMP activity in response to drugs and helps in predicting responses of FNAB with similar drugs.

Drug screening of FNAB may provide a closer representation of drug treatment responses in patients. This closer representation might be due to FNAB maintaining tumor heterogeneity, structure and molecular characteristics, all of which affect cellular responses to treatments and lack in 3D spheroids from isolated cells. Therefore, the same drug screen with spheroids could be done on FNAB tissue samples encapsulated *ex vivo*. PDX are a well-established methodology that was demonstrated in many studies to produce similar responses to patients. Therefore, drug candidates that alter MMP activity in FNAB could be tested using other technologies such as PDX models to confirm results found with FNAB and to prove the concept of the closer representation of FNAB to *in vivo* responses. Additionally, drug resistance (viability) of FNAB could be compared to tumors of PDX models as another indicator of the closer representation of the FNAB response to *in vivo* response. Other molecular characteristics and biomarkers might be compared between FNAB and PDX models in response to tested drugs. For instance, staining for apoptosis, proliferation, or suppression/activation of signal molecules and comparing them between FNAB and PDX models gives an indication of how close or far FNAB would predict cellular responses to *in vivo*.

4.2.7 FBS Effects on MMP and metabolic Activity

FBS added to assay media was heat inactivated and charcoal stripped as mentioned above in chapter 2. FBS heat inactivation and charcoal stripping reduce fluorescent background noise by reducing unspecific cleavage of the fluorescent peptide. This reduction of fluorescent background noise might be due to inactivating and stripping of proteases, growth factors and hormones from FBS (Cao et al., 2009). However, charcoal stripping also reduce other important compounds, such as vitamins, glucose, folic acid and phosphorus, which are necessary for cell growth and affect their responses (Cao et al., 2009). Therefore, it's important to determine which compounds in FBS that cause the increase of fluorescent background noise, to try to individually eliminate them from FBS without affecting other crucial compounds. Once compounds of interest are determined, their effects on cellular functions should be known, to control for any unwanted cellular co-variables during drug screenings. To test the effects of heat inactivation and charcoal stripping of FBS on fluorescence signal and cellular functions, processed and un-processed FBS might be incubated with functionalized hydrogels with and without encapsulated cells, and MMP and metabolic activity would be measured and compared. Other cellular biomarkers and functions, such as intracellular signaling, in response to processed and un-processed FBS might be tested, to further evaluate the effects of heat inactivation and charcoal stripping on MMP and metabolic activity.

4.3 Conclusion

To conclude, the value of 2D drug screening models has degraded over the years, due to its incompetency to accurately represent clinical outcomes. Therefore, HT 3D culture platforms are utilized. But because of the complexity and impracticalities introduced by HT 3D models, they are limited to viability assessment. Yet, potential treatments may be hidden underneath other cellular functions, hence it is important to consider them in drug screening and development. We developed, characterized, validated and demonstrated the utility of a HT assay for cellular encapsulation in 3D microenvironment to measure cellular functions such as MMP activity. Interestingly, sorafenib increased MMP activity in a dose dependent manner in fibrosarcoma. This MMP increase encourages us to further investigate other related cellular functions such as fibrosarcoma invasion and migration in response to sorafenib.

Cellular responses and functions using *in vitro* cultures are affected by their culture environment. The closer *in vitro* models representing *in vivo* microenvironment, the closer *in vitro* cellular responses might be to clinical responses. To improve tumor representation *in vitro*, we developed an *ex vivo* culture system, in which tissue samples lived for 24 hours and MMP and metabolic activity were detected. Further, tissue samples characterization (viability and histological fidelity) and MMP activity validation (with gelatin and in situ zymography) should be performed, before utilizing the assay for drug testing. The developed system opens new doors towards many applications pertaining biology fundamentals research, drug discovery, and precision medicine.

Bibliography

Anand, P., Fu, A., Teoh, S. H., & Luo, K. Q. (2015). Application of a fluorescence resonance energy transfer (FRET)-based biosensor for detection of drug-induced apoptosis in a 3D breast tumor model. *Biotechnology and Bioengineering*, *112*(8), 1673–1682. https://doi.org/10.1002/bit.25572

Anderson, S. B., Lin, C.-C., Kuntzler, D. V., & Anseth, K. S. (2011). The performance of human mesenchymal stem cells encapsulated in cell-degradable polymer-peptide hydrogels. *Biomaterials*, *32*(14), 3564–3574. https://doi.org/10.1016/j.biomaterials.2011.01.064

Annabi, N., Nichol, J. W., Zhong, X., Ji, C., Koshy, S., Khademhosseini, A., & Dehghani, F. (2010). Controlling the Porosity and Microarchitecture of Hydrogels for Tissue Engineering. *Tissue Engineering. Part B, Reviews*, *16*(4), 371–383. https://doi.org/10.1089/ten.teb.2009.0639

Baker, B. M., & Chen, C. S. (2012). Deconstructing the third dimension – how 3D culture microenvironments alter cellular cues. *J Cell Sci*, *125*(13), 3015–3024. https://doi.org/10.1242/jcs.079509

Barletta, E., Ramazzotti, M., Fratianni, F., Pessani, D., & Degl'Innocenti, D. (2015). Hydrophilic extract from Posidonia oceanica inhibits activity and expression of gelatinases and prevents HT1080 human fibrosarcoma cell line invasion. *Cell Adhesion & Migration*, *9*(6), 422–431. https://doi.org/10.1080/19336918.2015.1008330

Ben-David, U., Ha, G., Tseng, Y.-Y., Greenwald, N. F., Oh, C., Shih, J., … Golub, T. R. (2017). Patient-derived xenografts undergo mouse-specific tumor evolution. *Nature Genetics*, *49*(11), 1567–1575. https://doi.org/10.1038/ng.3967

Benya, P. D., & Shaffer, J. D. (1982). Dedifferentiated chondrocytes reexpress the differentiated collagen phenotype when cultured in agarose gels. *Cell*, *30*(1), 215–224. https://doi.org/10.1016/0092-8674(82)90027-7

Bläuer, M., Tammela, T. L., & Ylikomi, T. (2008). A novel tissue-slice culture model for non-malignant human prostate. *Cell and Tissue Research*, *332*(3), 489–498. https://doi.org/10.1007/s00441-008-0602-z

Böckelman, C., Beilmann-Lehtonen, I., Kaprio, T., Koskensalo, S., Tervahartiala, T., Mustonen, H., … Haglund, C. (2018). Serum MMP-8 and TIMP-1 predict prognosis in colorectal cancer. *BMC Cancer*, *18*(1), 679. https://doi.org/10.1186/s12885-018-4589-x

Boehnke, K., Iversen, P. W., Schumacher, D., Lallena, M. J., Haro, R., Amat, J., … Velasco, J. A. (2016). Assay Establishment and Validation of a High-Throughput Screening Platform for Three-Dimensional Patient-Derived Colon Cancer Organoid Cultures. *Journal of Biomolecular Screening*, *21*(9), 931–941. https://doi.org/10.1177/1087057116650965

Boespflug, A., Caramel, J., Dalle, S., & Thomas, L. (2017). Treatment of NRAS-mutated advanced or metastatic melanoma: rationale, current trials and evidence to date. *Therapeutic Advances in Medical Oncology*, *9*(7), 481–492. https://doi.org/10.1177/1758834017708160

Bremer, C., Bredow, S., Mahmood, U., Weissleder, R., & Tung, C. H. (2001). Optical imaging of matrix metalloproteinase-2 activity in tumors: feasibility study in a mouse model. *Radiology*, *221*(2), 523–529. https://doi.org/10.1148/radiol.2212010368

Caley, M. P., Martins, V. L. C., & O'Toole, E. A. (2015). Metalloproteinases and Wound Healing. *Advances in Wound Care*, *4*(4), 225–234. https://doi.org/10.1089/wound.2014.0581

Caliari, S. R., & Burdick, J. A. (2016). A Practical Guide to Hydrogels for Cell Culture. *Nature Methods*, *13*(5), 405–414. https://doi.org/10.1038/nmeth.3839

Cao, Z., West, C., Norton-Wenzel, C. S., Rej, R., Davis, F. B., Davis, P. J., & Rej, R. (2009). Effects of Resin or Charcoal Treatment on Fetal Bovine Serum and Bovine Calf Serum. *Endocrine Research*, *34*(4), 101–108. https://doi.org/10.3109/07435800903204082

Cathcart, J., Pulkoski-Gross, A., & Cao, J. (2015). Targeting matrix metalloproteinases in cancer: Bringing new life to old ideas. *Genes & Diseases*, *2*(1), 26–34. https://doi.org/10.1016/j.gendis.2014.12.002

Chai, S. C., Goktug, A. N., & Chen, T. (2015). Assay Validation in High Throughput Screening – from Concept to Application. In O. Vallisuta & S. Olimat (Eds.), *Drug Discovery and Development* (pp. 221–239). https://doi.org/10.5772/59765

Chalasani, A., Ji, K., Sameni, M., Mazumder, S. H., Xu, Y., Moin, K., & Sloane, B. F. (2017). Live-Cell Imaging of Protease Activity: Assays to Screen Therapeutic

Approaches. *Methods in Molecular Biology (Clifton, N.J.)*, *1574*, 215–225. https://doi.org/10.1007/978-1-4939-6850-3_16

Chen, L., Xiao, Z., Meng, Y., Zhao, Y., Han, J., Su, G., … Dai, J. (2012). The enhancement of cancer stem cell properties of MCF-7 cells in 3D collagen scaffolds for modeling of cancer and anti-cancer drugs. *Biomaterials*, *33*(5), 1437–1444. https://doi.org/10.1016/j.biomaterials.2011.10.056

Chiang, I.-T., Liu, Y.-C., Wang, W.-H., Hsu, F.-T., Chen, H.-W., Lin, W.-J., … Hwang, J.-J. (2012). Sorafenib inhibits TPA-induced MMP-9 and VEGF expression via suppression of ERK/NF-κB pathway in hepatocellular carcinoma cells. *In Vivo (Athens, Greece)*, *26*(4), 671–681.

DeForest, C. A., Polizzotti, B. D., & Anseth, K. S. (2009). Sequential click reactions for synthesizing and patterning three-dimensional cell microenvironments. *Nature Materials*, *8*(8), 659–664. https://doi.org/10.1038/nmat2473

Deshmukh, A. A., Weist, J. L., & Leight, J. L. (2018). Detection of proteolytic activity by covalent tethering of fluorogenic substrates in zymogram gels. *BioTechniques*, *64*(5), 203–210. https://doi.org/10.2144/btn-2018-0005

Dias, J. M., Go, N. F., Hart, C. P., & Mattheakis, L. C. (1998). Genetic recombination as a reporter for screening steroid receptor agonists and antagonists. *Analytical Biochemistry*, *258*(1), 96–102. https://doi.org/10.1006/abio.1998.2583

Duval, K., Grover, H., Han, L.-H., Mou, Y., Pegoraro, A. F., Fredberg, J., & Chen, Z. (2017). Modeling Physiological Events in 2D vs. 3D Cell Culture. *Physiology*, *32*(4), 266–277. https://doi.org/10.1152/physiol.00036.2016

Ehrbar, M., Sala, A., Lienemann, P., Ranga, A., Mosiewicz, K., Bittermann, A., … Lutolf, M. P. (2011). Elucidating the Role of Matrix Stiffness in 3D Cell Migration and Remodeling. *Biophysical Journal*, *100*(2), 284–293. https://doi.org/10.1016/j.bpj.2010.11.082

Esch, E. W., Bahinski, A., & Huh, D. (2015). Organs-on-chips at the frontiers of drug discovery. *Nature Reviews Drug Discovery*, *14*(4), 248–260. https://doi.org/10.1038/nrd4539

Fairbanks, B. D., Schwartz, M. P., Bowman, C. N., & Anseth, K. S. (2009). Photoinitiated polymerization of PEG-diacrylate with lithium phenyl-2,4,6-trimethylbenzoylphosphinate: polymerization rate and cytocompatibility. *Biomaterials*, *30*(35), 6702–6707. https://doi.org/10.1016/j.biomaterials.2009.08.055

Fairbanks, B. D., Schwartz, M. P., Halevi, A. E., Nuttelman, C. R., Bowman, C. N., & Anseth, K. S. (2009). A Versatile Synthetic Extracellular Matrix Mimic via Thiol-Norbornene Photopolymerization. *Advanced Materials*, *21*(48), 5005–5010. https://doi.org/10.1002/adma.200901808

Fakhouri, A. S., & Leight, J. L. (2019). Measuring Global Cellular Matrix Metalloproteinase and Metabolic Activity in 3D Hydrogels. *JoVE (Journal of Visualized Experiments)*, (143), e59123. https://doi.org/10.3791/59123

Fakhouri, A. S., Weist, J. L., Tomusko, A. R., & Leight, J. L. (2019). High-Throughput Three-Dimensional Hydrogel Cell Encapsulation Assay for Measuring Matrix

Metalloproteinase Activity. *ASSAY and Drug Development Technologies*, *17*(3), 100–115. https://doi.org/10.1089/adt.2018.877

Fernandez-Fuente, G., Mollinedo, P., Grande, L., Vazquez-Barquero, A., & Fernandez-Luna, J. L. (2014). Culture dimensionality influences the resistance of glioblastoma stem-like cells to multikinase inhibitors. *Molecular Cancer Therapeutics*, *13*(6), 1664–1672. https://doi.org/10.1158/1535-7163.MCT-13-0854

Folgueras, A. R., Pendás, A. M., Sánchez, L. M., & López-Otín, C. (2004). Matrix metalloproteinases in cancer: from new functions to improved inhibition strategies. *The International Journal of Developmental Biology*, *48*(5–6), 411–424. https://doi.org/10.1387/ijdb.041811af

Friedl, P., & Wolf, K. (2003). Tumour-cell invasion and migration: diversity and escape mechanisms. *Nature Reviews Cancer*, *3*(5), 362–374. https://doi.org/10.1038/nrc1075

Fukuda, J., Khademhosseini, A., Yeh, J., Eng, G., Cheng, J., Farokhzad, O. C., & Langer, R. (2006). Micropatterned cell co-cultures using layer-by-layer deposition of extracellular matrix components. *Biomaterials*, *27*(8), 1479–1486. https://doi.org/10.1016/j.biomaterials.2005.09.015

Geiser, A. G., Anderson, M. J., & Stanbridge, E. J. (1989). Suppression of tumorigenicity in human cell hybrids derived from cell lines expressing different activated ras oncogenes. *Cancer Research*, *49*(6), 1572–1577.

Gerlach, M. M., Merz, F., Wichmann, G., Kubick, C., Wittekind, C., Lordick, F., … Bechmann, I. (2014). Slice cultures from head and neck squamous cell carcinoma: a novel test system for drug susceptibility and mechanisms of resistance. *British Journal of Cancer*, *110*(2), 479–488. https://doi.org/10.1038/bjc.2013.700

Grant, D. S., Williams, T. L., Zahaczewsky, M., & Dicker, A. P. (n.d.). Comparison of antiangiogenic activities using paclitaxel (taxol) and docetaxel (taxotere). *International Journal of Cancer*, *104*(1), 121–129. https://doi.org/10.1002/ijc.10907

Gryshkov, O., Pogozhykh, D., Zernetsch, H., Hofmann, N., Mueller, T., & Glasmacher, B. (2014). Process engineering of high voltage alginate encapsulation of mesenchymal stem cells. *Materials Science and Engineering C*, *36*(1), 77–83. https://doi.org/10.1016/j.msec.2013.11.048

Guo, W. M., Loh, X. J., Tan, E. Y., Loo, J. S. C., & Ho, V. H. B. (2014). Development of a Magnetic 3D Spheroid Platform with Potential Application for High-Throughput Drug Screening. *Molecular Pharmaceutics*, *11*(7), 2182–2189. https://doi.org/10.1021/mp5000604

Ha, T.-Y., Hwang, S., Moon, K.-M., Won, Y.-J., Song, G.-W., Kim, N., … Hong, H.-N. (2015). Sorafenib inhibits migration and invasion of hepatocellular carcinoma cells through suppression of matrix metalloproteinase expression. *Anticancer Research*, *35*(4), 1967–1976.

Haas, M. J., Onstead-Haas, L., Kurban, W., Shah, H., Plazarte, M., Chamseddin, A., & Mooradian, A. D. (2017). High-Throughput Analysis Identifying Drugs That

Regulate Apolipoprotein A-I Synthesis. *Assay and Drug Development Technologies*, *15*(8), 362–371. https://doi.org/10.1089/adt.2017.782

Hakkinen, K. M., Harunaga, J. S., Doyle, A. D., & Yamada, K. M. (2011). Direct Comparisons of the Morphology, Migration, Cell Adhesions, and Actin Cytoskeleton of Fibroblasts in Four Different Three-Dimensional Extracellular Matrices. *Tissue Engineering. Part A*, *17*(5–6), 713–724. https://doi.org/10.1089/ten.tea.2010.0273

Hall, A., Marshall, C. J., Spurr, N. K., & Weiss, R. A. (1983). Identification of transforming gene in two human sarcoma cell lines as a new member of the ras gene family located on chromosome 1. *Nature*, *303*(5916), 396–400. https://doi.org/10.1038/303396a0

Hidalgo, M., Bruckheimer, E., Rajeshkumar, N. V., Garrido-Laguna, I., De Oliveira, E., Rubio-Viqueira, B., … Sidransky, D. (2011). A pilot clinical study of treatment guided by personalized tumorgrafts in patients with advanced cancer. *Molecular Cancer Therapeutics*, *10*(8), 1311–1316. https://doi.org/10.1158/1535-7163.MCT-11-0233

Hoarau-Véchot, J., Rafii, A., Touboul, C., & Pasquier, J. (2018). Halfway between 2D and Animal Models: Are 3D Cultures the Ideal Tool to Study Cancer-Microenvironment Interactions? *International Journal of Molecular Sciences*, *19*(1). https://doi.org/10.3390/ijms19010181

Hogrebe, N. J., & Gooch, K. J. (2016). Direct influence of culture dimensionality on human mesenchymal stem cell differentiation at various matrix stiffnesses using a

fibrous self-assembling peptide hydrogel. *Journal of Biomedical Materials Research. Part A*, *104*(9), 2356–2368. https://doi.org/10.1002/jbm.a.35755

Hopkins, A. L. (2008). Network pharmacology: the next paradigm in drug discovery. *Nature Chemical Biology*, *4*(11), 682–690. https://doi.org/10.1038/nchembio.118

Hughes, C. S., Postovit, L. M., & Lajoie, G. A. (2010). Matrigel: A complex protein mixture required for optimal growth of cell culture. *PROTEOMICS*, *10*(9), 1886–1890. https://doi.org/10.1002/pmic.200900758

Huh, D., Kim, H. J., Fraser, J. P., Shea, D. E., Khan, M., Bahinski, A., … Ingber, D. E. (2013). Microfabrication of human organs-on-chips. *Nature Protocols*, *8*(11), 2135–2157. https://doi.org/10.1038/nprot.2013.137

Huh, D., Matthews, B. D., Mammoto, A., Montoya-Zavala, M., Hsin, H. Y., & Ingber, D. E. (2010). Reconstituting Organ-Level Lung Functions on a Chip. *Science*, *328*(5986), 1662–1668. https://doi.org/10.1126/science.1188302

Imaninezhad, M., Hill, L., Kolar, G., Vogt, K., & Zustiak, S. P. (2019). Templated Macroporous Polyethylene Glycol Hydrogels for Spheroid and Aggregate Cell Culture. *Bioconjugate Chemistry*, *30*(1), 34–46. https://doi.org/10.1021/acs.bioconjchem.8b00596

Itoh, T., Tanioka, M., Yoshida, H., Yoshioka, T., Nishimoto, H., & Itohara, S. (1998). Reduced angiogenesis and tumor progression in gelatinase A-deficient mice. *Cancer Research*, *58*(5), 1048–1051.

Iversen, P. W., Beck, B., Chen, Y.-F., Dere, W., Devanarayan, V., Eastwood, B. J., … Sittampalam, G. S. (2004). HTS Assay Validation. In G. S. Sittampalam, N. P.

Coussens, K. Brimacombe, A. Grossman, M. Arkin, D. Auld, … X. Xu (Eds.), *Assay Guidance Manual* (pp. 937–967). Retrieved from http://www.ncbi.nlm.nih.gov/books/NBK83783/

Jedeszko, C., Sameni, M., Olive, M., Moin, K., & Sloane, B. F. (2008). Visualizing Protease Activity in Living Cells: From Two Dimensions to Four Dimensions. *Current Protocols in Cell Biology / Editorial Board, Juan S. Bonifacino ... [et Al.]*, *0 4*, Unit-4.20. https://doi.org/10.1002/0471143030.cb0420s39

Ji, C., Khademhosseini, A., & Dehghani, F. (2011). Enhancing cell penetration and proliferation in chitosan hydrogels for tissue engineering applications. *Biomaterials*, *32*(36), 9719–9729. https://doi.org/10.1016/j.biomaterials.2011.09.003

Johnson, J. I., Decker, S., Zaharevitz, D., Rubinstein, L. V., Venditti, J. M., Schepartz, S., … Sausville, E. A. (2001). Relationships between drug activity in NCI preclinical in vitro and in vivo models and early clinical trials. *British Journal of Cancer*, *84*(10), 1424–1431. https://doi.org/10.1054/bjoc.2001.1796

Kadono, Y., Shibahara, K., Namiki, M., Watanabe, Y., Seiki, M., & Sato, H. (1998). Membrane type 1-matrix metalloproteinase is involved in the formation of hepatocyte growth factor/scatter factor-induced branching tubules in madin-darby canine kidney epithelial cells. *Biochemical and Biophysical Research Communications*, *251*(3), 681–687. https://doi.org/10.1006/bbrc.1998.9531

Kinoshita, T., Higuchi, H., Kabashima-Niibe, A., Sakai, G., Hamamoto, Y., Takaishi, H., & Kanai, T. (2018). *Analysis of Sensitivity and Cell Death Pathways Mediated by*

Anti-cancer Drugs Using Three-dimensional Culture System. *14*, 1–12. https://doi.org/10.3923/ijcr.2018.1.12

Kleinman, H. K., & Martin, G. R. (2005). Matrigel: Basement membrane matrix with biological activity. *Seminars in Cancer Biology*, *15*(5), 378–386. https://doi.org/10.1016/j.semcancer.2005.05.004

Koblinski, J. E., Dosescu, J., Sameni, M., Moin, K., Clark, K., & Sloane, B. F. (2002). Interaction of human breast fibroblasts with collagen I increases secretion of procathepsin B. *The Journal of Biological Chemistry*, *277*(35), 32220–32227. https://doi.org/10.1074/jbc.M204708200

Kola, I. (2008). The state of innovation in drug development. *Clinical Pharmacology and Therapeutics*, *83*(2), 227–230. https://doi.org/10.1038/sj.clpt.6100479

Koshiba, T., Hosotani, R., Wada, M., Miyamoto, Y., Fujimoto, K., Lee, J. U., … Imamura, M. (1998). Involvement of matrix metalloproteinase-2 activity in invasion and metastasis of pancreatic carcinoma. *Cancer*, *82*(4), 642–650.

Kruitwagen, H. S., Oosterhoff, L. A., Vernooij, I. G. W. H., Schrall, I. M., van Wolferen, M. E., Bannink, F., … Spee, B. (2017). Long-Term Adult Feline Liver Organoid Cultures for Disease Modeling of Hepatic Steatosis. *Stem Cell Reports*, *8*(4), 822–830. https://doi.org/10.1016/j.stemcr.2017.02.015

Lai, Y., Wei, X., Lin, S., Qin, L., Cheng, L., & Li, P. (2017). Current status and perspectives of patient-derived xenograft models in cancer research. *Journal of Hematology & Oncology*, *10*(1), 106. https://doi.org/10.1186/s13045-017-0470-7

Ledford, H. (2011, September 29). Translational research: 4 ways to fix the clinical trial : Nature News. Retrieved March 4, 2019, from https://www.nature.com/news/2011/110928/full/477526a.html

Lee, S.-H., Miller, J. S., Moon, J. J., & West, J. L. (2005). Proteolytically Degradable Hydrogels with a Fluorogenic Substrate for Studies of Cellular Proteolytic Activity and Migration. *Biotechnology Progress*, *21*(6), 1736–1741. https://doi.org/10.1021/bp0502429

Leight, J. L., Alge, D. L., Maier, A. J., & Anseth, K. S. (2013). Direct measurement of matrix metalloproteinase activity in 3D cellular microenvironments using a fluorogenic peptide substrate. *Biomaterials*, *34*(30), 7344–7352. https://doi.org/10.1016/j.biomaterials.2013.06.023

Leight, J. L., Tokuda, E. Y., Jones, C. E., Lin, A. J., & Anseth, K. S. (2015). Multifunctional bioscaffolds for 3D culture of melanoma cells reveal increased MMP activity and migration with BRAF kinase inhibition. *Proceedings of the National Academy of Sciences of the United States of America*, *112*(17), 5366–5371. https://doi.org/10.1073/pnas.1505662112

Li, Y., Dal-Pra, S., Mirotsou, M., Jayawardena, T. M., Hodgkinson, C. P., Bursac, N., & Dzau, V. J. (2016). Tissue-engineered 3-dimensional (3D) microenvironment enhances the direct reprogramming of fibroblasts into cardiomyocytes by microRNAs. *Scientific Reports*, *6*, 38815. https://doi.org/10.1038/srep38815

Llano, E., Pendás, A. M., Freije, J. P., Nakano, A., Knäuper, V., Murphy, G., & López-Otin, C. (1999). Identification and Characterization of Human MT5-MMP, a New

Membrane-bound Activator of Progelatinase A Overexpressed in Brain Tumors. *Cancer Research*, *59*(11), 2570–2576.

Löffek, S., Schilling, O., & Franzke, C.-W. (2011). Biological role of matrix metalloproteinases: a critical balance. *European Respiratory Journal*, *38*(1), 191–208. https://doi.org/10.1183/09031936.00146510

Lutolf, M. P., & Hubbell, J. A. (2005). Synthetic biomaterials as instructive extracellular microenvironments for morphogenesis in tissue engineering. *Nature Biotechnology*, *23*(1), 47–55. https://doi.org/10.1038/nbt1055

Lutolf, M. P., Lauer-Fields, J. L., Schmoekel, H. G., Metters, A. T., Weber, F. E., Fields, G. B., & Hubbell, J. A. (2003). Synthetic matrix metalloproteinase-sensitive hydrogels for the conduction of tissue regeneration: Engineering cell-invasion characteristics. *Proceedings of the National Academy of Sciences*, *100*(9), 5413–5418. https://doi.org/10.1073/pnas.0737381100

Mabry, K. M., Schroeder, M. E., Payne, S. Z., & Anseth, K. S. (2016). Three-Dimensional High-Throughput Cell Encapsulation Platform to Study Changes in Cell-Matrix Interactions. *ACS Applied Materials & Interfaces*, *8*(34), 21914–21922. https://doi.org/10.1021/acsami.5b11359

Maffia, I., Kariv, I., & Oldenburg, K. R. (1999). Miniaturization of a mammalian cell-based assay: Luciferase reporter gene readout in a 3 microliter 1536-well plate. *Journal of Biomolecular Screening*, *4*(3), 137–142. https://doi.org/10.1177/108705719900400307

Maki, R. G. (2007). Gemcitabine and Docetaxel in Metastatic Sarcoma: Past, Present, and Future. *The Oncologist*, *12*(8), 999–1006. https://doi.org/10.1634/theoncologist.12-8-999

Marchenko, G. N., Ratnikov, B. I., Rozanov, D. V., Godzik, A., Deryugina, E. I., & Strongin, A. Y. (2001). Characterization of matrix metalloproteinase-26, a novel metalloproteinase widely expressed in cancer cells of epithelial origin. *The Biochemical Journal*, *356*(Pt 3), 705–718.

Meijer, T. G., Naipal, K. A., Jager, A., & van Gent, D. C. (2017). Ex vivo tumor culture systems for functional drug testing and therapy response prediction. *Future Science OA*, *3*(2). https://doi.org/10.4155/fsoa-2017-0003

Merz, F., Gaunitz, F., Dehghani, F., Renner, C., Meixensberger, J., Gutenberg, A., … Bechmann, I. (2013). Organotypic slice cultures of human glioblastoma reveal different susceptibilities to treatments. *Neuro-Oncology*, *15*(6), 670–681. https://doi.org/10.1093/neuonc/not003

Mokrý, J., Karbanová, J., Lukáš, J., Palečková, V., & Dvořánková, B. (2000). Biocompatibility of HEMA Copolymers Designed for Treatment of CNS Diseases with Polymer-Encapsulated Cells. *Biotechnology Progress*, *16*(5), 897–904. https://doi.org/10.1021/bp000113m

Mucha, A., Cuniasse, P., Kannan, R., Beau, F., Yiotakis, A., Basset, P., & Dive, V. (1998). Membrane Type-1 Matrix Metalloprotease and Stromelysin-3 Cleave More Efficiently Synthetic Substrates Containing Unusual Amino Acids in Their

P1′ Positions. *Journal of Biological Chemistry*, *273*(5), 2763–2768. https://doi.org/10.1074/jbc.273.5.2763

Muller, M., Trocme, C., Lardy, B., Morel, F., Halimi, S., & Benhamou, P. Y. (2008). Matrix metalloproteinases and diabetic foot ulcers: the ratio of MMP-1 to TIMP-1 is a predictor of wound healing. *Diabetic Medicine*, *25*(4), 419–426. https://doi.org/10.1111/j.1464-5491.2008.02414.x

Nagase, H., & Fields, G. B. (1996). Human matrix metalloproteinase specificity studies using collagen sequence-based synthetic peptides. *Peptide Science*, *40*(4), 399–416. https://doi.org/10.1002/(SICI)1097-0282(1996)40:4<399::AID-BIP5>3.0.CO;2-R

Nagase, H., Visse, R., & Murphy, G. (2006). Structure and function of matrix metalloproteinases and TIMPs. *Cardiovascular Research*, *69*(3), 562–573. https://doi.org/10.1016/j.cardiores.2005.12.002

Naipal, K. A. T., Verkaik, N. S., Sánchez, H., van Deurzen, C. H. M., den Bakker, M. A., Hoeijmakers, J. H. J., … van Gent, D. C. (2016). Tumor slice culture system to assess drug response of primary breast cancer. *BMC Cancer*, *16*. https://doi.org/10.1186/s12885-016-2119-2

Nakamura, H., Fujii, Y., Ohuchi, E., Yamamoto, E., & Okada, Y. (1998). Activation of the precursor of human stromelysin 2 and its interactions with other matrix metalloproteinases. *European Journal of Biochemistry*, *253*(1), 67–75.

Nakatani, T., Tsuboyama-Kasaoka, N., Takahashi, M., Miura, S., & Ezaki, O. (2002). Mechanism for peroxisome proliferator-activated receptor-alpha activator-

induced up-regulation of UCP2 mRNA in rodent hepatocytes. *The Journal of Biological Chemistry*, *277*(11), 9562–9569. https://doi.org/10.1074/jbc.M110132200

Nichol, J. W., Koshy, S. T., Bae, H., Hwang, C. M., Yamanlar, S., & Khademhosseini, A. (2010). Cell-laden microengineered gelatin methacrylate hydrogels. *Biomaterials*, *31*(21), 5536–5544. https://doi.org/10.1016/j.biomaterials.2010.03.064

Patterson, J., & Hubbell, J. A. (2010). Enhanced proteolytic degradation of molecularly engineered PEG hydrogels in response to MMP-1 and MMP-2. *Biomaterials*, *31*(30), 7836–7845. https://doi.org/10.1016/j.biomaterials.2010.06.061

Pauli, C., Hopkins, B. D., Prandi, D., Shaw, R., Fedrizzi, T., Sboner, A., … Rubin, M. A. (2017). Personalized In Vitro and In Vivo Cancer Models to Guide Precision Medicine. *Cancer Discovery*, *7*(5), 462–477. https://doi.org/10.1158/2159-8290.CD-16-1154

Ries, C., Egea, V., Karow, M., Kolb, H., Jochum, M., & Neth, P. (2007). MMP-2, MT1-MMP, and TIMP-2 are essential for the invasive capacity of human mesenchymal stem cells: differential regulation by inflammatory cytokines. *Blood*, *109*(9), 4055–4063. https://doi.org/10.1182/blood-2006-10-051060

Ryan, S.-L., Baird, A.-M., Vaz, G., Urquhart, A. J., Senge, M., Richard, D. J., … Davies, A. M. (2016). Drug Discovery Approaches Utilizing Three-Dimensional Cell Culture. *Assay and Drug Development Technologies*, *14*(1), 19–28. https://doi.org/10.1089/adt.2015.670

Salmaso, S., & Caliceti, P. (2013). Stealth Properties to Improve Therapeutic Efficacy of Drug Nanocarriers. *Journal of Drug Delivery*. https://doi.org/10.1155/2013/374252

Schnaeker, E.-M., Ossig, R., Ludwig, T., Dreier, R., Oberleithner, H., Wilhelmi, M., & Schneider, S. W. (2004). Microtubule-Dependent Matrix Metalloproteinase-2/Matrix Metalloproteinase-9 Exocytosis: Prerequisite in Human Melanoma Cell Invasion. *Cancer Research*, *64*(24), 8924–8931. https://doi.org/10.1158/0008-5472.CAN-04-0324

Sekhon, B. K., Roubin, R. H., Tan, A., Chan, W. K., & Sze, D. M.-Y. (2008). High-Throughput Screening Platform for Anticancer Therapeutic Drug Cytotoxicity. *ASSAY and Drug Development Technologies*, *6*(5), 711–722. https://doi.org/10.1089/adt.2008.148

Seliktar, D. (2012). Designing cell-compatible hydrogels for biomedical applications. *Science*, *336*(6085), 1124–1128. https://doi.org/10.1126/science.1214804

Seol, H. S., Kang, H., Lee, S.-I., Kim, N. E., Kim, T. I., Chun, S. M., … Jang, S. J. (2014). Development and characterization of a colon PDX model that reproduces drug responsiveness and the mutation profiles of its original tumor. *Cancer Letters*, *345*(1), 56–64. https://doi.org/10.1016/j.canlet.2013.11.010

Shelper, T. B., Lovitt, C. J., & Avery, V. M. (2016). Assessing Drug Efficacy in a Miniaturized Pancreatic Cancer In Vitro 3D Cell Culture Model. *Assay and Drug Development Technologies*, *14*(7), 367–380. https://doi.org/10.1089/adt.2016.737

Shukla, V., Barnhouse, V., Ackerman, W. E., Summerfield, T. L., Powell, H. M., Leight, J. L., … Ghadiali, S. N. (2018). Cellular Mechanics of Primary Human Cervical Fibroblasts: Influence of Progesterone and a Pro-inflammatory Cytokine. *Annals of Biomedical Engineering*, *46*(1), 197–207. https://doi.org/10.1007/s10439-017-1935-0

Singh M, Close DA, Mukundan S, Johnston PA, & Sant S. (2015). Production of Uniform 3D Microtumors in Hydrogel Microwell Arrays for Measurement of Viability, Morphology, and Signaling Pathway Activation. *Assay and Drug Development Technologies*, *13*(9), 570–583.

Sohail, A., Sun, Q., Zhao, H., Bernardo, M. M., Cho, J.-A., & Fridman, R. (2008). MT4-(MMP17) and MT6-MMP (MMP25), A unique set of membrane-anchored matrix metalloproteinases: properties and expression in cancer. *Cancer and Metastasis Reviews*, *27*(2), 289–302. https://doi.org/10.1007/s10555-008-9129-8

Sorafenib in Treating Patients With Metastatic, Locally Advanced, or Recurrent Sarcoma - Study Results - ClinicalTrials.gov. (n.d.). Retrieved July 6, 2018, from https://clinicaltrials.gov/ct2/show/results/NCT00245102

Sridhar, B. V., Brock, J. L., Silver, J. S., Leight, J. L., Randolph, M. A., & Anseth, K. S. (2015). Development of a cellularly degradable PEG hydrogel to promote articular cartilage extracellular matrix deposition. *Advanced Healthcare Materials*, *4*(5), 702–713. https://doi.org/10.1002/adhm.201400695

Sridhar, B. V., Doyle, N. R., Randolph, M. A., & Anseth, K. S. (2014). Covalently tethered TGF-β1 with encapsulated chondrocytes in a PEG hydrogel system

enhances extracellular matrix production. *Journal of Biomedical Materials Research. Part A*, *102*(12), 4464–4472. https://doi.org/10.1002/jbm.a.35115

Stolow, M. A., Bauzon, D. D., Li, J., Sedgwick, T., Liang, V. C., Sang, Q. A., & Shi, Y. B. (1996). Identification and characterization of a novel collagenase in Xenopus laevis: possible roles during frog development. *Molecular Biology of the Cell*, *7*(10), 1471–1483.

Stygar, D., Wang, H., Vladic, Y. S., Ekman, G., Eriksson, H., & Sahlin, L. (2002). Increased Level of Matrix Metalloproteinases 2 and 9 in the Ripening Process of the Human Cervix. *Biology of Reproduction*, *67*(3), 889–894. https://doi.org/10.1095/biolreprod.102.005116

Sung, K. E., Su, G., Pehlke, C., Trier, S. M., Eliceiri, K. W., Keely, P. J., … Beebe, D. J. (2009). Control of 3-dimensional collagen matrix polymerization for reproducible Human Mammary Fibroblast cell culture in microfluidic devices. *Biomaterials*, *30*(27), 4833–4841. https://doi.org/10.1016/j.biomaterials.2009.05.043

Tauro, M., McGuire, J., & Lynch, C. C. (2014). New approaches to selectively target cancer-associated matrix metalloproteinase activity. *Cancer Metastasis Reviews*, *33*(4), 1043–1057. https://doi.org/10.1007/s10555-014-9530-4

Thiery, J. P., Acloque, H., Huang, R. Y. J., & Nieto, M. A. (2009). Epithelial-Mesenchymal Transitions in Development and Disease. *Cell*, *139*(5), 871–890. https://doi.org/10.1016/j.cell.2009.11.007

Tignanelli, C. J., Herrera Loeza, S. G., & Yeh, J. J. (2014). KRAS and PIK3CA mutation frequencies in patient-derived xenograft models of pancreatic and colorectal

cancer are reflective of patient tumors and stable across passages. *The American Surgeon*, *80*(9), 873–877.

Tokito, A., Jougasaki, M., Tokito, A., & Jougasaki, M. (2016). Matrix Metalloproteinases in Non-Neoplastic Disorders. *International Journal of Molecular Sciences*, *17*(7), 1178. https://doi.org/10.3390/ijms17071178

Trappmann, B., Gautrot, J. E., Connelly, J. T., Strange, D. G. T., Li, Y., Oyen, M. L., … Huck, W. T. S. (2012). Extracellular-matrix tethering regulates stem-cell fate. *Nature Materials*, *11*(7), 642–649. https://doi.org/10.1038/nmat3339

Treatment of Soft Tissue Sarcomas, by Stage. (n.d.). Retrieved July 6, 2018, from https://www.cancer.org/cancer/soft-tissue-sarcoma/treating/by-stage.html

Uría, J. A., & López-Otín, C. (2000). Matrilysin-2, a new matrix metalloproteinase expressed in human tumors and showing the minimal domain organization required for secretion, latency, and activity. *Cancer Research*, *60*(17), 4745–4751.

Vanhoefer, U., Cao, S., Harstrick, A., Seeber, S., & Rustum, Y. M. (1997). Comparative antitumor efficacy of docetaxel and paclitaxel in nude mice bearing human tumor xenografts that overexpress the multidrug resistance protein (MRP). *Annals of Oncology: Official Journal of the European Society for Medical Oncology*, *8*(12), 1221–1228.

Vihinen, P., & Kähäri, V.-M. (2002). Matrix metalloproteinases in cancer: Prognostic markers and therapeutic targets. *International Journal of Cancer*, *99*(2), 157–166. https://doi.org/10.1002/ijc.10329

Visse, R., & Nagase, H. (2003). Matrix metalloproteinases and tissue inhibitors of metalloproteinases: structure, function, and biochemistry. *Circulation Research*, *92*(8), 827–839. https://doi.org/10.1161/01.RES.0000070112.80711.3D

Wang, Y., Mirza, S., Wu, S., Zeng, J., Shi, W., Band, H., … Duan, B. (2018). 3D hydrogel breast cancer models for studying the effects of hypoxia on epithelial to mesenchymal transition. *Oncotarget*, *9*(63), 32191–32203. https://doi.org/10.18632/oncotarget.25891

Weaver, B. A. (2014). How Taxol/paclitaxel kills cancer cells. *Molecular Biology of the Cell*, *25*(18), 2677–2681. https://doi.org/10.1091/mbc.E14-04-0916

Wen, Z., Liao, Q., Hu, Y., You, L., Zhou, L., & Zhao, Y. (2013). A spheroid-based 3-D culture model for pancreatic cancer drug testing, using the acid phosphatase assay. *Brazilian Journal of Medical and Biological Research*, *46*(7), 634–642. https://doi.org/10.1590/1414-431X20132647

Whitesides, G. M. (2006). The origins and the future of microfluidics. *Nature*, *442*, 368–373. https://doi.org/10.1038/nature05058

Williams, K. P., & Scott, J. E. (2009). Enzyme Assay Design for High-Throughput Screening. In W. P. Janzen & P. Bernasconi (Eds.), *High Throughput Screening: Methods and Protocols, Second Edition* (pp. 107–126). https://doi.org/10.1007/978-1-60327-258-2_5

Xue, M., McKelvey, K., Shen, K., Minhas, N., March, L., Park, S.-Y., & Jackson, C. J. (2014). Endogenous MMP-9 and not MMP-2 promotes rheumatoid synovial

fibroblast survival, inflammation and cartilage degradation. *Rheumatology*, *53*(12), 2270–2279. https://doi.org/10.1093/rheumatology/keu254

Yang, M., & Kurkinen, M. (1998). Cloning and characterization of a novel matrix metalloproteinase (MMP), CMMP, from chicken embryo fibroblasts. CMMP, Xenopus XMMP, and human MMP19 have a conserved unique cysteine in the catalytic domain. *The Journal of Biological Chemistry*, *273*(28), 17893–17900.

Yodkeeree, S., Chaiwangyen, W., Garbisa, S., & Limtrakul, P. (2009). Curcumin, demethoxycurcumin and bisdemethoxycurcumin differentially inhibit cancer cell invasion through the down-regulation of MMPs and uPA. *JNB The Journal of Nutritional Biochemistry*, *20*(2), 87–95.

Yodkeeree, S., Garbisa, S., & Limtrakul, P. (2008). Tetrahydrocurcumin inhibits HT1080 cell migration and invasion via downregulation of MMPs and uPA[1]. *APHS Acta Pharmacologica Sinica*, *29*(7), 853–860.

Zhang, J.-H., Chung, T. D. Y., & Oldenburg, K. R. (1999). A Simple Statistical Parameter for Use in Evaluation and Validation of High Throughput Screening Assays. *Journal of Biomolecular Screening*, *4*(2), 67–73. https://doi.org/10.1177/108705719900400206

Zhang, T., Zhang, L., Fan, S., Zhang, M., Fu, H., Liu, Y., … Su, X. (2015). Patient-Derived Gastric Carcinoma Xenograft Mouse Models Faithfully Represent Human Tumor Molecular Diversity. *PloS One*, *10*(7), e0134493. https://doi.org/10.1371/journal.pone.0134493

Zhu, Y., Tian, T., Li, Z., Tang, Z., Wang, L., Wu, J., … Shen, L. (2015). Establishment and characterization of patient-derived tumor xenograft using gastroscopic biopsies in gastric cancer. *Scientific Reports*, *5*, 8542. https://doi.org/10.1038/srep08542

Appendix A. Structure, substrates specificity, unique domains, substrates interactions and functions of different subclasses of MMPs

Structural Classification	Substrate Specificity	Name (MMP-#)	Unique Domains	Interact with Following Substrates	Functions
Gelatinases	Gelatinases	Gelatinase A (MMP-2)	3 repeats of fibronectin type II domains	Gelatin, collagens (type I, II, III, IV, V, VII, X, and XI), elastin, vitronectin, laminin, entactin, tenascin, SPARC, aggrecan, galectin-3, versican, myelin basic protein, fibronectin, chondroitinsulphate proteoglycan, IGFBP-3, laminin 5γ2 chain, degrading IL-1β, Monocyte chemoatractant protein-3, decorin, big endothelin, adrenomedullin, and Stromal cell-derived factor 1α (SDF-1).	Cell migration, neurite outgrowth, mesenchymal cell differentiation, increase IGF1, cell proliferation, epithelial cell migration, anti-inflammatory, Increase TGF-β, generate vasoconstrictor, convert vasoconstrictor to vasodilator, and neurons apoptosis.
		Gelatinase B (MMP-9)		Gelatin, collagens (type IV, V, XI, and XIV), elastin, vitronectin, laminin, SPARC, aggrecan, versican, decorin, myelin basic protein, ICAM-1, plasminogen, processing IL-1β, degrading IL-1β, IL-2Rα, precursor of TGFβ, and galactin-3.	Tumor cell resistance, angiostatin-like fragment formation, pro-inflammatory, anti-inflammatory, IL-2 response reduction, TGF-β bioavailability, thymic neovascularization, chondrocytes apoptosis, and osteoclast recruitment.

Continued on the next page.

Table 4: Structure, substrates specificity, unique domains, substrates interactions and functions of different subclasses of MMPs (Folgueras et al., 2004; Llano et al., 1999; Marchenko et al., 2001; Nagase, Visse, & Murphy, 2006; Nakamura, Fujii, Ohuchi, Yamamoto, & Okada, 1998; Sohail et al., 2008; Stolow et al., 1996; Uría & López-Otín, 2000; Visse & Nagase, 2003).

Structural Classification	Substrate Specificity	Name (MMP-#)	Unique Domains	Interact with Following Substrates	Function
Archetypal	Collagenases	Collagenase-1 (MMP-1)	No unique domains other than main common domains	Collagens (type I, II, III, VII, VIII, X, and XI), gelatin, vitronectin, laminin, entactin, tenascin, aggrecan, link protein, myelin basic protein, versican, fibronectin, IGFBP-3, processing IL-1β, degrading IL-1β, and Monocyte chemoatractant protein-3.	Cell and keratinocyte migration, platelet aggregation, increase IGF1, cell proliferation, apoptosis, pro-inflammatory, and anti-inflammatory.
		Collagenase-2 (MMP-8)		Collagens (type I, II, and III), and aggrecan.	Apoptosis.
		Collagenase-3 (MMP-13)		Collagens (type I, II, III, IV, VI, IX, X, and XIV), collagen telopeptides, gelatin, fibronectin, SPARC, aggrecan, perlecan, large tenascin-C3, perlecan, and Monocyte chemoatractant protein-3.	Osteoclast activation, release of bFGF, apoptosis, and anti-inflammatory.
		Collagenase-4 (MMP-18) (Xenopus)		Collagen type I.	Maturation of digestive tract, tail resorption, and hindlimb morphogenesis in tadpoles.
	Stromelysins	Stromelysin-1 (MMP-3)		Collagens (type III, IV , V , VII, IX, X, and XI), collagen telopeptides, gelatin, elastin, vitronectin, laminin, entactin, tenascin, SPARC, aggrecan, link protein, decorin, myelin basic protein, versican, fibulin, fibronectin, basement membrane, E-cadherin, plasminogen, perlecan, IGFBP-3, processing IL-1β, Monocyte chemoatractant protein-3, and decorin.	Increase cell migration and invasion, mammary epithelial cell apoptosis and alveolar formation, EMT, angiostatin-like fragment formation, release of bFGF, increase IGF1, cell proliferation, pro-inflammatory, anti-inflammatory, Increase TGF-β, and cell aggregation disruption.
		Stromelysin-2 (MMP-10)		Collagens (type III, IV, and V), gelatin, elastin, fibronectin, aggrecan, and link protein.	Activates proMMP-1, -7, -8, and -9.

Continued on the next page.

Structural Classification	Substrate Specificity	Name (MMP-#)	Unique Domains	Interact with Following Substrates	Function
Archetypal	Others	Metalloelastase (MMP-12)	No unique domains other than main common domains	Plasminogen, osteonectin, aggrecan, myelin basic protein, collagens (type I, V, and IV), gelatin, elastin, fibronectin, vitronectin, laminin, and entactin.	Angiostatin-like fragment formation.
		(MMP-19)		IGFBP-3, laminin 5γ2 chain, collagen type IV, gelatin, large tenascin-C, fibronectin, aggrecan, laminin, and entactin.	Increase IGF1, cell proliferation, and epithelial cell migration.
		Enamelysin (MMP-20)		Amelogenin, and aggrecan.	Autolysis
		CMMP (MMP-27) (Gallus)		Gelatin, and casein.	Autolysis
Matrilysins	Matrilysins	Matrilysin-1 (MMP-7)	No hemopexin domain	Fibronectin, plasminogen, IGFBP-3, decorin, E-cadherin, collagens (type I, and IV), gelatin, elastin, vitronectin, laminin, entactin, tenascin, SPARC, aggrecan, link protein, decorin, myelin basic protein, fibulin, and versican.	Increase cell invasion, adipocyte differentiation, angiostatin-like fragment formation, increase IGF1, cell proliferation, Increase TGF-β, and cell aggregation disruption,
		Matrilysins-2 (MMP-26)		Collagen type IV, gelatin, fibronectin, and vitronectin.	Activate proMMP-9, tumor progression, and angiogenesis.
Furin-activatable		Matrilysins-3 (MMP-11)	Furin cleavage site	IGFBP-1, gelatin, fibronectin, collagen type IV, and laminin.	Increase IGF1, and cell proliferation.
	Others	XMMP (MMP-21) (Xenopus)		Gelatin.	
		Epilysin (MMP-28)		Casein.	

Continued on the next page.

Structural Classification	Substrate Specificity	Name (MMP-#)	Unique Domains	Interact with Following Substrates	Function
Furin-activatable	Membrane Bound	MT1-MMP (MMP-14)	C-terminal transmembrane domain, and Furin cleavage site	Collagens (type I, II, and III), gelatin, fibronectin, tenascin, vitronectin, laminin, entactin, aggrecan, CD44, type I collagen, laminin 5γ2 chain, lamin 5β3, Monocyte chemoatractant protein-3, tissue transglutaminase on cell surface, and perlecan.	Cell migration, kidney tubulogenesis, epithelial cell migration, anti-inflammatory, cell adhesion, and spreading reduction.
		MT2-MMP (MMP-15)		Tissue transglutaminase on cell surface, aggrecan, perlecan, fibronectin, tenascin, entactin, and laminin.	Cell adhesion, and spreading reduction.
		MT3-MMP (MMP-16)		Tissue transglutaminase on cell surface, collagen type III, gelatin, fibronectin, vitronectin, and laminin.	
		MT5-MMP (MMP-24)		Fibronectin, gelatin, chondroitin sulphate proteoglycan, and dermatan sulphate proteoglycan.	Activating MMP-2
		MT4-MMP (MMP-17)	glycosylphosphatidylinositol (GPI) anchor, and Furin cleavage site	Gelatin, fibrinogen, and fibrin.	Activating MMP-2, and cancer progression.
		MT6-MMP (MMP-25)		Collagen type IV, gelatin, fibronectin, chondroitin sulphate proteoglycan, dermatan, and sulphate proteoglycan.	Cancer progression.
		CA-MMP (MMP-23)	No hemopexin domain, and Furin cleavage site	Gelatin	

Appendix B. MMP-Degradable Peptide Coupling with Dabcyl and Fluorescein Protocol

1. **OBJECTIVE**

To add dabcyl and then fluorescein onto a previously synthesized peptide.

2. **DEFINITIONS AND ACRONYMS**

1. DMF= N,N-Dimethylformamide, Anhydrous
2. DCM= Dichloromethane
3. TIPS= Triisopropylsilane
4. TFA=Trifluoroacetic acid
5. DIPEA= Diisopropylethylamine

3. **MATERIAL LIST**

1. Hydrazine (Cat # 215155-50g, Sigma-Aldrich)
2. DMF (Cat # 227056-2L, Sigma-Aldrich)
3. Dabcyl (Cat # 50-850-476, Fisher Scientific)
4. NHS-Fluorescein (Cat # PI-46409, Fisher Scientific)
5. DCM (Cat # 676853-4L, Sigma-Aldrich)
6. DIPEA (Cat # D125806-500ML, Sigma-Aldrich)
7. Phenol (Cat # 185450-100G, Sigma-Aldrich)
8. Ether (Cat # E1381, Fisher Scientific)
9. Kaiser Test Solutions (see Kaiser Test Protocol)

4. **DABCYL ADDITION**

1. Remove resin from the peptide synthesizer reaction vessel using DMF, and place into a glass peptide synthesis reaction vessel. Rinse 2-3 more times with DMF to remove as much resin as possible.
2. Clean the Liberty Blue reaction vessel with methanol and allow to dry in the fume hood before placing it back.
3. Fill glass reaction vessel with ~15-20 mL of DMF. Allow resin to swell while continuously stirring in DMF for 15 min.
4. Place a waste beaker below the glass vessel.
5. Open stopcocks and allow DMF to flow out. Use compressed gas to aid in making the fluid flow faster (do this for each wash/solution).
6. Wash resin with ~15-20mL of DMF three more times, ~1min for each wash.
7. Take two small samples (3-4 resin beads) of peptide and place in two tubes.
8. Test one tube via the Kaiser Test.
    1. Kaiser Test = add 20uL of each vial to sample, vortex, spin down, place in heat block @ 100°C for 2min. Positive= turns blue, Negative= no color change

9. Immerse resin with Dabcyl solution O/N
    1. Dabcyl solution: 100mg Dabcyl + 5mL DMF + 200µL DIPEA
    KEEP VESSEL COVERED WITH FOIL O/N

5. **DEPROTECTION, AND FLUORESCEIN ADDITION**

1. Rinse resin with ~15-20mL of DMF three times.
2. Take two small samples of resin and place in two tubes. Perform Kaiser Test on a sample before dabcyl addition, and a sample after dabcyl addition before continuing.
3. Make a 2% Hydrazine deprotection solution: 20mL DMF + 400µL Hydrazine.
4. Immerse resin with 10mL of hydrazine solution for 10min.
5. Drain and wash resin with ~15mL of DMF 3-4 times
6. Immerse resin with remaining hydrazine solution for 10min.
7. Drain and wash resin with ~15 mL of DMF 3-4 times.
8. Take two small samples of resin and place in two tubes. Perform Kaiser Test on a sample after dabcyl addition, and a sample after deprotection before continuing.
9. Immerse resin in Fluorescein solution O/N
    1. Fluorescein solution: 150mg Fluorescein + 2.5mL DMF +100µL DIPEA
10. *KEEP VESSEL WRAPPED IN FOIL O/N (sensing a theme here?)*

6. **CLEAVAGE OFF THE RESIN AND PRECIPITATION OF PEPTIDE**

1. Rinse resin with ~15-20mL of DMF three times.
2. Take a small sample of resin and place in a tube. Perform Kaiser Test on a sample after deprotection, and a sample after fluor. addition before continuing.
3. Wash resin 4 times with ~15mL of DCM. Allow resin to dry for a few minutes.
4. Prepare cleavage cocktail:
    1. Cocktail: 250mg Phenol + 125µL TIPS +125µL H_2O + 5mL TFA
5. Immerse resin in the cleavage cocktail for 2-3 hours.
    KEEP VESSEL COVERED IN FOIL (but you already knew this)
6. Drain liquid into a 50mL conical tube. *THIS IS YOUR PEPTIDE*
7. Add up to 48mL of cold ether to the peptide. Vortex well to precipitate.
8. Centrifuge tube at 3000rpm for 3 min*.
    *Remember! Balance needs to *weigh* the same, since ether is lighter then water.
9. Carefully pour off ether into a waste beaker without dumping the peptide.
10. Add 40-45mL of ether to the sample tube, vortex well, and spin down again. Pour off ether into waste beaker.
11. Repeat step 6.10
12. Rubber band a kimwipe over the tube. *WRAP TUBE IN FOIL (derp)* Allow tube to dry in the fume hood for ~1 hr*.

*Ether must be fully evaporated before placing sample in the desiccator to avoid explosions

13. Place tube in desiccator O/N

14. Perform degradation and Ellman's assays, or store peptide -20°C for long term storage.

Appendix C: Poly(Ethylene Glycol) Functionalization with Norbornene Protocol

1. **OBJECTIVE**
   To add norborbene to PEG monomers.

2. **DEFINITIONS AND ACRONYMS**
   1. PEG= polyethylene glycol
   2. NB= Norbornene
   3. DIC= N,N'-Diisopropylcarbodiimide
   4. DMAP= 4-(Dimethylamino)pyridine
   5. DCM= Dichloromethane, must be anhydrous!

3. **MATERIAL LIST**
   1. DCM, use the 100mL bottles(270997, Sigma-Aldrich)
   2. Norbornene (446440-25ML, Sigma-Aldrich)
   3. Pyridine (270970-100ML, Sigma-Aldrich)
   4. DIC (D125407-100G, Sigma-Aldrich)
   5. DMAP (107700-5G, Sigma-Aldrich)
   6. PEG (JenKem)

4. **DRYING THE PEG**
   1. Weigh out 2g of PEG into a 50mL conical tube
   2. Freeze tube O/N or at least 4hrs in the -70C (Ultra low freezer)
   3. Lyophilize tube O/N to remove any water in the sample

5. **ADDITION OF NORBORNENE**
   1. Add the dried PEG to 100mL round bottom flask.
   2. Add 15mL of DCM to the flask. Stir continuously until PEG dissolves completely.
   3. Add DMAP and pyridine to PEG flask. Allow to stir continuously under Argon for 30min.
   4. In another flask, add 10mL DCM, then add the NB*, and DIC. Allow to stir continuously under Argon for 30min.
   5. Pour contents from PEG flask into NB flask. Allow to stir O/N.
      ***NOTE: use a syringe for dispensing NB, change gloves after handling NB**

6. **PRECIPITATION AND FILTRATION OF PEG-NB**
   1. Fill a large flask with ~900mL of cold ether, add a large stir bar.
   2. Add PEG-NB solution dropwise, slowly, into the stirring ether.
   3. Filter precipitate using a vacuum filter funnel and another large flask*.
   4. Place solid from funnel into a 50mL conical tube, leave tube in hood (~1-2hrs) w/ kimwipe to evaporate the ether.
   5. Place PEG-NB in desiccator until it looks "light and fluffy" (~2-4hrs).

6. Add 20mL of DI H_2O to dried PEG-NB, vortex till fully dissolved.
7. Cut a section of dialysis tubing to ~14cm in length, clamp one end. Pipet solution into the dialysis tubing, and clamp other end. Immerse dialysis tube in 2500-3000mL of DI H_2O.
8. Leave tube immersed for 24-48hrs (the longer the better). Change water at least 3 times during this period.
9. Pipette solution into a 50mL falcon tube after dialysis, and freeze for lyophilization.

***NOTE: All items that come in contact with NB will need to be placed in a 10% bleach bath after cleaning with acetone.**

7. LYOPHILIZATION AND QUALITY CHECK

1. Lyophilize PEG-NB. May take up to 3 days to fully freeze dry.
2. Test dried PEG-NB to see if it will polymerize into a gel.
3. Check purity via NMR on 3-4mg of dried sample.

Some common PEG-NB recipes:

	PEG arms:	4			
MF:	**4 arm PEG (g)**	**NB (uL)**	**Pyridine (uL)**	**DIC (uL)**	**DMAP (mg)**
MW (g/mol)	20000	138.7	79.1	126	122.17
mmoles of amines:	0.4	2	2	1	0.02
Equivalence:	1	5	5	2.5	0.05
Density (g/mL)	-	1.129	0.98	0.8	-
Amount:	2	245.70	161.43	157.50	2
	PEG arms:	8			
MF:	**8 arm PEG (g)**	**NB (uL)**	**Pyridine (uL)**	**DIC (uL)**	**DMAP (mg)**
MW (g/mol)	10000	138.7	79.1	126	122.17
mmoles of amines:	1.6	8	8	4	0.08
Equivalence:	1	5	5	2.5	0.05
Density (g/mL)	-	1.129	0.98	0.8	-
Amount:	2	982.82	645.71	630.00	10
	PEG arms:	8			
MF:	**8 arm PEG (g)**	**NB (uL)**	**Pyridine (uL)**	**DIC (uL)**	**DMAP (mg)**
MW (g/mol)	40000	138.7	79.1	126	122.17
mmoles of amines:	0.4	2	2	1	0.02
Equivalence:	1	5	5	2.5	0.05
Density (g/mL)	-	1.129	0.98	0.8	-
Amount (g):	2	245.70	161.43	157.50	2